

THE PREPARATION AND CHARACTERIZATION OF
LANTHANUM ALUMINATE POWDER AND
RF-SPUTTERED THIN FILMS

by

Carol C. Poirot

ProQuest Number: 10783649

All rights reserved

INFORMATION TO ALL USERS

The quality of this reproduction is dependent upon the quality of the copy submitted.

In the unlikely event that the author did not send a complete manuscript and there are missing pages, these will be noted. Also, if material had to be removed, a note will indicate the deletion.



ProQuest 10783649

Published by ProQuest LLC (2018). Copyright of the Dissertation is held by the Author.

All rights reserved.

This work is protected against unauthorized copying under Title 17, United States Code
Microform Edition © ProQuest LLC.

ProQuest LLC.
789 East Eisenhower Parkway
P.O. Box 1346
Ann Arbor, MI 48106 – 1346

T-3956

A thesis submitted to the Faculty and the Board of Trustees of the Colorado School of Mines in partial fulfillment of requirements for the degree of Master of Science (Materials Science).

Golden, Colorado

Date Sept 19, 1990

Signed: Carol C. Poirot

Carol C. Poirot

Approved: John U. Trefny

Dr. John U. Trefny

Baki Yarar Sept. 18, 1990

Dr. Baki Yarar

Golden, Colorado
Date 19 SEPTEMBER 1990

Date 19 SEPTEMBER 1990

W.D. Copeland

Dr. William D. Copeland
Professor of Metallurgical
Engineering and Coordinator of
Materials Science Program

ABSTRACT

The motivation for this was to develop reliable techniques for depositing high-quality, thin, lanthanum aluminate layers which could be incorporated into high-temperature superconducting devices for microwave applications. A process was developed to prepare high-quality lanthanum aluminate powder. Ionic solutions of lanthanum and aluminum were combined, coprecipitated, filtered, dried at 150 °C and calcined at 950 °C in air. The resulting powder was used to make sputtering targets for the deposition study. This study consisted in rf-magnetron sputtering of thin films of lanthanum aluminate onto sapphire substrates. The effects of different deposition parameters and post-annealing treatments were investigated. Randomly oriented lanthanum aluminate films were prepared by post-annealing amorphous films at temperatures greater than 800 °C in air. The quality of these polycrystalline films was unsuitable for device applications. A high-quality, well-oriented lanthanum aluminate film was deposited onto a well-oriented, crystalline EBCO superconductive film. The morphology of this film was smooth at 3000X magnification and appeared to be suitable for high-temperature superconducting device applications. This result showed that matching the lattice constant of the film and substrate is an important consideration when trying to grow crystalline films of lanthanum aluminate.

TABLE OF CONTENTS

| | <u>Page</u> |
|--|-------------|
| ABSTRACT | iii |
| LIST OF FIGURES | vi |
| LIST OF TABLES | xi |
| ACKNOWLEDGEMENTS | xvi |
| Chapter | |
| 1.0 INTRODUCTION | 1 |
| 1.1 Background and Motivation | 1 |
| 1.2 Comparison of Common High T_c Superconducting Substrate and Buffer Layer Materials | 3 |
| 1.2.1 Lattice Parameters | 3 |
| 1.2.2 Electrical Properties | 4 |
| 1.2.2 Chemical Stability. | 9 |
| 1.2.3 Thermal Properties | 11 |
| 1.3 Summary of the Physical Properties of Lanthanum Aluminate | 12 |
| 2.0 Lanthanum Aluminate Powder Preparation | 15 |
| 2.1 Literature Review for Lanthanum Aluminate Powder Preparation and Characterization | 15 |
| 2.2 Procedure To Make Lanthanum Aluminate Powder | 17 |
| 2.3 Results and Analysis of Lanthanum Aluminate Powder | 25 |
| 2.4. Results and Conclusions for Lanthanum Aluminate Powder Preparation | 34 |
| 3.0 RF-Magnetron Sputtering and Characterization of Lanthanum Aluminate Thin Films. | 41 |
| 3.1 Literature Review for Lanthanum Aluminate Thin Films; Deposition Techniques | 41 |
| 3.1.1 Thin Film Deposition Techniques | 41 |
| 3.1.2 Deposition Techniques for Lanthanum Aluminate Thin Films | 43 |
| 3.2 Deposition Processes of Lanthanum Aluminate Thin Films | 44 |
| 3.3 Lanthanum Aluminate Thin Characterization Procedures | 50 |
| 3.4 Lanthanum Aluminate Thin Film Results | 55 |
| 3.4.1 Initial Lanthanum Aluminate Deposition onto Superconducting Films | 55 |

| | | |
|----------------------------|---|-----|
| 3.4.2 | Radial Composition Study of Lanthanum Aluminate Films . . . | 63 |
| 3.4.3 | Effects of Sputtering Gas Pressure in Lanthanum Aluminate Deposition | 70 |
| 3.4.4 | Post-Annealing Effects on Lanthanum Aluminate Films . . . | 81 |
| 3.4.5 | Metallic Buffer Layers | 100 |
| 3.4.6 | Post In-Situ Annealing of Lanthanum Aluminate Films . . . | 118 |
| 3.4.7 | Lattice Matching | 127 |
| 3.5 | Lanthanum Aluminate Thin Film Deposition Summary. | 141 |
| 4.0 | Recommendations for Future Studies of Lanthanum Aluminate Film Depositions. | 143 |
| 5.0 | Overall Summary | 145 |
| | | |
| REFERENCES CITED | | 149 |

LIST OF FIGURES

| <u>Figure</u> | | <u>Page</u> |
|---------------|---|-------------|
| 2.2.1 | Solubilities of lanthanum and aluminum at different pH values | 21 |
| 2.4.1 | Diffraction pattern for powder made from lanthanum hydroxide and aluminum chloride. Processing method included hydrolysis, filtration, calcination at 500 °C in air and pellet form. | 35 |
| 2.4.2 | Diffraction pattern for powder made from lanthanum and aluminum nitrates. Processing method included hydrolysis, filtration, calcination at 500°C in air and pellet form. . . | 35 |
| 2.4.3 | Diffraction pattern for powder made from lanthanum hydroxide and aluminum chloride. Processing included hydrolysis, filtration, calcination at 950°C in oxygen and pellet form | 36 |
| 2.4.4 | Diffraction pattern for powder made from lanthanum hydroxide and aluminum chloride Processing included hydrolysis, filtration, calcination at 950°C in air and powder form. . . | 36 |
| 2.4.5 | Diffraction pattern for powder made from lanthanum hydroxide and aluminum chloride. Processing method included hydrolysis, evaporation, calcination at 950°C in oxygen and pellet form. | 37 |
| 2.4.6 | Diffraction pattern for powder made from lanthanum and aluminate nitrates. Processing included hydrolysis, filtration, calcination at 950°C in oxygen and pellet form | 37 |
| 2.4.7 | Diffraction pattern for powder made from lanthanum and aluminum nitrate. Processing method included evaporation, calcination at 950°C in air and powder form | 38 |
| 2.4.8 | Diffraction pattern for powder made from lanthanum and aluminum nitrates. Processing method included evaporation, calcination at 950°C for 24 hours in oxygen and powder form | 38 |

| <u>Figure</u> | <u>Page</u> |
|---|-------------|
| 3.2.1 Schematic drawing of the vacuum chamber used to deposit lanthanum aluminate films. | 45 |
| 3.2.2 Schematic diagram showing the deposition apparatus and the off-axis substrates holder configuration. | 46 |
| 3.4.1 SEM micrograph showing the smooth continuous dielectric film deposited onto an EBCO film. . . | 57 |
| 3.4.2 XRD pattern for the dielectric film deposited onto an EBCO film. | 58 |
| 3.4.3 SEM micrograph showing the morphology of the dielectric film deposited onto a YBCO film. | 60 |
| 3.4.4 XRD pattern for the dielectric film deposited onto a YBCO film. | 62 |
| 3.4.5 SEM micrographs showing the morphology of the YBCO and LaAlO ₃ films for radial distance study. | 67 |
| 3.4.6 The XRD pattern for the dielectric film deposited onto a YBCO film centered on the rotating substrate holder. | 68 |
| 3.4.7 XRD pattern for the dielectric film deposited onto the YBCO film placed 1 cm radially from the center of the substrate holder. | 68 |
| 3.4.8 XRD pattern for the dielectric film deposited onto a YBCO film placed 1.3 cm from the center of the substrate holder. | 69 |
| 3.4.9 SEM micrographs for LaAlO ₃ films deposited onto sapphire at 9 and 6 mTorr with argon to oxygen ratios of 2.0:1.0 and 3.0:1.0 respectively. . . | 74 |
| 3.4.10 SEM micrographs for LaAlO ₃ films deposited onto sapphire at 9 and 12 mTorr with argon to oxygen ratios of 3.0:1.0. | 75 |
| 3.4.11 SEM micrographs for LaAlO ₃ films deposited onto silicon at 9 and 6 mTorr with argon to oxygen ratio of 2.0:1.0 and 3.0:1.0 respectively. | 76 |

| <u>Figure</u> | <u>Page</u> |
|--|-------------|
| 3.4.12 XRD patterns for LaAlO ₃ films deposited onto sapphire at 5.7 and 10 mTorr and oxygen to argon ratios of 2.2:1.0 and 3.3:1.0 respectively. | 78 |
| 3.4.13 XRD pattern for LaAlO ₃ films deposited onto sapphire at 9.0 and 6.0 mTorr and argon to oxygen ratio of 2.0:1.0 and 3.0:1.0 respectively. | 79 |
| 3.4.14 XRD patterns for LaAlO ₃ films deposited onto sapphire at 9.1 and 12 mTorr and argon to oxygen ratios of 3.0:1.0. | 80 |
| 3.4.15 SEM micrographs showing amorphous LaAlO ₃ films before post-annealing treatments. | 83 |
| 3.4.16 XRD patterns of amorphous LaAlO ₃ films before post-annealing treatments. | 85 |
| 3.4.17 SEM micrographs showing randomly oriented LaAlO ₃ films after post-annealing treatments . . | 86 |
| 3.4.18 XRD patterns for randomly oriented LaAlO ₃ films after post-annealing treatments. | 89 |
| 3.4.19 Rocking curve analyses for post-annealed LaAlO ₃ films. | 91 |
| 3.4.20 XRD patterns for amorphous LaAlO ₃ films for minimum crystallization temperature study. | 94 |
| 3.4.21 XRD patterns for randomly oriented, post-annealed LaAlO ₃ films in minimum crystallization temperature study. | 97 |
| 3.4.22 Micrographs of post-annealed films for minimum crystallization temperature study. | 99 |
| 3.4.23 XRD pattern for LaAlO ₃ film deposited onto a thick copper buffer layer. | 104 |
| 3.4.24 SEM micrographs of a thick copper buffer layer and LaAlO ₃ overlayer. | 105 |

| <u>Figure</u> | <u>Page</u> |
|---|-------------|
| 3.4.25 XRD pattern for LaAlO ₃ film deposited onto thin copper buffer layer on sapphire. | 109 |
| 3.4.26 SEM micrograph of LaAlO ₃ film deposited onto thin copper buffer layer on silicon. | 109 |
| 3.4.27 SEM micrograph of LaAlO ₃ film deposited onto thin copper buffer layer on sapphire. | 110 |
| 3.4.28 XRD patterns for LaAlO ₃ films deposited onto Ag/sapphire and Ag/silicon. | 111 |
| 3.4.29 SEM micrographs for LaAlO ₃ films deposited onto Ag/sapphire and Ag/silicon. | 112 |
| 3.4.30 SEM micrographs of post-annealed LaAlO ₃ films on Ag/sapphire and Ag/silicon. | 117 |
| 3.4.31 XRD pattern for post-annealed LaAlO ₃ film deposited onto Ag/sapphire | 118 |
| 3.4.32 SEM micrograph of post-in-situ annealed LaAlO ₃ film on MgO. | 123 |
| 3.4.33 SEM micrographs of post-in-situ annealed LaAlO ₃ films on sapphire. | 124 |
| 3.4.34 SEM micrographs of post-in-situ annealed LaAlO ₃ films on MgO. | 125 |
| 3.4.35 SEM micrographs of post-in-situ annealed LaAlO ₃ films on YSZ. | 126 |
| 3.4.36 XRD pattern and rocking curve analysis for crystalline EBCO before LaAlO ₃ film deposition. | 130 |
| 3.4.37 Plot of q against 001 | 131 |
| 3.4.38 Resistance versus temperature curve for EBCO film before LaAlO ₃ film deposition. | 133 |
| 3.4.39 SEM micrograph of EBCO film before LaAlO ₃ film deposition. | 134 |
| 3.4.40 Graph of EDS data for EBCO film. | 134 |
| 3.4.41 XRD pattern and rocking curves analysis for EBCO and LaAlO ₃ films. | 137 |

T-3956

| <u>Figure</u> | | <u>Page</u> |
|---------------|---|-------------|
| 3.4.42 | SEM micrographs of LaAlO_3 deposited onto sapphire and MgO. | 138 |
| 3.4.43 | SEM micrograph of LaAlO_3 film deposited onto crystalline EBCO film. | 139 |

LIST OF TABLES

| <u>Table</u> | | <u>Page</u> |
|--------------|--|-------------|
| 1.2.1 | Lattice Mismatch of Buffer and Substrate Materials With the Basal Plane of YBCO | 5 |
| 1.2.2 | Dielectric Constants for Substrates | 8 |
| 1.2.3 | Loss Tangents for Substrates | 8 |
| 1.2.4 | Thermal Expansion Coefficients of Various Substrate and Buffer Materials | 13 |
| 2.2.1 | Solubility Product Constants in Water | 22 |
| 2.2.2 | Solubility of Lanthanum Ions | 22 |
| 2.2.3 | Solubility of Aluminum Ions | 22 |
| 2.2.4 | Decomposition Temperatures of Lanthanum and Aluminum Nitrates and Hydroxides. | 24 |
| 2.3.5 | X-Ray Diffraction Scanning Parameters Theta/Two Theta Scan. | 27 |
| 2.3.6 | d-Spacings for Lanthanum Aluminate Powder | 27 |
| 2.3.7 | Calculated d-Spacings for Powder Product Made from Lanthanum Hydroxide and Aluminum Chloride Starting Materials, Filtered, and Calcined at 950 °C in Oxygen (Pellet) | 28 |
| 2.3.8 | Calculated d-Spacings for Powder Product Made from Lanthanum Hydroxide and Aluminum Chloride Starting Materials, Filtered, and Calcined at 950 °C in Air (Powder). | 28 |
| 2.3.9 | Calcined d-Spacings for Powder Product Made from Lanthanum Hydroxide and Aluminum Chloride Starting Materials, Evaporated, and Calcined at 500 °C in Air (Pellet). | 29 |
| 2.3.10 | Calculated d-Spacing for Powder Product Made from Lanthanum and Aluminum Nitrate Starting Materials, Filtered, and Calcined at 950 °C in Oxygen (Pellet). | 30 |

| <u>Table</u> | <u>Page</u> |
|--|-------------|
| 2.3.11 Calculated d-Spacings for Powder Product Made from Lanthanum and Aluminum Nitrate Starting Materials, Without Hydrolysis, and Calcined at 950 °C in Oxygen (Powder) . . . | 31 |
| 2.3.12 Lattice Constants for Lanthanum Aluminate (Pseudo-Cubic Structure). | 33 |
| 2.3.13 Lattice Constants for Lanthanum Aluminate Powder Products | 33 |
| 2.3.14 Powder Product Structural Determination | 34 |
| 3.2.1 Calibration of Substrate Heater | 49 |
| 3.3.1 d-Spacing and Lattice Constants for Lanthanum Aluminate Powder. | 54 |
| 3.4.1 Deposition Parameters onto EBCO Film. | 56 |
| 3.4.2 EDS Compositional Analyses Results For LaAlO ₃ Deposited onto EBCO Film | 56 |
| 3.4.3 d-Spacings For LaAlO ₃ Deposited onto EBCO Film | 59 |
| 3.4.4 Deposition Parameters onto YBCO Film. | 60 |
| 3.4.5 EDS Compositional Analyses Results For LaAlO ₃ Deposited onto YBCO Film | 61 |
| 3.4.6 d-Spacings For LaAlO ₃ Deposited onto YBCO Film. | 62 |
| 3.4.7 Radial Placement of YBCO Film Samples | 64 |
| 3.4.8 Deposition Parameters for Radial Composition Study | 64 |
| 3.4.9 Composition of As-Deposited Films For Radial Study. | 66 |
| 3.4.10 XRD d-Spacings for Sample Placed 1 cm From Center of Substrate Holder (S062189 A LaAlO ₃) | 69 |
| 3.4.11 XRD d-Spacings for Sample Placed 1.3 cm From Center of Substrate Holder (S062189 SrTiO ₃). | 70 |

| <u>Table</u> | <u>Page</u> |
|--|-------------|
| 3.4.12 Deposition Parameters for Gas Pressure Study. . | 71 |
| 3.4.13 EDS Compositional Results for Lanthanum Aluminate Films Deposited onto Sapphire and Silicon at Different Sputtering Pressures | 72 |
| 3.4.14 XRD Analysis Results for Dielectric Films Deposited onto Sapphire with Different Sputtering Gas Pressures. | 81 |
| 3.4.15 Deposition Parameters For Post-Annealing Study of Lanthanum Aluminate Films on Sapphire and Silicon Substrates | 82 |
| 3.4.16 Compositional Analysis of As-Deposited Films onto Sapphire and Silicon Substrates. . . | 85 |
| 3.4.17 Post-Annealing Conditions for Lanthanum Aluminate Deposited onto Sapphire and Silicon Substrates. | 87 |
| 3.4.18 Compositional Analysis of Post-Annealed Lanthanum Aluminate Films Deposited onto Sapphire and Silicon. | 87 |
| 3.4.19 Calculated d-Spacings for Post-Annealed Lanthanum Aluminate Films | 92 |
| 3.4.20 Deposition Parameters for Minimum Crystallization Temperature for Post-Annealed Lanthanum Aluminate Films | 93 |
| 3.4.21 Heating Conditions for Minimum Crystallization Temperature Study | 96 |
| 3.4.22 Summary of XRD Analysis For Post-Annealed LaAlO ₃ Films on Sapphire and Silicon Substrates. | 96 |
| 3.4.23 Compositional Results for Minimum Crystallization Temperature Study | 98 |
| 3.4.24 Comparison of Metallic Lattice Constants With Lanthanum Aluminate, Sapphire, and Silicon | 101 |

| <u>Table</u> | <u>Page</u> |
|--|-------------|
| 3.4.25 Deposition Parameters for RF-Sputtering Copper buffer Layer onto Sapphire and Silicon Substrates. | 101 |
| 3.4.26 Deposition Parameters for Depositing Lanthanum Aluminate onto Copper Buffer Layers. | 103 |
| 3.4.27 XRD Analysis Summary For LaAlO ₃ Deposited onto a Thick Copper Buffer Layer on Silicon . . | 103 |
| 3.4.28 Compositional Results of LaAlO ₃ \Cu Films on Silicon Substrate. | 106 |
| 3.4.29 Deposition Parameters of LaAlO ₃ onto Sapphire and Silicon with a Copper Buffer Layer | 106 |
| 3.4.30 Composition of Film Deposited onto Cu/Sapphire | 108 |
| 3.4.31 Composition of Film Deposited onto Cu/Silicon | 108 |
| 3.4.32 Deposition Parameters of Lanthanum Aluminate onto Silver Buffer Layer on Sapphire and Silicon Substrates | 114 |
| 3.4.33 Compositional Analysis of Lanthanum Aluminate Deposited onto Ag\Sapphire and Ag\Silicon. | 114 |
| 3.4.34 Post-Annealing Conditions of Lanthanum Aluminate Films Deposited onto Silver Buffer Layers. | 115 |
| 3.4.35 Compositional Results of Post-Annealed Lanthanum Aluminate Deposited onto Silver Buffer Layers | 115 |
| 3.4.36 d-Spacings for Post-Annealed Lanthanum Aluminate Film on Ag\Sapphire | 116 |
| 3.4.37 Deposition and Post-In-Situ Annealing Parameters For Lanthanum Aluminate Films Deposited onto Sapphire, MgO, And YSZ Substrates. | 120 |

| <u>Table</u> | <u>Page</u> |
|--|-------------|
| 3.4.38 EDS Compositional Results for Post-In-Situ Annealing Study of Lanthanum Aluminate Films Deposited onto Sapphire, MgO, and YSZ Substrates. | 121 |
| 3.4.39 Deposition Parameters of Lanthanum Aluminate onto Crystalline EBCO Film, Sapphire and MgO Substrates. | 129 |
| 3.4.40 Compositional Analysis of EBCO Film on SrTiO ₃ Before Lanthanum Aluminate Film Deposition. | 133 |
| 3.4.41 Calculated d-Spacings for XRD Pattern of LaAlO ₃ Deposited onto Crystalline EBCO Superconducting Film. | 136 |
| 3.4.42 Compositional Analysis for Lanthanum Aluminate Deposited onto EBCO Film on SrTiO ₃ . | 140 |
| 3.4.43 Compositional Analysis for Lanthanum Aluminate Deposited onto Sapphire and MgO Substrates. | 140 |

ACKNOWLEDGEMENTS

I would like to take this opportunity express my gratitude to my advisors Dr. J Trefny and Dr. B. Yarar for their encouragement and support they offered while I was working on this research study. I would also like to thank Dr. N. Wada for serving on my graduate thesis committee as the committee chairman.

A special thanks to Dr. C Platt and Dr. A. Lee of TRW Space and Technology Group. The technical and practical advice they provided assisted me with this research study. I would like to thank J. Ahn for the many hours he worked on the SEM/EDS analyses of the thin films. I also appreciate the support from my fellow graduate students L. Greco, P. Michael, P. Ahrenkiel, and S. Fellows.

I am grateful for the financial sponsorship awarded to me by TRW Space and Technology Group. This study was performed under subcontract number HTS.MA. DARPA/ONR 15606.01, Rev C of TRW Space and Technology Group.

Chapter 1

1.0 INTRODUCTION

1.1 BACKGROUND AND MOTIVATION

Low-temperature superconducting circuits have demonstrated excellent performance properties in various high-frequency applications such as passive microwave devices, high-speed counters, and ultra-high-speed microprocessors (1). These devices are typically constructed from Josephson Junctions, which consist of two superconducting layers separated by a thin insulating layer (approximately 10 Å thick) (2). The construction of Josephson Junctions is contingent upon the ability to deposit high quality superconducting and dielectric thin films (1). One of the factors limiting industrial applications of the low temperature superconducting devices is the cost of cooling the devices to their operating temperatures. Liquid helium (4.2 K) is the expensive coolant required for operating these devices (2). When high temperature superconductors were discovered, many researchers were optimistic that economical superconducting devices could be developed for industrial applications. The high temperature superconductors have critical temperature

transitions above the boiling point of liquid nitrogen (77 K), thereby allowing the superconducting devices to operate at higher temperatures than at 4.2 K provided by liquid helium. Liquid nitrogen is an economical coolant, since it is a byproduct in the process of making liquid oxygen (3).

As observed in the development of the low temperature superconducting devices, high temperature superconducting devices will be contingent upon the development of processing techniques of high quality superconducting and dielectric thin films (1). These deposition techniques need to be reliable as well as reproducible. Ideally, one would like to deposit superconducting thin films onto substrate materials which are commonly used in high frequency applications such as sapphire and silicon. However, these substrates tend to react with the superconducting films and degrade their superconducting properties (4,5). Many researchers have focused on investigating possible buffer layer materials which would limit the chemical and interdiffusion interactions between the substrate and the superconducting film. The first requirement for buffer materials is that they are chemically inert at elevated processing temperatures, thereby preventing possible interdiffusion between the substrate and film. The buffer material should also display favorable dielectric properties

for high frequency applications such as low dielectric constant and loss tangent. Additionally, the buffer material should also have similar lattice parameters and thermal expansion coefficients to the superconductor and substrate from the highest processing temperature to below the temperature at which the device is intended to be used.

1.2 COMPARISON OF COMMON HIGH T_c SUPERCONDUCTING SUBSTRATE AND BUFFER LAYER MATERIALS

1.2.1 LATTICE PARAMETERS

The strain between high T_c superconducting thin films and buffer layer\substrate materials can be minimized by matching the lattice parameters of these materials with those of the superconductors. Typically in thin film superconductor applications using $\text{ReBa}_2\text{Cu}_3\text{O}_{7-x}$ compounds (where Re is usually yttrium or erbium), or more commonly referred to as 1-2-3 superconductors, the preferred superconducting film orientation is with the c-axis perpendicular to the substrate plane (6,7). (In this report all data and analyses will adhere to the more common convention where the c-axis is defined as 11.69 Å in contrast to the convention used in the Powder Diffraction

Index to label the lattice constants of the 1-2-3 superconductors (8).) This orientation is preferred since it maximizes the current flow along the c-axis (7). Therefore the buffer layer and substrate lattice parameters should be matched with the a (3.8856 Å) and b (3.8185 Å) lattice constants for yttrium barium copper oxide (YBCO) (8). Table 1.2.1 lists the percent difference of lattice parameters between YBCO and some buffer layer and substrate materials. As seen in this Table, lanthanum aluminate closely matches the basal plane of YBCO with a maximum lattice mismatch of 2.769 percent. More importantly the lattice parameters are between those of the YBCO basal plane and sapphire [1T02], 3.479 Å (9). The sapphire [1T02] substrate is often referred to as the r-plane and is commonly used in high frequency applications (5,10).

1.2.2 ELECTRICAL PROPERTIES

Current microwave applications typically operate in the frequency range of 1 to 30 GHz, leaving a portion of the microwave band unused (i.e., the frequency range from 30 GHz to THz). Microwave applications include radar, passive microwave devices, telecommunications, high speed counters, and ultra-high-speed processors (1). Higher frequency

TABLE 1.2.1
Lattice Mismatch of Buffer and Substrate Materials
With the Basal Plane of YBCO

| Compound | a axis | | b axis | | Ref. |
|----------------------|--------|-----|------------------------------|--------|------|
| | (Å) | (Å) | Percent Difference a axis | b axis | |
| LaAlO ₃ | 3.778 | - | 2.769 | 1.061 | (11) |
| LaGaO ₃ | 3.875 | - | 0.2783 | 1.480 | (11) |
| SrTiO ₃ | 3.905 | - | 0.4993 | 2.265 | (12) |
| MgO | 4.213 | - | 8.426 | 10.33 | (13) |
| YSZ | 5.139 | - | 32.26 | 34.58 | (14) |
| SrLaAlO ₄ | 3.755 | - | 3.361 | 1.663 | (15) |
| KTaO ₃ | 3.989 | - | 2.592 | 4.274 | (16) |
| CaNdAlO ₄ | 3.688 | - | 5.085 | 3.418 | (17) |
| BaTiO ₃ | 4.035 | - | 3.845 | 5.670 | (16) |
| NdGaO ₃ | 3.851 | - | 0.891 | 0.851 | (16) |
| Ag | 4.086 | - | 5.158 | 6.884 | (16) |
| Si | 5.4301 | - | 39.75 | 42.21 | (16) |
| Cu | 3.6153 | - | 6.956 | 5.321 | (16) |
| Nb | 3.307 | - | 14.89 | 13.14 | (16) |

applications are not technically possible with current semiconductor technology, in part due to the limited sensitivity of these devices. Researchers are optimistic that with high T_c superconducting devices such as the superconducting tunnel junctions, high-frequency microwave applications may be possible (18). These types of superconducting devices require that the non-superconducting packaging materials have specific electrical properties. Ideally the electric properties of the buffer layer should not interfere with or alter the electrical properties of the superconductor. In microwave frequency applications with

high T_c superconductors the buffer layer should have a low dielectric constant and loss tangent.

A material with a lower dielectric constant has a smaller electric displacement in contrast to a material with a large dielectric constant. This relationship can be derived from the constitutive equation:

$$\mathbf{D} = \epsilon \mathbf{E} \quad (1.1) \quad (19)$$

where \mathbf{D} is the electric displacement, ϵ is the permittivity, and \mathbf{E} is the electric field applied. By definition the permittivity is related to the dielectric constant and the permittivity constant;

$$\epsilon = K_e \epsilon_0 \quad (1.2) \quad (19)$$

where K_e is the dielectric constant of the material and ϵ_0 is the permittivity constant. Substituting equation (1.2) into equation (1.1) shows that the electric displacement is linearly dependent on the dielectric constant of the material

$$\mathbf{D} = K_e \epsilon_0 \mathbf{E} . \quad (1.3)$$

When an electric field is applied to a dielectric material, the material polarizes as described by the following equation:

$$\mathbf{D} = \epsilon_0 \mathbf{E} + \mathbf{P} \quad (1.4) \quad (19)$$

where \mathbf{P} is the polarization vector of the material. When an alternating electric field is applied to a material the

polarization vector also varies. At low frequencies the alternating electric field and the polarization vector are nearly in phase. However, at high frequencies the polarization vector cannot change as rapidly as the electric field due to the inertia of the charged particles. This effect creates a power loss in the material. The loss tangent is a measure of the power loss in a material:

$$\tan \delta_c = \epsilon'' / \epsilon' \quad (1.5)$$

where δ_c is the loss angle, ϵ'' is the imaginary part and ϵ' the real part of the complex permittivity (20).

Tables 1.2.2 and 1.2.3 list the dielectric constants and loss tangents for some substrate materials. Lanthanum aluminate has a low dielectric constant and loss tangent making it an ideal substrate and buffer layer material for most high frequency applications (10). Other common substrates such as strontium titanate, magnesium oxide, and yttrium-stabilized zirconia have dielectric properties which are not as favorable for microwave applications as lanthanum aluminate.

TABLE 1.2.2
Dielectric Constants for Substrates

| Substrate | Dielectric Constant | Reference |
|----------------------------------|---------------------|-----------|
| LaAlO ₃ | 16 | (21) |
| α-Al ₂ O ₃ | 8.6 | (21) |
| MgO | 9.65 | (21) |
| Si | 11.7 | (21) |
| YSZ | 25 | (21) |
| LaGaO ₃ | 27 | (21) |
| KTaO ₃ | 4000 | (21) |
| SrTiO ₃ | 277 | (22) |
| | 215-310 | (10) |
| NdGaO ₃ | 20.2 | (22) |

TABLE 1.2.3
Loss Tangents for Substrates

| Substrate | Loss Tangent (x 10 ⁻⁴) | Measurement Frequency | Reference |
|--------------------------------|---------------------------------------|--------------------------|-----------|
| LaAlO ₃ | 5.8 | 10 GHz | (21) |
| | 70 | 1 MHz | (22) |
| (@ 77 K) | 0.83 | 10 GHz | (10) |
| Al ₂ O ₃ | 10 | - | (10) |
| (@ 77 K) | 0.00015 | 9 GHz | (10) |
| MgO | 91 | 1 MHz | (21) |
| YSZ | 54 | 1 MHz | (22) |
| LaGaO ₃ | 18 | 1 MHz | (21) |
| SrTiO ₃ | 125 | 1 MHz | (22) |
| CaNdAlO ₄ | 10 | 200-600 GHz | (17) |
| SrLaAlO ₄ | < 1 | - | (23) |

1.2.3 CHEMICAL STABILITY

One difficult technical challenge is to make a thin insulating layer between two superconducting layers for device applications. The insulating layer needs to be on the order of a few angstroms thick for high T_c applications. To successfully deposit an insulating layer with this thickness there should not be any significant chemical interaction between the superconductor and insulating films. Thus, the chemical stability of the buffer layer becomes a critical component in developing processing techniques for making high T_c superconducting devices.

Recent studies have concentrated on characterizing the chemical interactions between high T_c superconductors and substrate\buffer layer materials. Common high frequency substrate materials such as sapphire and silicon easily react with superconducting films when processing temperatures are higher than 700 to 900°C (4,5). A study performed by C. Cheung and E. Ruckenstein (4) showed that silicon, alumina, and zirconia were highly reactive with YBCO while magnesium oxide, and silver were not. Strontium titanate reacted slightly with YBCO. The authors mixed superconducting powder with substrate powder and then heat-treated the mixtures from 600 to 945°C. X-ray diffraction

(XRD) patterns for silicon and YBCO mixtures heat-treated above 945°C indicated that a significant amount of superconducting material reacted with silicon. The impurity phases identified were CuO, Ba₂SiO₄, and Y₂BaCuO_x. The XRD patterns for the alumina and YBCO mixture showed slight chemical interaction at 800°C where the impurity phase was BaAl₂O₄. At heat treatments of 945°C CuO and Y₂BaCuO_x phases were also observed in the alumina-YBCO XRD patterns. Again, significant amounts of impurity phases, BaZrO₃, CuO, and Y₂BaCuO_x were observed for zirconia samples treated at 945°C. Strontium titanate was less reactive with YBCO than silicon, alumina, and zirconia even though a small amount of unknown impurity phase was observed upon treatment at 945°C (4).

In contrast, recent studies by R. Simon et al. showed that lanthanum aluminate substrates did not react with EBCO superconducting films during processing at temperatures of 830°C (21,24). This was later confirmed by a mixed powder study performed by A. Bono (25). This study concluded that there was no observable interaction between the lanthanum aluminate and YBCO powder following heat treatment at 1000°C. The only phase changes in the XRD patterns were ascribed to the orthorhombic to tetragonal transition of the YBCO (25). The chemical stability of lanthanum aluminate makes it an ideal candidate for buffer material in high T_c

superconducting applications.

1.2.4 THERMAL PROPERTIES

The buffer layer material for superconducting films should have suitable thermal properties such as a similar coefficient of thermal expansion (CTE) to the 1-2-3 superconductors and exhibit no structural or phase changes from high processing temperatures to low superconducting application temperatures. The coefficient of thermal expansion of the buffer material should closely match with the superconductor to reduce film cracking that can occur. The basal plane of YBCO has an average CTE of $12.9 \times 10^{-6} \text{ K}^{-1}$ (26). Table 1.2.4 compares the coefficients of thermal expansion of different substrate and buffer materials. Sapphire and silicon CTE's are significantly different from that of YBCO. This difference in thermal expansion of the substrate and superconducting film causes the film to crack as reported by several research groups (26,27). The CTE for lanthanum aluminate is comparable to the basal plane of YBCO and therefore should be suitable for buffer layer applications (22,27). Another advantage is that the CTE of lanthanum aluminate is in between that of YBCO and sapphire.

Potential buffer layers should be thermodynamically stable over a large temperature range. Lanthanum aluminate has a rhombohedral structure at room temperature with the following lattice constants: $a = 5.357 \text{ \AA}$ and $\alpha = 60^\circ 6'$ (32). The rhombohedral structure deviates slightly from a cubic structure and is often approximated by using a pseudo-cubic structure with the lattice constants $a = 3.790 \text{ \AA}$ and $\alpha = 90^\circ 05'$ (16). Lanthanum aluminate has a phase transition from a rhombohedral to a cubic structure at approximately 435°C (10,16,33). This slight phase change should cause little roughening of the surface superconducting film (10). Lanthanum gallate is another good buffer layer candidate except that it has a phase transition at 150°C which degrades the quality of the superconducting films deposited onto it (22).

1.3 SUMMARY OF THE PHYSICAL PROPERTIES OF LANTHANUM ALUMINATE

The rhombohedral structure of lanthanum aluminate deviates slightly from a cubic structure and is often described as pseudo-cubic (16). There is less than a 3 percent difference between the lattice constant with the YBCO basal plane and the pseudo-cubic constant of lanthanum

TABLE 1.2.4

Thermal Expansion Coefficients of Various
Substrate and Buffer Materials

| Material | CTE ($\times 10^{-6} \text{ } ^\circ\text{C}^{-1}$) | Reference |
|--------------------------------|---|-----------|
| LaAlO ₃ | 10 | (28) |
| LaGaO ₃ | 10.3 | (22) |
| Al ₂ O ₃ | 8.8 | (29) |
| MgO | 13.5 | (29) |
| YSZ | 9.2 | (22) |
| SrTiO ₃ | 10.4 | (22) |
| Si | 2.2 | (30) |
| Ag | 19 | (31) |
| Cu | 16.6 | (31) |

aluminate (8,11). The dielectric properties of lanthanum aluminate are superior to strontium titanate and slightly better than magnesium oxide (MgO) and yttrium-stabilized zirconia (YSZ) (Tables 1.2.2 and 1.2.3). Even though the dielectric constant and loss tangent for lanthanum aluminate are not as low as sapphire, they are still in the acceptable range for most microwave applications (10). Lanthanum aluminate has been proven to be chemically stable up to processing temperatures of 1000°C (25). Lanthanum gallate is another suitable substrate and buffer layer candidate for high T_c superconductors. The major disadvantage of lanthanum gallate is that it has a phase transition from cubic to tetragonal at 150°C which causes defects in the

YBCO films. Lanthanum aluminate also has a phase transition that occurs within the processing temperatures, but since the transition is from pseudo-cubic to cubic the disruption to the YBCO film because of the transition is minimal (10). For the above reasons we chose to investigate the deposition processes of lanthanum aluminate films onto sapphire substrates.

Unlike lanthanum aluminate single crystals, lanthanum aluminate in the form of powder and sputtering targets was not commercially available at the start of this project. Therefore, a study was initiated to prepare and characterize lanthanum aluminate powder. The purpose of this study was to develop a reliable processing method to prepare high quality lanthanum aluminate powder. The powder was then used to make rf-sputtering targets for the lanthanum aluminate deposition studies. The deposition studies consisted of investigating the effects of different deposition parameters such as substrate positioning, sputtering gas pressures, post-annealing, use of metallic buffer layers, in-situ-post annealing, and substrate lattice matching.

Chapter 2

2.0 LANTHANUM ALUMINATE POWDER PREPARATION AND CHARACTERIZATION

2.1 LITERATURE REVIEW FOR LANTHANUM ALUMINATE POWDER PREPARATION AND CHARACTERIZATION

Lanthanum aluminate powder has been prepared using a variety of processing techniques such as mixing oxide powders followed by heat treatment (34,35), chemical solution precursors followed by coprecipitation (36-40), sol-gel processing (41), and molten reaction (42). The most widely used powder preparation techniques are mixing oxide powders and chemical solution precursors. Mixing stoichiometric one-to-one ratios of lanthanum and aluminum oxide powders followed by calcination is the simplest method for preparing lanthanum aluminate powders. This process requires higher temperature treatments and typically requires regrinding and heat-treatment of the powder to ensure homogeneity of the product (43). Use of the chemical precursor technique allows for precise control of the stoichiometry and purity of the powder product. Another advantage of using precursors is that fine homogeneous powder products can be made using lower processing

temperatures (43).

Roth (34) made lanthanum aluminate by combining a correct molar ratio of high purity powders of lanthanum and aluminum oxide and then pressing the powder into small pellets and calcining them at 1100°C for 4 hours. The product was ground, mixed, and pressed into pellets again. The pellets were then calcined at 1550°C for five hours. X-ray diffraction analysis showed the structure of the powder product to be rhombohedral and of a perovskite-type with pseudo-cubic lattice parameters of $a = 3.788 \text{ \AA}$ and $\alpha = 90^\circ 41'$ (34). These pseudo-cubic lattice parameters values matched closely with other published data for lanthanum aluminate indicating that the powder product was lanthanum aluminate. In another study performed by Keith and Roy, lanthanum aluminate powder was made by mixing oxide powders. One heat-treatment consisted of heating the powders to 1640°C for 90 minutes and another heat-treatment calcined the powder at 700°C for three days with 5000 psi of stream pressure. XRD analysis showed that both heat treatments produced powders which were pseudo-cubic and had a perovskite-type structure. The lattice constant for the pseudo cubic cell was determined to be $3.778 \pm 0.001 \text{ \AA}$.

Vidyasagar, Golpalakrishnan, and Rao (37) prepared lanthanum aluminate using hydroxide precursor solutions. To make the hydroxide precursor they combined one-to-one molar

ratios of lanthanum hydroxide and aluminum hydroxide with a nitrate solution. They then added ammonium hydroxide to facilitate precipitation of the hydroxides. The precipitate was collected by filtering; then it was washed and dried. They report the decomposition temperature of $\text{La}_{0.5}\text{Al}_{0.5}(\text{OH})_3$ to be 645 K and the formation temperature of LaAlO_3 to be about 1170 K (37). Aslanysan, Nadzharyan, and Nikogosyan (38) also prepared aqueous solutions of rare earth metals and aluminum ions to make monoaluminates. The precipitating agents used were ammonia, (NH_3) and $(\text{NH}_4)_2\text{CO}_3$. The precipitates were collected and dried at 100-160°C. They report that after heat treatment at 200-600°C the powder is amorphous and that the crystallization temperature for monoaluminates is between 805 to 930°C (38). Chemical precursor solutions provide flexibility in the selection of lanthanum and aluminum salts as well as the precipitating agent used in hydrolysis reactions. Processing temperatures are significantly reduced when the precursor technique is implemented.

2.2 PROCEDURE TO MAKE LANTHANUM ALUMINATE POWDER

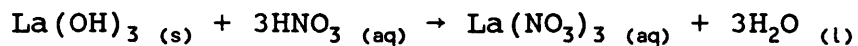
The motivation for making lanthanum aluminate was to generate a supply of high quality powder which would be used

to make rf-sputtering targets. The lanthanum aluminate powder was to be hot pressed into 38 mm (approximate diameter) pellets for rf-sputtering targets. A chemical precursor technique was chosen to prepare the lanthanum aluminate powder, since the homogeneity and stoichiometry of the powder product could be precisely controlled. Aqueous ionic precursor solutions were made by dissolving lanthanum and aluminum salts. The ionic solutions were then combined into one-to-one molar ratios of lanthanum to aluminum ions. Three different processing procedures were compared. In the first and second procedures, hydrolysis reactions were used to coprecipitate lanthanum and aluminum hydroxides. The first process filtered and washed the precipitates. The second evaporated the solvent from the precipitate after completion of the hydrolysis reaction. The third process evaporated the solvent from the precursor solution without hydrolysis. The materials from all three processes were either dried overnight in a drying oven at 100 to 150°C or on a hot plate (500°C). The powders were then ground with a pestle and mortar and calcined at either 500 or 950°C.

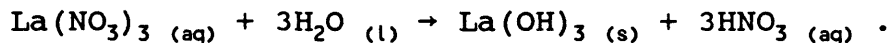
The effects of different lanthanum and aluminum salts used to make the solution precursors were investigated. The salts used to make lanthanum salt solutions were lanthanum hydroxide ($\text{La}(\text{OH})_3$) and lanthanum nitrate ($\text{La}(\text{NO}_3)_3$). The starting material for aluminum salt solution was aluminum

chloride (AlCl_3) and aluminum nitrate ($\text{Al}(\text{NO}_3)_3$). Finally, the effects of heat-treatment parameters were compared. Small amounts of lanthanum aluminum hydroxide were calcined both in pellet and powder form in either oxygen or air environments.

In all of the three processes the lanthanum and aluminum salt solutions were prepared similarly. Lanthanum hydroxide precursor was made by dissolving lanthanum hydroxide with nitric acid in an aqueous solution. The chemical reactions are as follows:



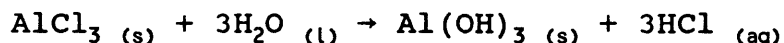
and



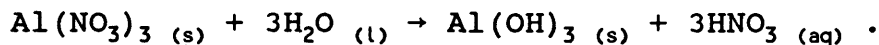
Lanthanum nitrate can be dissolved directly in water and the chemical reaction is:



Aluminum chloride and aluminum nitrate both dissolve in water. The chemical reactions for these salt solutions are:



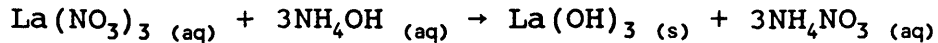
and



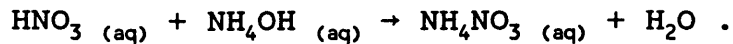
All starting materials were at least 99.99 % pure.

The first and second processes used ammonium hydroxide, NH_4OH , to coprecipitate lanthanum and aluminum hydroxide.

The hydrolysis reactions are as follows:



and



The solubility product constants listed in Table 2.2.1 were used to calculate the solubilities of lanthanum and aluminum hydroxides in an aqueous solution at the different pH levels listed in Tables 2.2.2 and 2.2.3. For example the equation used to calculate the solubility of lanthanum hydroxide is

$$K_{sp} = [\text{La}^{3+}] [\text{OH}^-]^3 \quad (2.1)$$

where K_{sp} is the solubility product constant, $[\text{La}^{3+}]$ is the molar concentration of lanthanum ions, $[\text{OH}^-]$ the molar concentration of OH^- , and $[\text{La}(\text{OH})_3]$ the molar concentration of lanthanum hydroxide (44). Figure 2.2.1 shows a plot of the solubilities of lanthanum and aluminum hydroxides at different pH values. The solubility curve defines the conditions, i.e., concentration and pH, where both ions and hydroxide precipitates exist in equilibrium. The region to the right of the solubility curve is the region where the concentration of the hydroxide precipitates in the solution is greater than the ion concentration and vice versa in the region to the left. The ion concentration used to make the precursor solutions was 1×10^{-2} molar. The pH level required for hydrolysis is approximately 8.2 (see Figure 2.2.1). Therefore the pH level selected to coprecipitate lanthanum and aluminum hydroxides was 8.50 and was obtained by adding

ammonium hydroxide which had a pH of 13.20.

The salt solution of lanthanum and aluminum ions usually had a low pH value between 1.0 and 2.0. Aluminum hydroxide at 1×10^{-2} molar concentration begins to precipitate at a pH value of approximately 3.3 (see Figure 2.2.1), while lanthanum hydroxide precipitates at approximately 8.2. The solution was magnetically stirred to break up the aluminum hydroxide and occluded impurities in the precipitates while ammonium hydroxide was slowly added to the solution and for thirty minutes after a minimum pH level of 8.5 was reached.

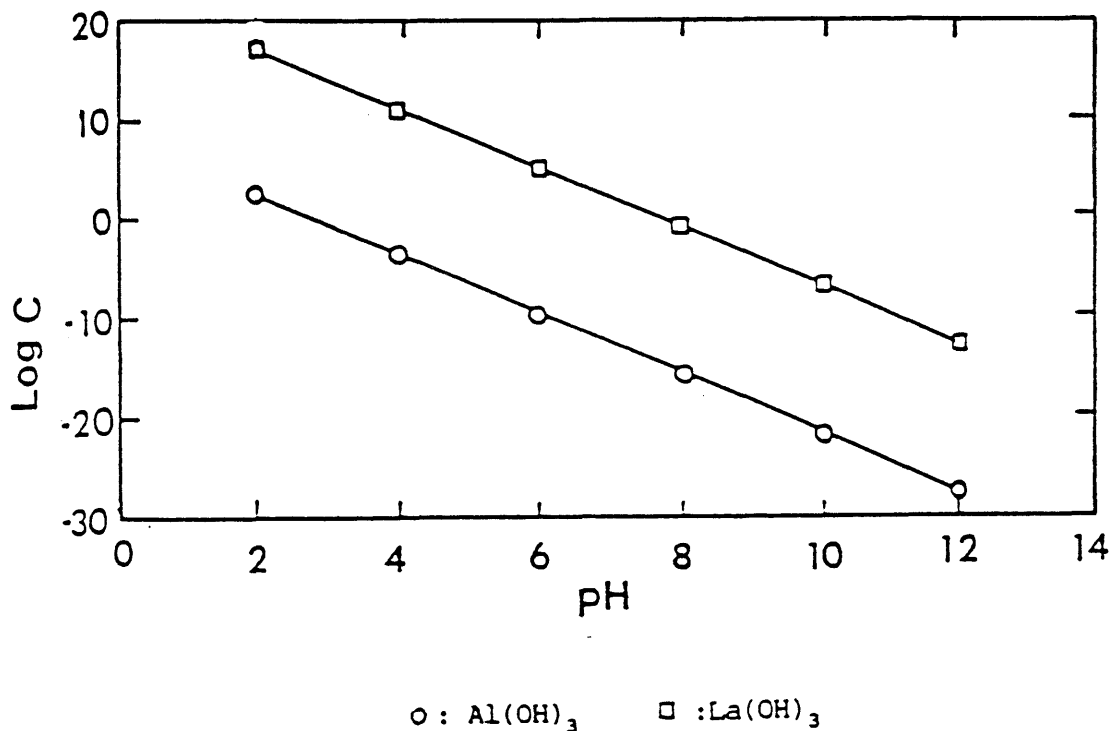


Figure 2.2.1: Solubilities of lanthanum and aluminum at different pH values.

TABLE 2.2.1

Solubility Product Constants in Water

| | | |
|----------------------------|-----------------------|------|
| $[\text{Al}(\text{OH})_3]$ | 1.9×10^{-33} | (45) |
| $[\text{La}(\text{OH})_3]$ | 10^{-20} | (45) |

TABLE 2.2.2

Solubility of Lanthanum Hydroxide

| pH | $[\text{H}^+]$ (molar) | $[\text{OH}^-]^3$ (molar) | $[\text{La}^{3+}]$ (molar) |
|----|---------------------------|------------------------------|-------------------------------|
| 2 | 1.0×10^{-1} | 1.0×10^{-35} | 1.0×10^{16} |
| 4 | 1.0×10^{-3} | 1.0×10^{-29} | 1.0×10^{10} |
| 6 | 1.0×10^{-5} | 1.0×10^{-23} | 1.0×10^4 |
| 8 | 1.0×10^{-7} | 1.0×10^{-17} | 1.0×10^{-2} |
| 10 | 1.0×10^{-9} | 1.0×10^{-11} | 1.0×10^{-8} |
| 12 | 1.0×10^{-11} | 1.0×10^{-5} | 1.0×10^{-14} |

TABLE 2.2.3

Solubility of Aluminum Hydroxide

| pH | $[\text{H}^+]$ (molar) | $[\text{OH}^-]^3$ (molar) | $[\text{Al}^{3+}]$ (molar) |
|----|---------------------------|------------------------------|-------------------------------|
| 2 | 1.0×10^{-1} | 1.0×10^{-35} | 2.0×10^2 |
| 4 | 1.0×10^{-3} | 1.0×10^{-29} | 2.0×10^{-4} |
| 6 | 1.0×10^{-5} | 1.0×10^{-23} | 2.0×10^{-10} |
| 8 | 1.0×10^{-7} | 1.0×10^{-17} | 2.0×10^{-16} |
| 10 | 1.0×10^{-9} | 1.0×10^{-11} | 2.0×10^{-22} |
| 12 | 1.0×10^{-11} | 1.0×10^{-5} | 2.0×10^{-28} |

The first process allowed the precursor solution to sit overnight so that the particles could grow. This step prevented unnecessary loss of material in the filtering step. The filter cake, $\text{La}(\text{OH})_3\text{Al}(\text{OH})_3$ gel, was dried in an air bath until it had a dry powder consistency, $\text{LaAl}(\text{OH})_6$. The filter cake was further dried overnight at 100-150°C. After drying, the material was ground into a fine powder and was ready for calcination. The calcination parameters are described later sections.

The second process evaporated the solvent from the precursor solution until it was dry. During evaporation the solution was magnetically stirred so the remaining solution would be a homogenous mixture of lanthanum and aluminum hydroxide. The dried material, $\text{LaAl}(\text{OH})_6$ was collected and ground to a fine consistency.

After the powder had been dried overnight, the samples were prepared for different calcination treatments. Due to the limited amount of $\text{LaAl}(\text{OH})_6$ powder prepared using the first and second processing techniques, only a subset of calcination parameters was investigated. Approximately 250 mg of powder prepared using the first and second processes was measured and pressed into pellets 13 mm in diameter using 9000 pounds of pressure in a static hydraulic press. The pellets were placed in a flat alumina crucible and calcined at 500°C in air or at 950°C in oxygen for five

and one half hours. Approximately 100 mg of the same powder samples were weighed and placed onto aluminum slats for calcination. The powder samples were fired in air at either 500 or 950°C for five and one half hours. These calcination temperatures were selected to compare the products calcined below and above most of the decomposition temperatures for occluded powder impurities and lanthanum aluminum hydroxide (see Table 2.2.4).

TABLE 2.2.4

Decomposition Temperatures of Lanthanum
and Aluminum Nitrates and Hydroxides

| Compound | Melting Temp. (°C) | Boiling Temp. (°C) | Decomposition Temp. (°C) | Reference |
|---|--------------------------|--------------------------|--------------------------------|-----------|
| AlCl_3 | 190 | 187.2 | - | (31) |
| Al(OH)_3 | 300 | - | - | (31) |
| $\text{Al(NO}_3)_3$ | 73.5 | - | 150 | (31) |
| LaCl_3 | 860 | >1000 | - | (31) |
| La(OH)_3 | - | - | 300-400 | (46) |
| $\text{La(NO}_3)_3$ | 40 | - | 126 | (31) |
| NH_4NO_3 | - | 520 | - | (31) |
| $\text{NH}_4\text{ClAlCl}_3$ | 304 | - | - | (31) |
| $\text{La}_{0.5}\text{Al}_{0.5}(\text{OH})_3$ | - | - | 372 | (37) |

The third process simply combined one-to-one molar ratios of lanthanum and aluminum salt solutions made from $\text{La(NO}_3)_3$ and $\text{Al(NO}_3)_3$ and evaporated the solvent from the solution. The powder material was stirred and heated on a

hot plate until most of the nitrates had decomposed. The powder was then ground and measured into approximately 250 mg samples for calcination. The samples were calcined at 500 and 950°C in powder and pellet form and in oxygen or air environment.

2.3 RESULTS AND ANALYSIS OF LANTHANUM ALUMINATE POWDER

The lanthanum aluminate powder products were characterized with x-ray diffraction (XRD) and energy dispersive spectroscopy (EDS). Using x-ray diffraction the structure and purity of the product was determined. Using energy dispersive spectroscopy the impurity elements present in the products were identified.

A Rigaku Rotaflex x-ray powder diffractometer was used in all of the powder diffraction measurements. The radiation source was Cu k-alpha with a wavelength of 1.540598 Å. Typical scanning parameters are listed in Table 2.5. All samples were ground into a fine powder using an alumina mortar and pestle. The powder was mounted onto a glass slide with double stick tape. This method was chosen since only small quantities of the powder product were available for analysis. The x-ray diffraction patterns were recorded on a strip chart.

The scanning electron microscope (SEM) that was used for impurity identification was a JOEL JXA-840. The apparatus has EDS for qualitative compositional analysis. The software used to collect and process the EDS data was standardless semi-quantitative analysis (SSQ) by Tracor Northern. With the aid of this software, impurity elements were identified. The powder was typically analyzed at a magnification range of 100X to 1000X.

Bragg's law was used to calculate the d-spacings from the XRD patterns:

$$d_{hkl} = \lambda / 2 \sin(\theta) \quad (2.2)$$

where d_{hkl} is the d-spacing in Å, λ is the x-ray wavelength, and θ is half the Bragg diffraction angle (47). The calculated d-spacing of the product x-ray diffraction patterns were compared with d-spacings reported by other researchers (Tables 2.3.6-2.3.11). Some product d-spacings and relative peak heights are listed in Tables 2.3.7-2.3.11. The d-spacings listed in Tables 2.3.7 and 2.3.8 closely match with the strong intensity Bragg peaks previously published data listed in Table 2.3.6. The relative peak heights were compared to the relative intensities listed in Table 2.3.6. The normalized peak heights matched fairly well with the relative peak intensities. The difference observed between them was because the relative peak intensity calculated integrated the area beneath the Bragg

TABLE 2.3.5

X-Ray Diffraction Scanning Parameters
Theta/Two-Theta Scan

| | |
|----------------------------|---------------|
| Filament Voltage | 40 kV |
| Filament Current | 60 mA |
| Scanning Range | 20-90 degrees |
| Scanning Speed | 2 degrees\min |
| Step Width for Two-Theta | 0.1 degrees |
| Count Time per Step | 0.5 seconds |
| Strip Chart Recorder Speed | 20 mm\minute |

TABLE 2.3.6

d-Spacings for Lanthanum Aluminate Powder

| S. Gella and V. Bala (32) | | M. Mizuno et. al. (48) | |
|---------------------------|----------------------|------------------------|---------------------------|
| d-spacing (Å) | Intensity Ranking | d-spacing (Å) | Intensity (Normalized) |
| 3.797 | s | 3.792 | 80 |
| 2.657 | vs | 2.682 | 100 |
| 2.286 | vw-w | 2.287 | 3 |
| 2.188 | s | 2.191 | 45 |
| - | - | 2.185 | 40 |
| 1.896 | s | 1.896 | 60 |
| 1.736 | vvw | 1.740 | 3 |
| 1.696 | m | 1.695 | 20 |
| - | - | 1.6925 | 11 |
| 1.548 | s | 1.548 | 30 |
| - | - | 1.5460 | 30 |
| - | - | 1.5440 | 13 |
| 1.342 | w-m | 1.3145 | 14 |
| 1.339 | m | 1.3390 | 19 |
| 1.264 | m | 1.2640 | 8 |
| - | - | 1.2620 | 6 |
| 1.199 | m | 1.1980 | 16 |
| 1.198 | m-s | - | - |

TABLE 2.3.7

Calculated d-Spacings for Powder Product
 Made from Lanthanum Hydroxide and Aluminum
 Chloride Starting Materials, Filtered, and
 Calcined at 950°C in Oxygen (Pellet)

| Two*Theta (Degrees) | d-Spacing (Å) | Intensity Ranking | Normalized Peak Height |
|------------------------|------------------|----------------------|---------------------------|
| 23.45 | 3.791 | 2 | 49.1 |
| 33.40 | 2.681 | 1 | 100.0 |
| 41.20 | 2.189 | 3 | 42.8 |
| 47.95 | 1.896 | 4 | 32.0 |
| 54.05 | 1.695 | 6 | 16.8 |
| 59.70 | 1.547 | 5 | 30.5 |
| 70.20 | 1.340 | 7 | 14.7 |
| 75.10 | 1.264 | 8 | 7.9 |

TABLE 2.3.8

Calculated d-Spacings for Powder Product
 Made from Lanthanum Hydroxide and Aluminum
 Chloride Starting Materials, Filtered, and
 Calcined at 950°C in Air (Powder)

| Two*Theta (Degrees) | d-Spacing (Å) | Intensity Ranking | Normalized Intensity |
|------------------------|------------------|----------------------|-------------------------|
| 23.60 | 3.767 | 2 | 51.6 |
| 33.55 | 2.669 | 1 | 100.0 |
| 41.40 | 2.180 | 3 | 48.6 |
| 48.10 | 1.890 | 4 | 39.5 |
| 54.20 | 1.691 | 6 | 21.9 |
| 59.80 | 1.545 | 5 | 34.7 |
| 70.3 | 1.338 | 7 | 17.4 |
| 75.2 | 1.262 | 8 | 9.5 |

TABLE 2.3.9

Calculated d-Spacings for Powder Product
Made from Lanthanum Hydroxide and Aluminum
Chloride Starting Materials, Evaporated, and
Calcined at 500°C in Air (Pellet)

| Two*Theta (Degrees) | d-Spacing (Å) | Intensity Ranking | Normalized Peak Height |
|------------------------|------------------|----------------------|---------------------------|
| 25.40 | 3.504 | 2 | 86.2 |
| 26.00 | 3.424 | 9 | 23.0 |
| 28.50 | 3.129 | 7 | 27.6 |
| 30.80 | 2.901 | 3 | 71.3 |
| 34.10 | 2.627 | 1 | 100.0 |
| 39.40 | 2.285 | 11 | 14.3 |
| 40.70 | 2.215 | 4 | 41.7 |
| 44.10 | 2.052 | 5 | 36.8 |
| 45.40 | 1.996 | 11 | 14.3 |
| 46.20 | 1.963 | 12 | 13.4 |
| 50.80 | 1.800 | 8 | 25.4 |
| 51.50 | 1.773 | 8 | 25.4 |
| 56.70 | 1.622 | 6 | 33.3 |
| 58.20 | 1.584 | 10 | 21.0 |
| 60.50 | 1.529 | 13 | 12.0 |

TABLE 2.3.10

Calculated d-Spacings for Powder Product
 Made from Lanthanum and Aluminum Nitrate
 Starting Materials, Filtered, and Calcined
 at 950°C in Oxygen (Pellet)

| Two*Theta (Degrees) | d-Spacing (Å) | Intensity Ranking | Normalized Peak Height |
|------------------------|------------------|----------------------|---------------------------|
| 23.40 | 3.799 | 2 | 46.6 |
| 25.00 | 3.559 | 7 | 22 |
| 26.00 | 3.424 | 10 | 13 |
| 27.50 | 3.241 | 5 | 33 |
| 29.00 | 3.077 | 9 | 19 |
| 29.60 | 3.016 | 8 | 22 |
| 30.80 | 2.901 | 7 | 23 |
| 33.40 | 2.681 | 1 | 100.0 |
| 41.20 | 2.189 | 3 | 39.6 |
| 43.80 | 2.065 | 10 | 13 |
| 45.60 | 1.988 | 11 | 11 |
| 47.90 | 1.898 | 4 | 36 |
| 54.10 | 1.694 | 7 | 23 |
| 55.10 | 1.665 | 12 | 11 |
| 55.40 | 1.657 | 11 | 12 |
| 59.70 | 1.548 | 6 | 30 |
| 70.10 | 1.341 | 8 | 17 |

TABLE 2.3.11

Calculated d-Spacings for Powder Product
Made from Lanthanum and Aluminum Nitrate
Starting Materials, without Hydrolysis,
and Calcined at 950°C in Oxygen (Powder)

| Two*Theta (Degrees) | d-Spacing (Å) | Intensity Ranking | Normalized Peak Height |
|------------------------|------------------|----------------------|---------------------------|
| 23.60 | 3.767 | 2 | 49.0 |
| 26.20 | 3.399 | 10 | 8.8 |
| 27.80 | 3.207 | 14 | 6.1 |
| 29.20 | 3.056 | 9 | 9.9 |
| 30.00 | 2.976 | 6 | 21.0 |
| 33.50 | 2.673 | 1 | 100.0 |
| 39.80 | 2.263 | 13 | 6.8 |
| 41.30 | 2.184 | 3 | 41.0 |
| 46.20 | 1.963 | 11 | 8.9 |
| 48.10 | 1.890 | 4 | 34.3 |
| 52.20 | 1.751 | 12 | 7.1 |
| 54.10 | 1.694 | 7 | 19.0 |
| 55.50 | 1.654 | 13 | 6.3 |
| 56.10 | 1.638 | 15 | 5.1 |
| 59.80 | 1.545 | 5 | 31.0 |
| 70.20 | 1.340 | 8 | 16.0 |

peak. The relative peak height was consistent with the intensity ranking presented by S. Gella and V. Bala (32).

The x-ray product diffraction patterns that agreed with published d-spacing data for lanthanum aluminate powder were used to calculate the lattice constants of these products (Table 2.3.12). By definition the d-spacing, d_{hkl} , is equal to the inverse magnitude of the reciprocal lattice vector, r_{hkl}^* ,

$$d_{hkl} = 1 / | r_{hkl}^* | \quad (2.3)$$

where h, k, l are the Miller indices (47). The structure of lanthanum aluminate can be approximated by assuming a pseudo-cubic structure (32). Therefore the diffraction data were interpreted by assuming a simple cubic structure. The reciprocal lattice vector for a simple cubic lattice is

$$r_{hkl}^* = a / (h^2 + k^2 + l^2)^{0.5} \quad (2.4)$$

where a is the lattice parameter. By substituting this expression into equations 2.3 and 2.4 and then into equation 2.2 an expression may be obtained relating the Bragg peak positions with the lattice parameter

$$a = (\lambda) (h^2 + k^2 + l^2)^{0.5} / (2) (\sin(\theta)). \quad (2.5)$$

Table 2.3.12 lists the published pseudo-cubic lattice parameters for lanthanum aluminate. Table 2.3.13 lists the lattice parameters for some powder products.

Deviation from the simple cubic structure was calculated for the diffraction patterns to determine if the pseudo-cubic approximation is appropriate. The method used to calculate the structure is described by Schwartz and Cohen (47) for indexing powder diffraction patterns for powders with unknown structures. This calculation was done by taking the ratio of the x^{th} reciprocal lattice vector squared, r_x^{*2} , and the smallest reciprocal lattice vector squared, r_1^{*2} . By noting that r_{hkl}^{*2} is equal to $1/d_{hkl}^2$ and substitute this expression into Bragg's law, we obtain

$$(\lambda)^2 = 4(\sin^2(\theta)) / r_{hkl}^{*2}. \quad (2.6)$$

Solving this equation for the reciprocal lattice gives

$$r_{hkl}^{*2} = 4(\sin^2(\theta)) / (\lambda)^2. \quad (2.7)$$

Now, taking the ratio of the reciprocal lattice vectors, we may simplify to get the following expression

$$r_x^{*2} / r_1^{*2} = \sin^2(\theta)_x / \sin^2(\theta)_1. \quad (2.8)$$

The expected values for the reciprocal lattice ratios for a simple cubic structure are listed in Table 2.3.14.

TABLE 2.3.12

Lattice Constants for Lanthanum Aluminate
(Pseudo-Cubic Structure)

| Lattice Constant (Å) | Reference |
|-------------------------|-----------|
| 3.778 | (35) |
| 3.788 | (34) |
| 3.790 | (32) |
| 3.778 | (11) |

TABLE 2.3.13

Lattice Constants for Lanthanum Aluminate
Powder Products (Pseudo-Cubic Structure)

| Lattice Constant (Å) | Data from Table |
|-------------------------|--------------------|
| 3.79 | 7 |
| 3.78 | 8 |

TABLE 2.3.14

Deviation from Pseudo-Cubic Structure

| Simple Cubic Structure | | Powder Product (Data from Table 7) | |
|------------------------|---|------------------------------------|---|
| hkl | $\frac{\sin^2(\theta)_x}{\sin^2(\theta)_1}$ | Bragg Peak Location(Degrees) | $\frac{\sin^2(\theta)_x}{\sin^2(\theta)_1}$ |
| 100 | 1 | 23.5 | 1 |
| 110 | 2 | 33.4 | 1.99 |
| 111 | 3 | 41.2 | 2.98 |
| 200 | 4 | 48.0 | 3.99 |
| 210 | 5 | 54.1 | 4.99 |
| 211 | 6 | 59.8 | 5.99 |
| 220 | 8 | 70.2 | 7.97 |
| 300 | 9 | 75.1 | 8.96 |

2.4 RESULTS AND CONCLUSIONS FOR LANTHANUM ALUMINATE POWDER PREPARATION

The XRD patterns of the powder products fired at 500°C show no lanthanum aluminate Bragg peaks. The shape of the diffraction pattern shows that the structure of the material is amorphous (Figures 2.4.1 and 2.4.2). On the other hand, most of the XRD patterns of powder products fired at 950°C contained lanthanum aluminate Bragg diffraction peaks (Figures 2.4.3 - 2.4.8). This result is consistent with the Vidyasagar, Gopalakrishnan, and Rao study (37), where they reported the formation temperature of lanthanum aluminate to be around 897°C.

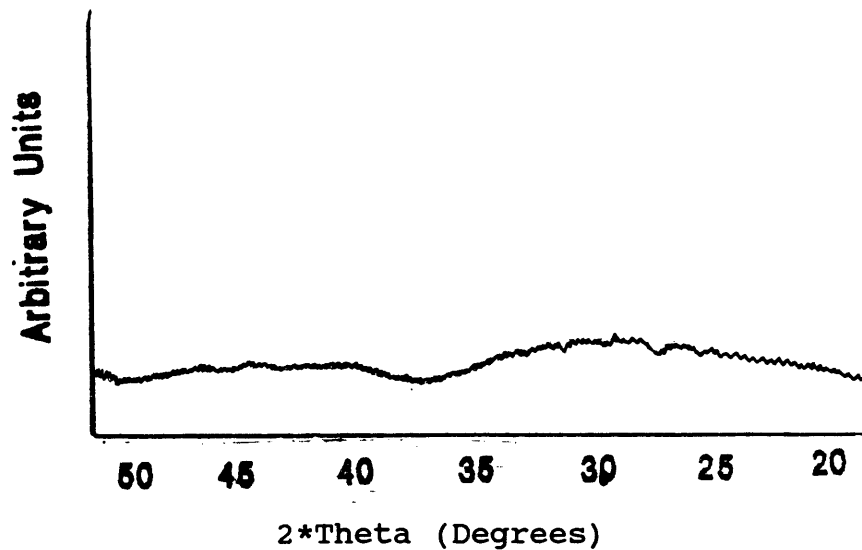


Figure 2.4.1: Diffraction pattern for powder made from lanthanum hydroxide and aluminum chloride. Processing method included hydrolysis, filtration, calcination at 500°C in air and pellet form.

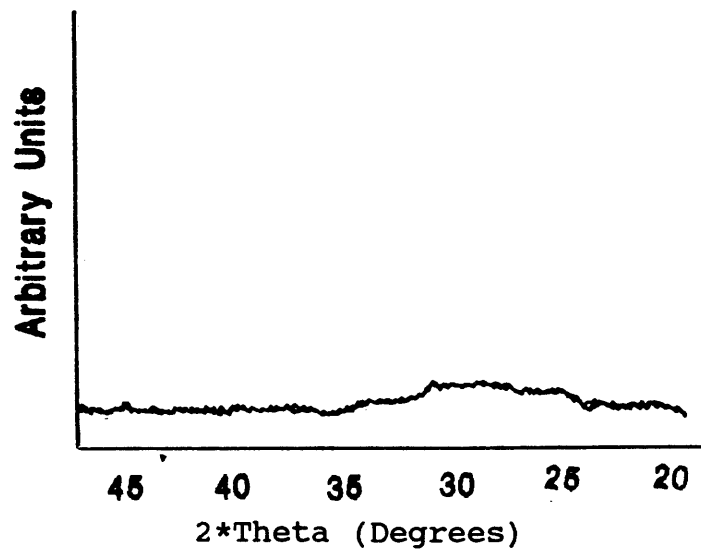


Figure 2.4.2: Diffraction pattern for powder made from lanthanum and aluminum nitrates. Processing method included hydrolysis, filtration, calcination at 500°C in air and pellet form.

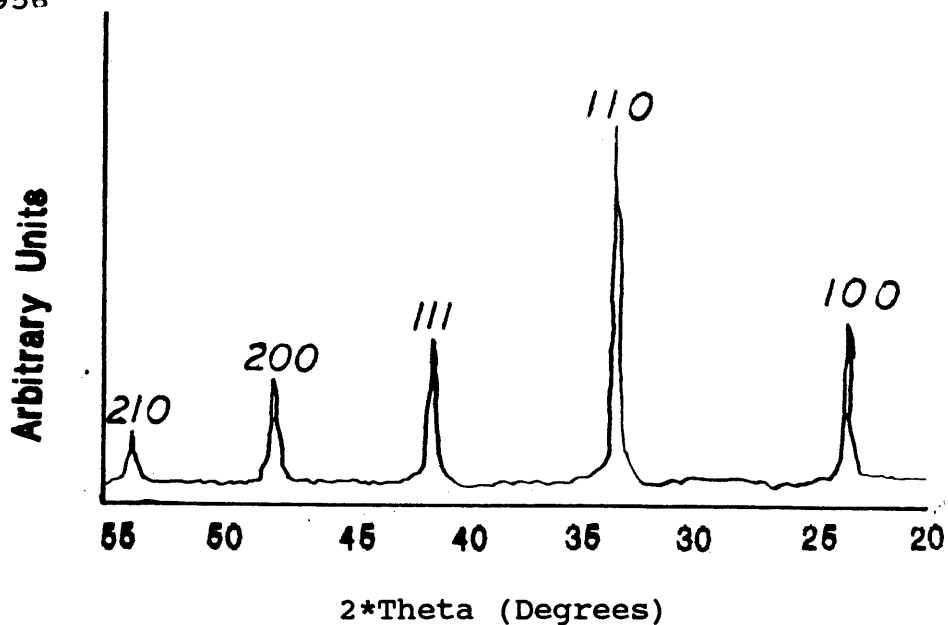


Figure 2.4.3: Diffraction pattern for powder made from lanthanum hydroxide and aluminum chloride. Processing method included hydrolysis, filtration, calcination at 950°C in oxygen and pellet form.

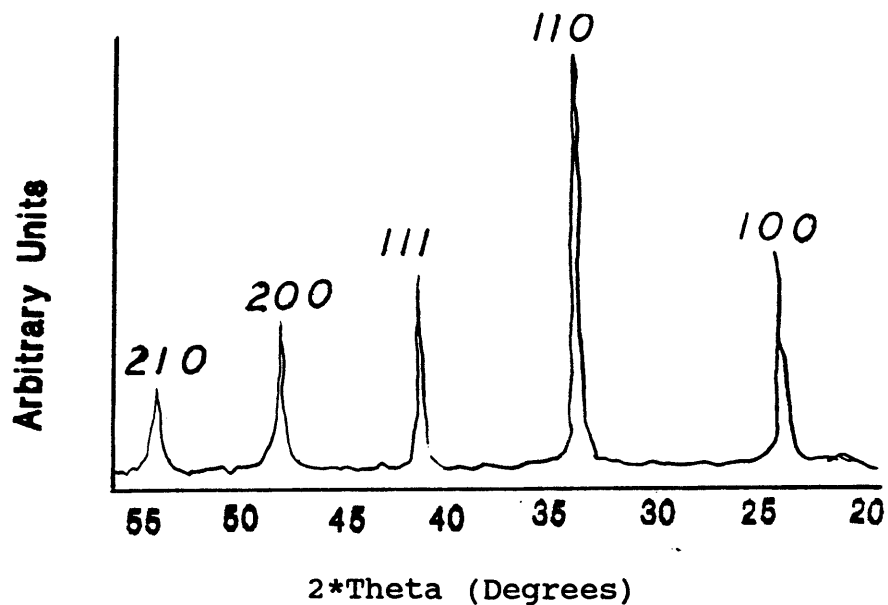


Figure 2.4.4: Diffraction pattern for powder made from lanthanum hydroxide and aluminum chloride. Processing method included hydrolysis, filtration, calcination at 950°C in air and powder form.

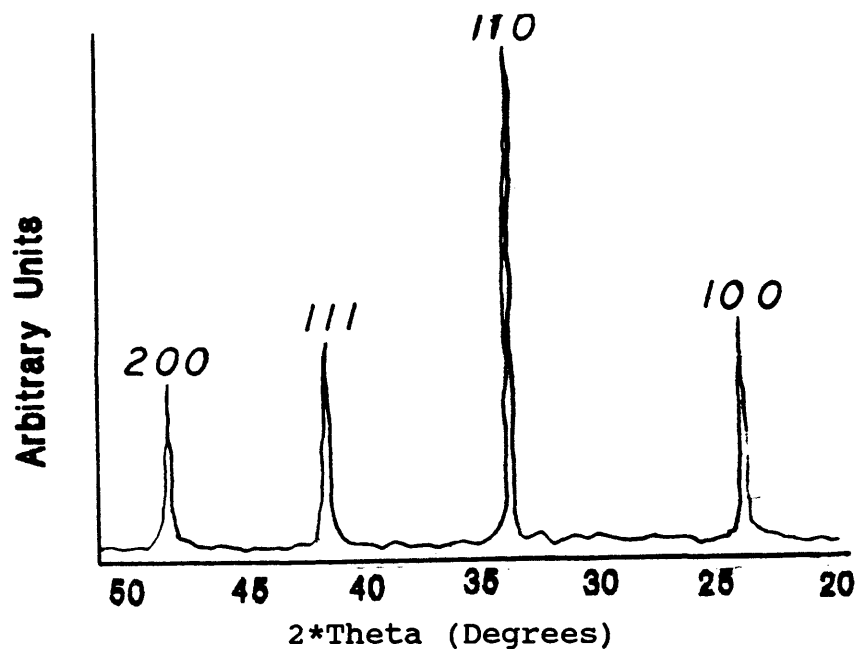


Figure 2.4.5: Diffraction pattern for powder made from lanthanum hydroxide and aluminum chloride. Processing method included hydrolysis, evaporation, calcination at 950°C in oxygen and pellet form.

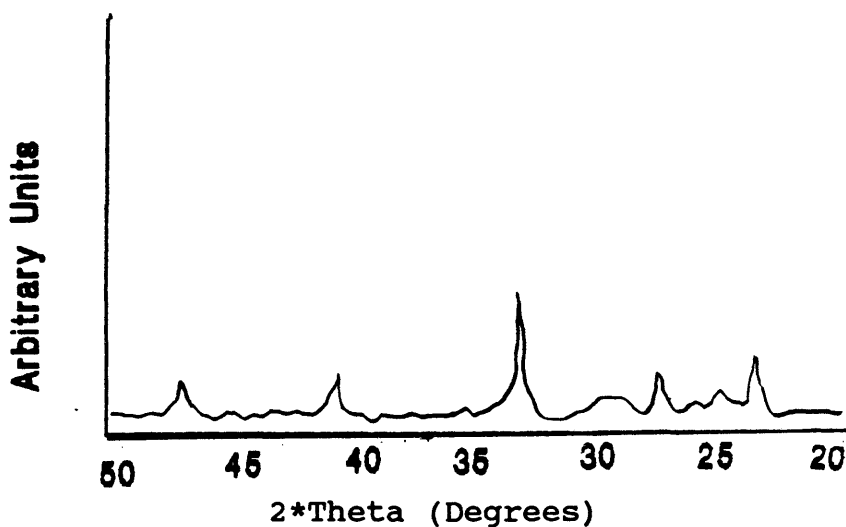


Figure 2.4.6: Diffraction pattern for powder made from lanthanum and aluminum nitrates. Processing method included hydrolysis, filtration, calcination at 950°C in oxygen and pellet form.

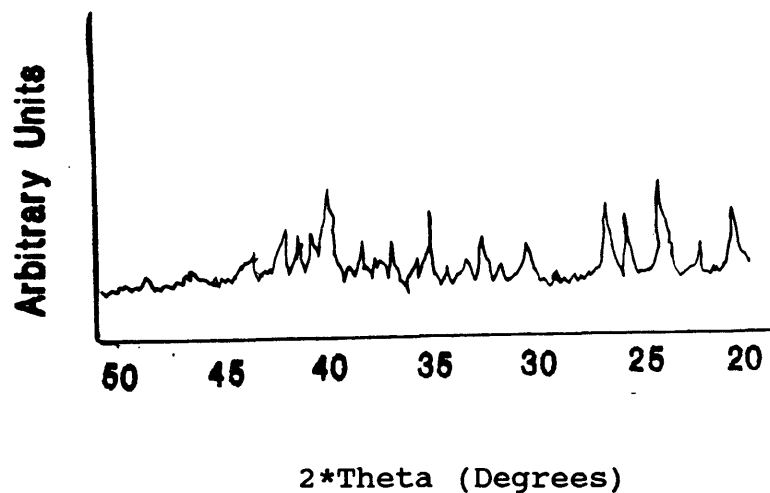


Figure 2.4.7: Diffraction pattern for powder made from lanthanum and aluminum nitrates. Processing method included evaporation, calcination at 950°C in air and powder form.

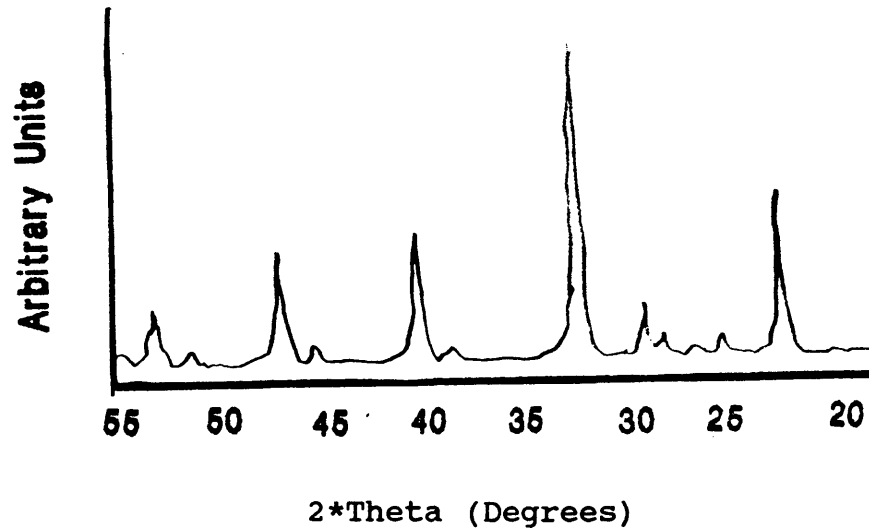


Figure 2.4.8: Diffraction pattern for powder made from lanthanum and aluminum nitrates. Processing method included evaporation, calcination at 950°C for 24 hours in oxygen and powder form.

The purities of the powder products were compared for each processing method. The best results were achieved from the salt solution made from lanthanum hydroxide and aluminum chloride (Figures 2.4.3 and 2.4.4). The XRD patterns have no observable impurity peaks. No substantial difference was observed in the XRD patterns for products prepared using either filtration or evaporation for precipitation collection (Figures 2.4.4 and 2.4.5). The calculated pseudo-cubic lattice parameters for the powder products in Figures 2.4.3 and 2.4.4 are 3.79 ± 0.01 and 3.78 ± 0.01 Å respectively. No differences in the XRD patterns were observed in products that were calcined in oxygen or air as well as in powder or pellet form (Figures 2.4.3 and 2.4.4).

Higher impurity levels were observed in the XRD patterns when greater amounts of nitrates were used to prepare the salt solutions (see Figures 2.4.6 and 2.4.8). A test was performed to see if longer calcination times would remove the impurities in the powder. Two powder samples prepared by using the third method were calcined at 950°C, one for five and one half hours and the other for twenty-four hours. Comparison of the XRD patterns shows that the relative impurity level decreases with increasing calcination times (Figures 2.4.7 and 2.4.8). However, even with the longer calcination times the impurity level was much greater than observed in the powder products made from

lanthanum hydroxide and aluminum chloride.

SEM analysis showed that chlorine and iron impurities were in many of the powder products. No correlation was found between the presence of chlorine and the starting material. This is most likely due to sample contamination during calcination since samples prepared with aluminum nitrate and chloride were calcined simultaneously. As expected, chlorine was present in samples fired at 500 and 950°C. The boiling point of lanthanum chloride is greater than 1000°C (see Table 2.2.4).

The optimal processing method for lanthanum aluminate was the first method where the salt solution was prepared from lanthanum hydroxide and aluminum chloride. Ammonium hydroxide was added to the solution to coprecipitate lanthanum and aluminum hydroxide. The precipitate was filtered, washed and dried overnight at 100-150°C. The material was then calcined at 950°C in air or oxygen and in powder or pellet form. To minimize processing costs lanthanum aluminum hydroxide should be calcined in air at 950°C.

Chapter 3

3.0 RF-MAGNETRON SPUTTERING AND CHARACTERIZATION OF LANTHANUM ALUMINATE THIN FILMS

3.1 LITERATURE REVIEW FOR LANTHANUM ALUMINATE THIN FILMS; DEPOSITION TECHNIQUES

3.1.1 THIN FILM DEPOSITION TECHNIQUES

There are many different processing methods to deposit thin films of material onto a substrate such as vapor phase deposition (VPD), chemical vapor deposition (CVD), molecular beam epitaxy (MBE), and spray pyrolysis (6). The most common technique is VPD which consists of the following deposition methods: sputtering, evaporation, and laser ablation. All of these processing methods require medium (10^{-6} - 10^{-7} Torr) to ultra-high (approximately 10^{-10} Torr) vacuum conditions. One advantage of depositing films in medium to ultra-high vacuum is that high-purity, thin-film samples can be produced. The drawbacks of using vacuum systems are the cost of the apparatus and the slow processing times. Nevertheless, Leskela et al. (6) reported that VPD techniques are the most commonly used for producing

high quality high T_c superconducting films.

Recently, more articles have reported the use of CVD, or more precisely, metal-organic chemical vapor deposition (MOCVD) to deposit high T_c superconducting films. The advantage of this technique is the deposition of high quality superconducting films at lower processing temperatures on sapphire substrates. The MBE technique has been used to grow highly oriented superconducting films with good electrical properties. The major disadvantage of this deposition technique is that it requires an expensive ultra-high vacuum system (6).

Spray pyrolysis is a more convenient technique since it does not require vacuum conditions. A metalorganic solution is sprayed onto a heated substrate using an air brush. The samples are heated at high processing temperatures typically 800 - 900°C. However, the films produced using this technique are of lower quality than films produced using the methods mentioned above (6).

The simplest methods to deposit high quality thin films are the VPD; of these techniques sputtering is the most common. There is a variety of different sputtering techniques such as dc-magnetron, dc-diode, dc-triode, rf-magnetron, rf-diode and ion beam. The dc techniques are only suitable if the target is made of a conducting or semiconducting material (6). Since lanthanum aluminate is a

dielectric material the dc sputtering techniques were not considered here. Lanthanum aluminate has a high melting point (2110°C) which makes it difficult to use evaporation as a film deposition method (49). The laser ablation technique would be suitable for depositing lanthanum aluminate, but the apparatus is costly. Therefore rf-magnetron sputtering was chosen to deposit lanthanum aluminate thin films in this study.

3.1.2 DEPOSITION TECHNIQUES FOR LANTHANUM ALUMINATE THIN FILMS

The deposition technique of rf-magnetron sputtering has some inherent systematic problems such as oxygen depletion, and re-sputtering that affect the quality of films produced. These effects can be reduced by modifying some of the deposition parameters. Oxygen depletion in the film is a common problem when magnetron sputtering is the deposition technique. The oxygen-depleted films appear dark or as metallic. However, this problem can be corrected by adding oxygen to the sputtering gas (argon) (50). Re-sputtering occurs when ions bombard the surface of the film and cause changes in the film stoichiometry. There are several deposition parameters that can be altered to minimize

re-sputtering. The simplest to implement are using higher deposition pressures and placing the substrates in an off-axis orientation with respect to the plasma. Both methods reduce the probability of an energized ion striking the surface of the film (6).

3.2 DEPOSITION PROCESSES OF LANTHANUM ALUMINATE THIN FILMS

For the present work, a Varian 3118 evaporator chamber was converted into a single source rf-magnetron sputtering chamber. The chamber was connected to a diffusion pump as shown in Figure 3.2.1. Base pressures of 5×10^{-6} Torr could be achieved with this apparatus. The pumping speed was found to be too high when trying to deposit thin films at pressures greater than 10 mTorr by rf-sputtering. This made it difficult to stabilize the sputtering gas pressure. To correct this problem a steel plate was placed over the majority of the gate valve opening to reduce the diffusion pump speed. With the modified pumping configuration the typical base pressure was 1×10^{-4} Torr.

The planar rf-magnetron sputtering head held a 38 mm diameter target. The stoichiometric, hot-pressed lanthanum aluminate target was made from powder prepared using the optimal processing technique previously described in

chapter 2. The rf-power source was an ENI Power Systems solid state power generator which could supply up to 700 Watts of power at a frequency of 13.56 MHz (Figure 3.2.2). The rf-power supply was connected to an automatic RF Plasma Products automatic tuner.

The film thickness was monitored by a Sloan digital deposition controller with a 5 MHz quartz crystal. The quartz crystal was 0.5 inches in diameter and was coated with silver.

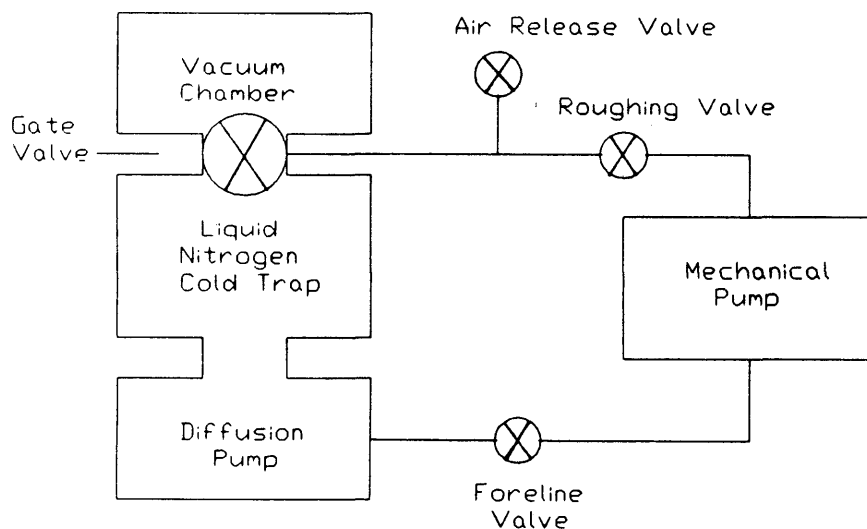


Figure 3.2.1: Schematic diagram of the vacuum chamber used to deposit lanthanum aluminate films.

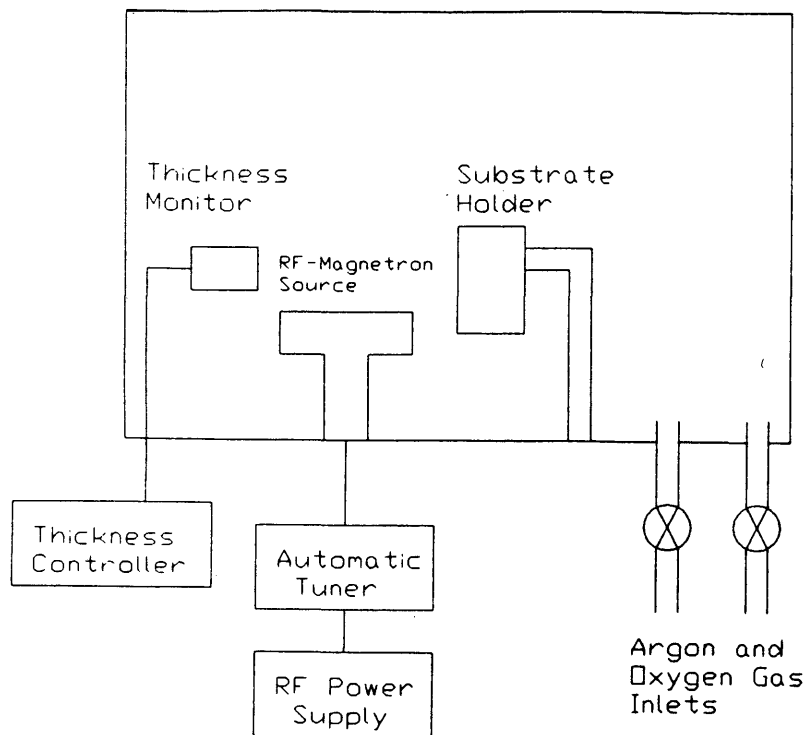


Figure 3.2.2: Schematic diagram showing the deposition apparatus and the off-axis substrate holder configuration.

Argon was the primary sputtering gas. Oxygen was added to the sputtering gas mixture to preserve film stoichiometry (50). Two adjustable gas inlet valves were used to control the flow and partial pressures of argon and oxygen respectively. The purities of the argon and oxygen gases were 99.998%.

Initially a rotating substrate was used to deposit the lanthanum aluminate thin films in order to maximize the film

uniformity. The holder could accommodate substrates up to 3 inches in length. The rotation rate could be adjusted by simply varying the voltage supplied to the motor. The typical rotation rate was 60 rpm. The substrate holder orientation could be adjusted in three independent directions thereby allowing freedom to position the substrates with respect to the target.

Later the rotating substrate holder was replaced with a fixed, heated substrate holder. The substrates were heated by a small 600 Watt halogen lamp placed directly behind the steel plate which supported them. Acting on advice from Dr. A. Lee of TRW, a water cooling system was installed to extend the operating life of the halogen lamps. With these modifications, a 1 cm² area on the substrate holder could be heated up to 750°C during film deposition and to more than 800°C for post-deposition, in-situ annealing heat treatments. When the applied voltage to the halogen lamp was greater than 100 volts, the plasma would interact with the halogen lamp and cause it to burn out. This limited the maximum substrate temperature during deposition to 750°C. The substrate deposition temperature was monitored with a thermocouple placed near the substrates on the steel plate. Silver paint was used to attach the substrates to the steel plate in order to insure good thermal contact.

To calibrate the substrate heater the temperature was

measured for specific voltage settings applied to the halogen lamp. Temperature measurements were taken for both substrate heating and cooling (See Table 3.2.1). A linear regression of these data yields the following equation for substrate temperature at a given voltage:

$$T \pm 15 = (6.88 \pm 0.12)V + 78$$

From this linear regression the uncertainty of the temperature measured with the thermocouple was approximately $\pm 15^\circ\text{C}$.

The pressures were monitored using either a Bayard-Alpert ionization or a thermocouple pressure gauge. The ionization gauge was used to measure pressures up to 30 mTorr. Pressures higher than 30 mTorr were monitored with the thermocouple gauge. This procedure was implemented to extend the life of the ionization gauges since factory specifications recommend against using them above 20 mTorr, except in an argon only environment. Off-axis orientation was used in all film depositions to minimize re-sputtering effects (Figure 3.2.2) (6, 50).

The plasma did not ignite at pressures lower than 20 mTorr. To overcome this problem the gate valve was closed for a few seconds to ignite the plasma and then reopened.

A substrate heating regimen was suggested by TRW to slowly evaporate the solvents from the silver paint. The procedure was to slowly heat to 150°C , hold there for about

TABLE 3.2.1

Calibration of Substrate Heater

| Heating Cycle | | Cooling Cycle | |
|---------------------------|---------------------|---------------------------|---------------------|
| Variac Reading (Volts) | Temperature (°C) | Variac Reading (Volts) | Temperature (°C) |
| 15 | 140 | 20 | 210 |
| 20 | 190 | 25 | 250 |
| 25 | 235 | 30 | 295 |
| 35 | 325 | 35 | 335 |
| 45 | 400 | 40 | 370 |
| 55 | 470 | 45 | 400 |
| 65 | 530 | 50 | 440 |
| 75 | 595 | 55 | 475 |
| 85 | 650 | 60 | 505 |
| 90 | 685 | 65 | 535 |
| 93 | 700 | 70 | 565 |
| | | 75 | 600 |
| | | 80 | 630 |
| | | 85 | 660 |
| | | 90 | 690 |
| | | 93 | 705 |

10 minutes, increase the temperature to 600°C, and hold there for 10 - 20 minutes. These temperatures were appropriate for atmospheric conditions. At pressures in the mTorr range most of the solvents were observed to evaporate around 300 - 400°C. Therefore in this temperature range the temperature was increased very slowly.

After film deposition the substrates were cooled very quickly to about 200°C at a cooling rate of approximately 50°C/minute. Typically, when the chamber reached 200°C, it was then filled with oxygen to approximately 2000 mTorr.

3.3 LANTHANUM ALUMINATE THIN FILM CHARACTERIZATION PROCEDURES

Initially the x-ray diffraction patterns for the lanthanum aluminate film samples were collected by using the powder diffractometer described in Section 2.3. All of the data was processed with the Micro-peak software program developed by Materials Data Inc. This program identifies diffraction peak locations and their relative intensities and also the corresponding d-spacings of the sample. The film samples were mounted on glass slides or with clay in the powder sample holders. Unfortunately, these methods for collecting x-ray diffraction patterns had too many systematic errors which sometimes resulted in the loss of data and time. The most significant systematic error occurred in mounting the sample because the slightest misalignment (by a half a degree or less) could result in the absence of very strong diffraction peaks in the XRD pattern.

To minimize this type of systematic error, the XRD patterns were collected by using a four-circle diffractometer. The samples were mounted with clay onto a pin which was then placed into a goniometer. The sample was visually aligned with the pin as near as possible to a vertical position. Once the pin was placed into the goniometer, the surface of the sample was rotated until it was parallel with one of the axes of the goniometer. The goniometer was then mounted in the four-circle diffractometer. The surface of the film was then aligned using the telescope on the diffractometer.

The deposited films were too thin to observe with the transmission configuration. Therefore the sample was first aligned by maximizing a substrate peak in the transmission configuration. The substrate was then by rotated 85° from the position where the film surface was perpendicular to the incident x-ray beam. Then a θ - 2θ reflection scan was performed. This data collection method worked well for randomly oriented samples, but not for well-oriented crystalline samples. The data collection procedure was again modified to better align the sample before collecting the XRD pattern.

After aligning the sample by using the sighting telescope, the edge of the substrate was aligned so that it was essentially parallel to the incident x-ray beam. The

substrate Bragg diffraction peaks were maximized by adjusting the orientation of the substrate. Once the substrate Bragg peaks were maximized, then a θ - 2θ scan was performed.

When analyzing a well-oriented crystalline film, the sample was aligned again by maximizing the intensity of the largest diffraction peak of the crystal. For example when a lanthanum aluminate crystalline film oriented in the (h00) direction was analyzed, the (100) Bragg peak was maximized since it is expected to have the largest intensity in the diffraction pattern for this family of planes.

To determine the degree of orientation of crystalline films, rocking curve analyses were performed. The first step was to maximize the intensity of the Bragg diffraction peak of interest. Then the detector was set at 2θ and the sample was rotated through θ . Typically, for the rocking-curve analyses, the sample was "rocked" 2 degrees on each side of θ . The rocking curve measurement consists of a plot of diffracted beam intensity versus θ . For a perfect crystal the width of the peak should be on the order of 0.003° . For practical applications a single crystal typically has a peak width of 0.03 to 0.3° (51).

Molybdenum is the radiation source used in the four-circle powder diffractometer. Molybdenum has two similar characteristic wavelengths which cannot be separated by the

monochrometer. The wavelengths are $K_{\alpha 1}$ and $K_{\alpha 2}$ and their respective values are 0.70930 Å and 0.71359 Å. The ratio of the relative intensities of $K_{\alpha 1}:K_{\alpha 2}$ is 2:1. Therefore a weighted averaged value for the wavelength (0.71073 Å) was used in calculations of d-spacings and lattice constants unless otherwise noted.

To calibrate the four-circle diffractometer for lanthanum aluminate a diffraction pattern for lanthanum aluminate powder was collected. The d-spacings were calculated using Equation 2.2 and are listed in Table 3.3.1. The lanthanum aluminate was ground into a fine powder, placed in a glass capillary and mounted into a goniometer. By using Equation 2.5 the lattice parameter for each Bragg peak was calculated (Table 3.3.1) and the standard deviation of these values was 3.788 ± 0.009 Å.

The SEM and EDS analyses were performed by Mr. J. Ahn. The same SEM apparatus as previously described in Section 2.3 was used. Since lanthanum aluminate is a dielectric material, the samples were pre-coated with a conducting layer of carbon to prevent localized charge build-up that can occur on nonconducting samples during SEM analysis (52). The carbon coatings were deposited onto the films by evaporation. All compositional films analyses were performed using 15 KV electrons and a magnification of 500X unless otherwise noted. For consistency in comparing film

morphologies, SEM photomicrographs were taken at magnifications of 500X and 3000X. The EDS detection limits is approximately 1 atomic percent of a given element.

TABLE 3.3.1

d-Spacings and Lattice Constants for
Lanthanum Aluminate Powder

| Pseudo- Cubic h k l | d-Spacing (Å) | Lattice Constant (Å) | Normalized Peak Height |
|---------------------------|------------------|-------------------------|---------------------------|
| 1 0 0 | 3.808 | 3.808 | 49.3 |
| 1 1 0 | 2.680 | 3.790 | 100.0 |
| 1 1 1 | 2.180 | 3.775 | 45.2 |
| 2 0 0 | 1.892 | 3.784 | 43.2 |
| 2 1 0 | 1.692 | 3.783 | 23.5 |
| 2 1 1 | 1.544 | 3.782 | 46.4 |
| 2 2 0 | 1.336 | 3.779 | 21.9 |
| 3 0 0 | 1.265 | 3.796 | 14 |
| 3 1 0 | 1.198 | 3.790 | 19.9 |
| 3 1 1 | 1.143 | 3.791 | 13 |
| 2 2 2 | 1.095 | 3.795 | 7.3 |

3.4 LANTHANUM ALUMINATE THIN FILM RESULTS

3.4.1 INITIAL LANTHANUM ALUMINATE DEPOSITION ONTO SUPERCONDUCTING FILMS

Initial lanthanum aluminate deposition studies consisted of rf-sputtering lanthanum aluminate onto 1-2-3 superconducting films supplied by Dr. C. Platt from TRW. The first attempt to deposit lanthanum aluminate was onto an EBCO superconducting film. The deposition parameters are listed in Table 3.4.1. SEM micrographs showed that the as-deposited film was smooth and continuous with small rectangular and square particles on the surface (see Figure 3.4.1). From the micrograph the sizes of the particles were estimated to be about 0.5 to 2.5 microns. The EDS compositional analysis results are listed in Table 3.4.2. All areas of the film were analyzed at 10 KV and the overall film composition was analyzed at 300 magnification, while the continuous film and particles were analyzed at magnifications of 12000 and 5000 respectively. The particles had higher impurity concentrations of chlorine and potassium than did the continuous film. The source of the chlorine contamination was the rf-sputtering target; however, the source of the potassium contamination remains unknown. The potassium contamination was never observed in

TABLE 3.4.1

Initial Deposition Parameters onto EBCO Film

| RF-Sputtering Parameters | |
|---------------------------------------|------------------------|
| Target | LaAlO ₃ |
| Orientation | Off-Axis |
| Rotating Substrate Holder | |
| Substrate Temperature | Ambient |
| Substrate Height | - |
| Substrate Distance | - |
| RF-Power | 100 W |
| Base Pressure | 7.6 x 10 ⁻⁶ |
| Average Argon Pressure | 10.5 mTorr |
| Average Oxygen Pressure | 9.5 mTorr |
| Average Total Sputtering Gas Pressure | 20.0 mTorr |
| Argon : Oxygen | 1.1 : 1.0 |
| Deposition Time | 3 Hours |

TABLE 3.4.2

EDS Compositional Analyses Results
For LaAlO₃ Deposited onto EBCO Film

| Element | Overall (Atomic Percent) | Continuous Film (Atomic Percent) | Particle (Atomic Percent) |
|---------|-----------------------------|-------------------------------------|------------------------------|
| La | 38.89 ± 1.0 | 40.51 ± 1.0 | 27.67 ± 1.0 |
| Al | 50.08 ± 1.0 | 50.92 ± 1.0 | 34.26 ± 1.0 |
| Cl | 7.48 ± 1.0 | 5.51 ± 1.0 | 19.25 ± 1.0 |
| K | 3.55 ± 1.0 | 3.06 ± 1.0 | 18.82 ± 1.0 |

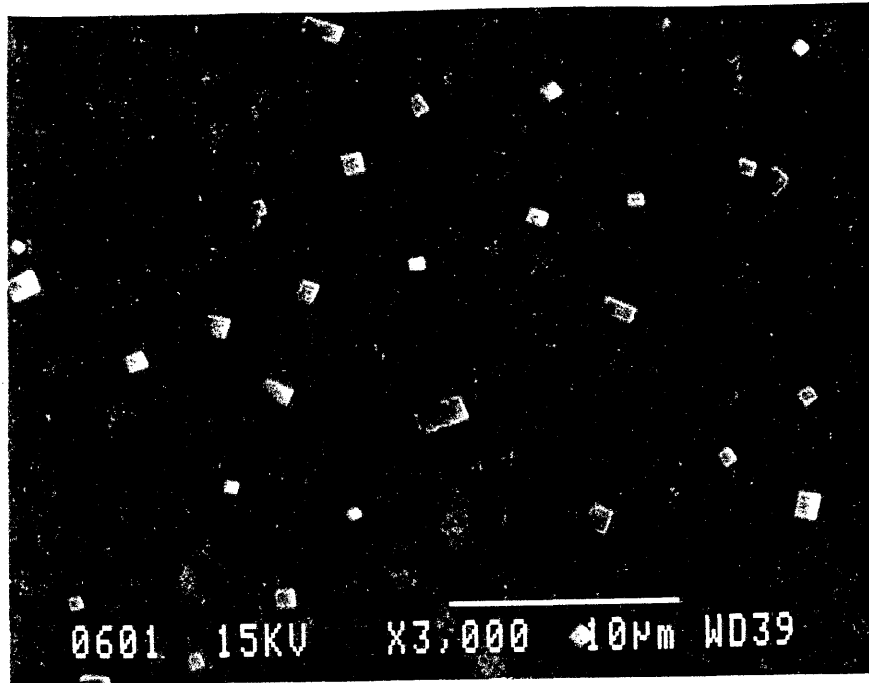


Figure 3.4.1: SEM micrograph showing the smooth continuous dielectric film deposited onto an EBCO film. The square and rectangular particles on the surface are rich in chlorine and potassium impurities.

later lanthanum aluminate depositions.

The lanthanum aluminate and EBCO film sample was mounted onto a glass slide for x-ray diffraction analysis. A Rigaku Rotaflex powder diffractometer was used to record the diffraction pattern for this sample (Figure 3.4.2). The incident x-ray beam covered approximately a 2 cm² area which was larger than the sample. Therefore, the amorphous background shape observed in the diffraction pattern can be attributed to the glass slide. The d-spacings for the Bragg peaks are listed in Table 3.3. In the diffraction pattern

the Bragg diffraction peaks at 2θ equal to 23.46° and 75.02° correspond to the (100) and (300) lanthanum aluminate respectively. We are unable to explain the absence of the (200) Bragg peak from the XRD pattern. We experienced difficulty of precisely identifying the remaining Bragg peaks in the diffraction pattern as being due to the EBCO film or the substrate material. The problem in identifying is most likely caused by misalignment of the sample with respect to the incident x-ray beam.

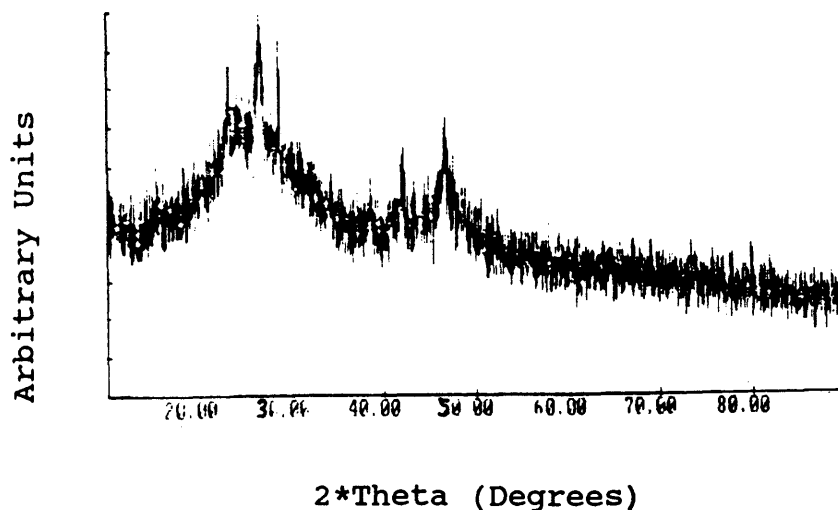


Figure 3.4.2: XRD pattern for dielectric film deposited onto an EBCO film. The amorphous shape of the pattern was attributed to the glass slide holding the sample.

TABLE 3.4.3

d-Spacings For LaAlO₃ Deposited onto EBCO Film

| 2θ (Degrees) | d-Spacing (Å) | Relative Peak Height |
|------------------------|------------------|-------------------------|
| 12.86 | 6.878 | 54.4 |
| 20.78 | 4.271 | 66.2 |
| 23.02 | 3.860 | 92.5 |
| 23.46 | 3.789 | 82.2 |
| 28.48 | 3.131 | 100.0 |
| 31.48 | 2.840 | 78.6 |
| 42.10 | 2.145 | 69.4 |
| 51.34 | 1.778 | 49.8 |
| 58.78 | 1.570 | 45.2 |
| 75.02 | 1.265 | 34.9 |

The second film deposition of lanthanum aluminate onto a YBCO film was performed according to the sputtering parameters listed in Table 3.4.4. The SEM micrograph in Figure 3.4.3 shows the film as continuous with large cracks ranging from about 0.3 to 12 microns in length. Again, there are large particles on the surface of the film. However, these particles do not have a specific shape as previously observed. The film was analyzed at 10 KV and the compositional analyses were performed at magnifications of 300, 5000, and 7000 for overall, particle, and continuous film areas respectively. The EDS compositional analyses are listed in Table 3.4.5.

TABLE 3.4.4

Initial Deposition Parameters onto YBCO Film

RF-Sputtering Parameters

| | |
|---------------------------|--------------------|
| Target | LaAlO ₃ |
| Orientation | Off-Axis |
| Rotating Substrate Holder | |
| Substrate Temperature | Ambient |
| Substrate Height | - |
| Substrate Distance | - |
| RF-Power | 100 W |
| Base Pressure | 8×10^{-6} |
| Average Argon Pressure | 14.5 mTorr |
| Average Oxygen Pressure | 10.0 mTorr |
| Average Total Sputtering | |
| Gas Pressure | 24.5 mTorr |
| Argon : Oxygen | 1.45 : 1.0 |
| Deposition Time | 3 Hours |

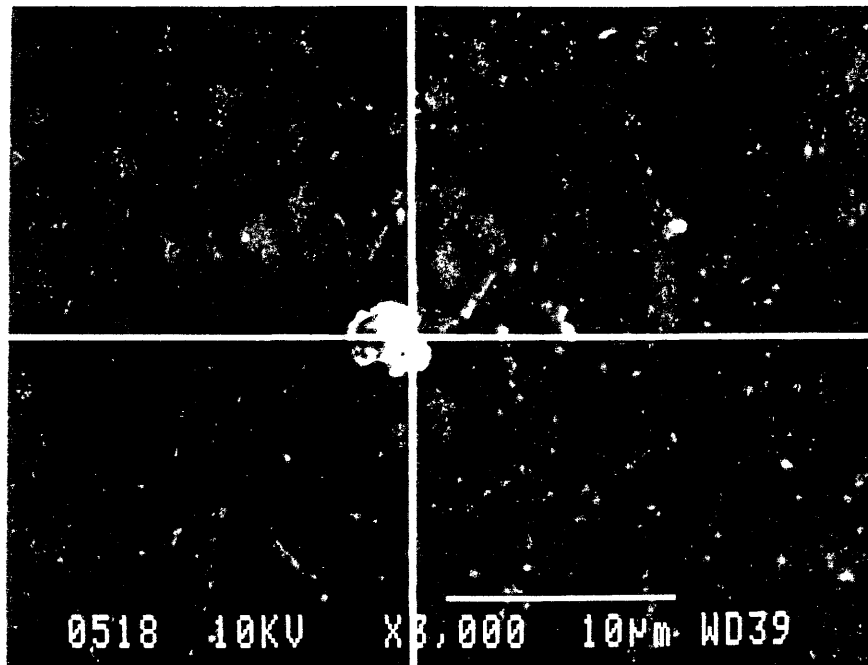


Figure 3.4.3: SEM micrograph showing the morphology of the dielectric film deposited onto a YBCO film. The film is continuous with large cracks.

TABLE 3.4.5
EDS Compositional Analyses Results
For LaAlO_3 Deposited onto YBCO Film

| Element | Overall (Atomic Percent) | Continuous Film (Atomic Percent) | Particle (Atomic Percent) |
|---------|-----------------------------|-------------------------------------|------------------------------|
| La | 27.80 \pm 1.0 | 28.65 \pm 1.0 | 25.63 \pm 1.0 |
| Al | 43.11 \pm 1.0 | 43.92 \pm 1.0 | 38.43 \pm 1.0 |
| Y | 9.60 \pm 1.0 | 9.48 \pm 1.0 | 0.0 |
| Ba | 18.05 \pm 1.0 | 16.43 \pm 1.0 | 0.0 |
| Cl | 1.44 \pm 1.0 | 1.52 \pm 1.0 | 1.77 \pm 1.0 |
| Zr | 0.0 | 0.0 | 34.18 \pm 1.0 |

For XRD analysis the film sample was again mounted on a glass slide and the powder diffractometer was used to record the diffraction pattern (Figure 3.4.4). The Bragg diffraction peaks are labeled and identified in Table 3.4.6. The underlying YBCO film in this case was deposited onto a lanthanum aluminate crystalline substrate. The lanthanum aluminate peaks observed in the diffraction pattern are most likely from the substrate since their relative peak heights are large. However, it is difficult to draw any conclusions about the lanthanum aluminate film except that it is not randomly oriented. The deposited film can either be amorphous or oriented crystal.

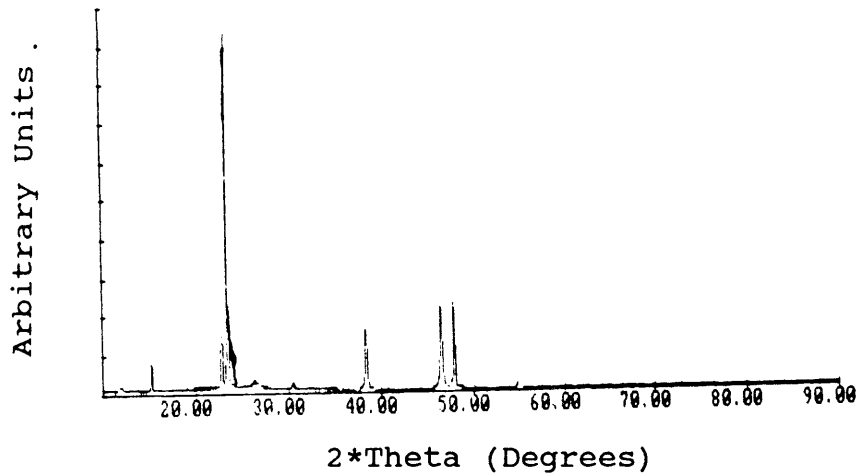


Figure 3.4.4: XRD pattern for the dielectric film deposited onto a YBCO film.

TABLE 3.4.6

d-Spacings For LaAlO_3 Deposited onto YBCO Film

| $2*\theta$ (Degrees) | d-Spacing (Å) | Relative Peak Height | LaAlO_3 hkl | YBCO hkl |
|-------------------------|------------------|-------------------------|-------------------------|-------------|
| 15.14 | 5.848 | 7.9 | | 002 |
| 22.78 | 3.900 | 19.9 | | 003 |
| 23.46 | 3.789 | 100.0 | 100 | |
| 26.44 | 3.368 | 3.2 | | |
| 30.54 | 2.925 | 2.6 | | 004 |
| 38.42 | 2.341 | 18.1 | | 005 |
| 46.52 | 1.951 | 22.3 | | 006 |
| 47.94 | 1.896 | 23.4 | 200 | |
| 48.08 | 1.891 | 12.3 | | |
| 54.88 | 1.672 | 2.6 | | 007 |

3.4.2 RADIAL COMPOSITION STUDY OF LANTHANUM ALUMINATE FILMS

Recent studies have shown that the substrate-target distance parameter affects the composition and phase of rf-sputtered YBCO films (7,53). Based on these observations we performed a study to determine if the composition of rf-sputtered lanthanum aluminate films varied with substrate positioning. YBCO superconducting film samples on lanthanum aluminate or strontium titanate substrates were placed at different radial distances on the rotating substrate holder, which was located approximately 4 cm from the target center. (Table 3.4.7). The YBCO films were visually inspected for noticeable differences before deposition of the lanthanum aluminate overlayers. Both YBCO film samples deposited onto LaAlO_3 substrates were very smooth except for polishing lines on the substrates. The YBCO film deposited onto SrTiO_3 substrate was basically smooth except for some rough sections in the film. The deposition parameters for the lanthanum aluminate overlayers are described in Table 3.4.8. After deposition the films were again visually inspected. The sample placed in the center of the substrate holder was uniformly blue-green in color, while the samples placed 1.0 and 1.3 cm from the center varied in color. This result indicates that uniform deposition occurred for the sample in the center and that, for the other samples, the film

TABLE 3.4.7

Radial Placement of YBCO Film Samples

| Sample Id | Position on Substrate Holder (Distance from Center of Holder in cm) |
|--------------------------------|--|
| S062189B LaAlO ₃ -1 | 0 |
| S062189A LaAlO ₃ -1 | 1.0 |
| S062189B SrTiO ₃ | 1.3 |

TABLE 3.4.8

Deposition Parameters for Radial Composition Study

| RF-Sputtering Parameters | |
|---------------------------|------------------------|
| Target | LaAlO ₃ |
| Off-Axis Orientation | |
| Rotating Substrate Holder | |
| Substrate Temperature | 115°C |
| Substrate Height | - |
| Substrate Distance | - |
| RF-Power | 100 W |
| Base Pressure | 8.4 x 10 ⁻⁶ |
| Average Argon Pressure | 13.5 mTorr |
| Average Oxygen Pressure | 9.0 mTorr |
| Average Total Sputtering | |
| Gas Pressure | 22.5 mTorr |
| Argon : Oxygen | 1.5 : 1.0 |
| Deposition Time | 3 Hours |

deposition was not uniform and the film thickness varied.

SEM and EDS analyses were performed on both the as-deposited and the masked portion (YBCO film) of the film. The SEM micrographs show the as-deposited films partially filling gaps present in the microstructure of the YBCO films (Figure 3.4.5). The EDS compositional analyses for the as-deposited films are listed in Table 3.4.9. There are slight differences in the compositional make-up of these films; however, no specific correlation between radial distance and film composition was observed. It is worth noting that a small amount of yttrium was detected in the film placed farthest from the center of the substrate holder. This suggests that this deposited film may be slightly thinner than the other films closer to the center of the holder.

The XRD pattern for a sample placed in the center of the substrate holder showed it to be amorphous (Figure 3.4.6). The absence of any YBCO or LaAlO_3 diffraction peaks may have been caused by sample misalignment previously described in Section 3.3. The XRD pattern (Figure 3.4.7) for a sample mounted 1 cm from the center had a lanthanum aluminate peak at 23.40° , but the other diffraction peaks did not match any of the powder diffraction peaks documented for YBCO, lanthanum aluminate or silver. (See d-spacings listed in Table 3.4.10.) Similarly, the XRD pattern (Figure 3.4.8)

for the sample mounted 1.3 cm from the center had a diffraction peak at 23.45° , but no other identifiable peaks. (See d-spacings listed in Table 3.4.11.) These anomalies again can be attributed to systematic errors in aligning the film samples.

TABLE 3.4.9

Composition of As-Deposited Films For
Radial Study

| Sample Id | Element | Overall Film (Atomic Percent) | Particle (Atomic Percent) |
|------------------------------------|---------|----------------------------------|------------------------------|
| S062189 B LaAlO ₃ -1 | La | 40 ± 1 | 38 ± 1 |
| | Al | 49 ± 1 | 39 ± 1 |
| | Cl | 11 ± 1 | 10 ± 1 |
| | Si | 0 | 11 ± 1 |
| | S | 0 | 2 ± 1 |
| S062189 A LaAlO ₃ -1 | La | 41 ± 1 | 38 ± 1 |
| | Al | 48 ± 1 | 50 ± 1 |
| | Cl | 10 ± 1 | 11 ± 1 |
| S062189 B SrTiO ₃ | La | 38 ± 1 | 39 ± 1 |
| | Al | 50 ± 1 | 50 ± 1 |
| | Cl | 11 ± 1 | 11 ± 1 |
| | Y | 2 ± 1 | 1 ± 1 |

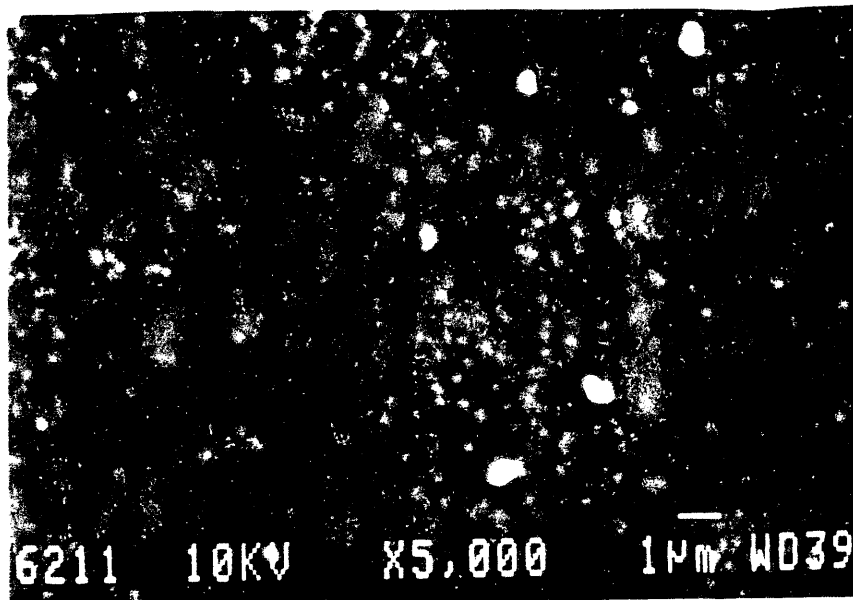
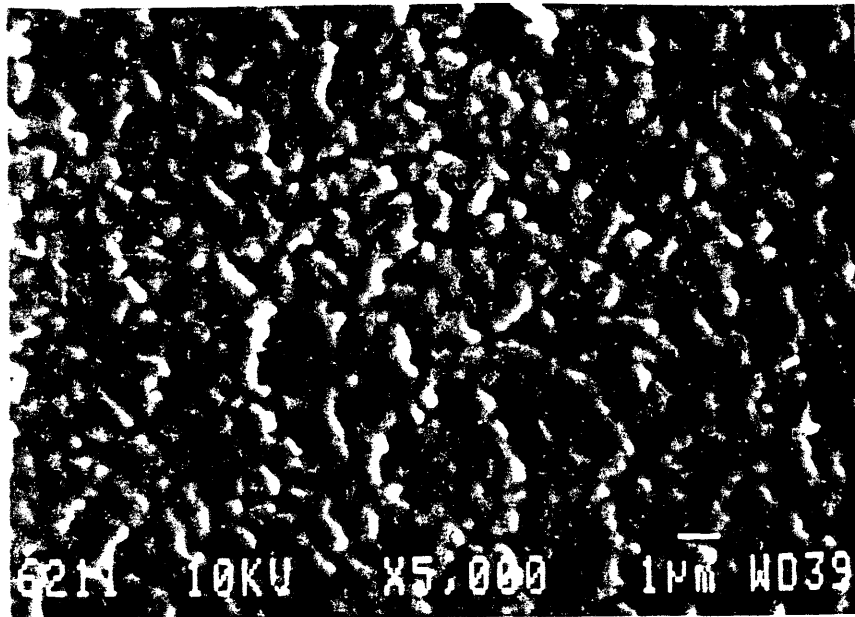


Figure 3.4.5: The top micrograph shows the morphology of the YBCO superconducting film. The bottom micrograph shows the morphology of the dielectric film deposited onto the YBCO film. The radial distance for this sample was 1 cm.

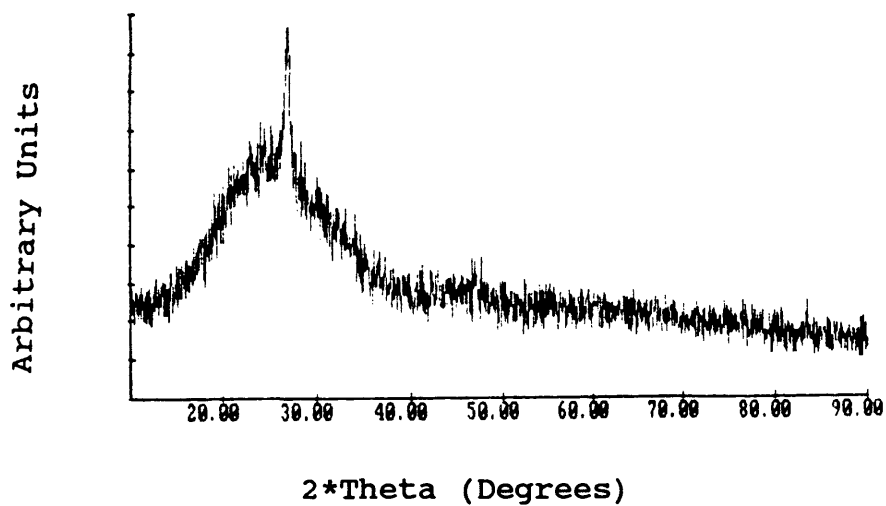


Figure 3.4.6: The XRD pattern for the dielectric film deposited onto a YBCO film centered on the rotating substrate holder.

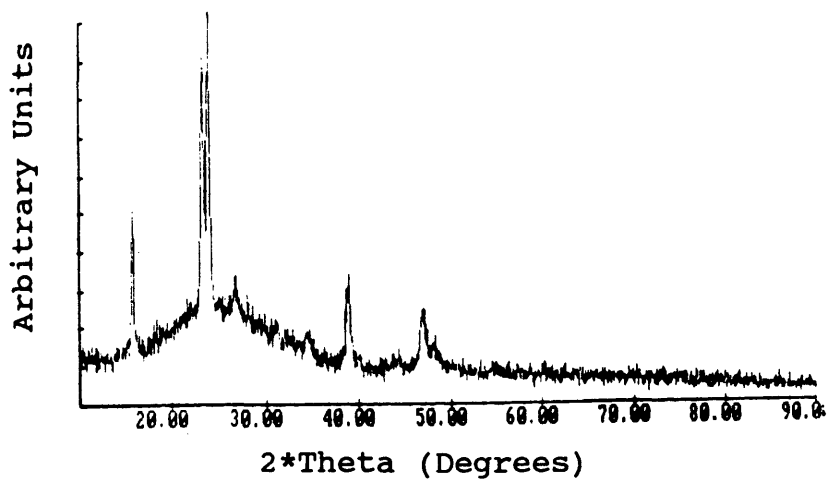


Figure 3.4.7: XRD pattern for the dielectric film deposited onto the YBCO film placed 1 cm radially from the center of the substrate holder.

TABLE 3.4.10

XRD d-Spacings for Sample Placed 1 cm From
Center of Substrate Holder
(S062189 A LaAlO_3)

| $2 * \theta$ | d-Spacing (Å) | Relative Peak Height |
|--------------|------------------|-------------------------|
| 15.80 | 5.605 | 51.3 |
| 23.40 | 3.798 | 94.4 |
| 24.05 | 3.698 | 100.0 |
| 26.90 | 3.312 | 34.4 |
| 39.04 | 2.305 | 33.9 |
| 46.95 | 1.934 | 25.7 |

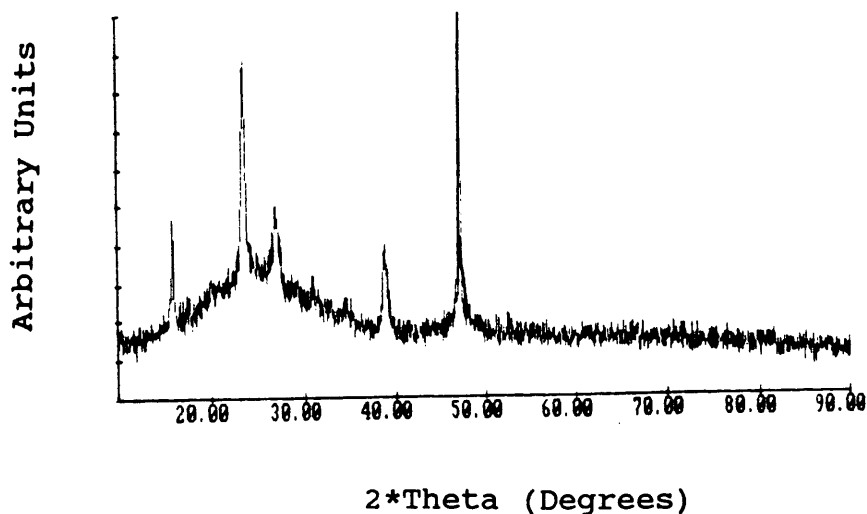


Figure 3.4.8: XRD pattern for the dielectric film deposited onto the YBCO film placed 1.3 cm radially from the center of the substrate holder.

TABLE 3.4.11

XRD d-Spacings for Sample Placed 1.3 cm
From Center of Substrate Holder
(S062189 SrTiO₃)

| $2 * \theta$ | d-Spacing (Å) | Relative Peak Height |
|--------------|------------------|-------------------------|
| 15.85 | 5.589 | 46.9 |
| 23.45 | 3.791 | 89.4 |
| 26.81 | 3.323 | 50.4 |
| 38.90 | 2.313 | 40.0 |
| 47.27 | 1.921 | 100.0 |

3.4.3 EFFECTS OF SPUTTERING GAS PRESSURE IN LANTHANUM ALUMINATE DEPOSITION

The effects of sputtering gas total pressure and the partial pressures of argon and oxygen on film quality deposited onto sapphire [1102], silicon (110), and glass were investigated. The sputtering gas pressures used for this study were approximately 6, 9, and 12 mTorr and the partial pressure of argon to oxygen ratios were 2:1 and 3:1. The remaining deposition parameters are listed in Table 3.4.12.

The EDS compositional results are listed in Table 3.4.13. The compositional analysis of the lanthanum aluminate target gave the following element atomic percentages: 33.09 La, 47.51 Al, 18.35 Cl, and 1.06 K.

TABLE 3.4.12

Deposition Parameters for Gas Pressure Study

| RF-Sputtering Parameters | Samples | | | | | |
|---|---------------------|---------------------|---------------------|---------------------|---------------------|---------------------|
| | LAO-1 | LAO-2 | LAO-3 | LAO-5 | LAO-6 | LAO-7 |
| Target Orientation | LAO off- axis | LAO off- axis | LAO off- axis | LAO off- axis | LAO off- axis | LAO off- axis |
| Rotating Substrate Holder | | | | | | |
| Substrate Height (cm) | 2 | 2 | 2 | 2 | 2 | 2 |
| RF-Power (Watts) | 100 | 100 | 100 | 100 | 100 | 100 |
| Base Pressure ($\times 10^{-4}$ Torr) | 3.0 | 1.6 | 0.28 | 1.6 | 1.6 | 1.9 |
| Sputtering Gas Pressure (mTorr) | 5.7 | 10.0 | 9.0 | 6.0 | 9.1 | 12.0 |
| Argon Pressure (mTorr) | 3.9 | 7.9 | 6.0 | 4.5 | 6.8 | 9.0 |
| Oxygen Pressure (mTorr) | 1.8 | 2.4 | 3.0 | 1.5 | 2.3 | 3.0 |
| Ar / O ₂ | 2.2 | 3.3 | 2.0 | 3.0 | 3.0 | 3.0 |
| Deposition Time (Hours) | 2 | 2 | 0.42 | 2 | 2 | 2 |

TABLE 3.4.13

EDS Compositional Results for Lanthanum Aluminate
Films Deposited onto Sapphire and Silicon
At Different Sputtering Pressures

| Substrate | Sample Id. | Atomic Percent ($\pm 1\%$) | | | La/Al |
|-----------|------------|------------------------------|-------|------|--------|
| | | La | Al | Cl | |
| Sapphire | LAO-1 | 14.41 | 84.19 | 1.41 | - |
| | LAO-2 | 17.17 | 81.37 | 1.46 | - |
| | LAO-3 | 2.70 | 97.04 | 0.27 | - |
| | LAO-5 | 17.34 | 81.15 | 1.50 | - |
| | LAO-6 | 20.40 | 78.16 | 1.43 | - |
| | LAO-7 | 18.46 | 80.12 | 1.42 | - |
| | Silicon | LAO-1 | 8.23 | 9.44 | 0.61 |
| LAO-2 | | 10.82 | 13.85 | 1.16 | 0.781 |
| LAO-3 | | 1.32 | 2.24 | 0.12 | 0.589 |
| LAO-5 | | 10.05 | 11.91 | - | 0.8438 |
| LAO-6 | | 13.83 | 15.48 | 1.02 | 0.893 |
| LAO-7 | | 12.60 | 14.77 | 0.96 | 0.85 |

The ratio of lanthanum to aluminum for the target was computed to be 0.6965. The films deposited onto silicon differ in composition from the target stoichiometry. The film compositions are closer to the desired film stoichiometry, since the ratio of lanthanum to aluminum is closer to 1:1 (Table 3.4.13). The EDS analysis samples the substrate as well as the film making it difficult to draw significant conclusions about the composition of the films deposited onto sapphire. Lanthanum aluminate has a slightly greater deposition rate onto sapphire than silicon, since

more lanthanum is detected on sapphire than silicon. All the films deposited onto sapphire and silicon have lower or even unmeasurable concentrations of chlorine and potassium as compared to the target. The total sputtering pressures and argon and oxygen partial pressures did not greatly affect the stoichiometry of the films.

However, slightly higher deposition rates were observed with an argon to oxygen ratio of 3:1. The morphology of the films did not vary greatly with the pressure changes. The films were smooth and continuous with some pinholes (Figures 3.4.9 - 3.4.11).

The XRD patterns show that the deposited films on both sapphire and silicon substrates are amorphous. Since our research mainly concentrated on the deposition of LaAlO_3 onto sapphire substrates, only the XRD patterns for lanthanum aluminate films deposited onto sapphire are presented (Figures 3.4.12 - 3.4.14). Table 3.4.14 summarizes the XRD analysis of the diffraction patterns. No lanthanum aluminate diffraction peaks were observed in the diffraction patterns. Samples LAO-1 through LAO-3 were analyzed with the powder diffractometer and the most of the diffraction peaks observed are from the sapphire substrate. Samples LAO-5 through LAO-7 were analyzed with the four-circle diffractometer. The films were aligned perpendicular with respect to the incident x-ray beam and then rotated by 85°

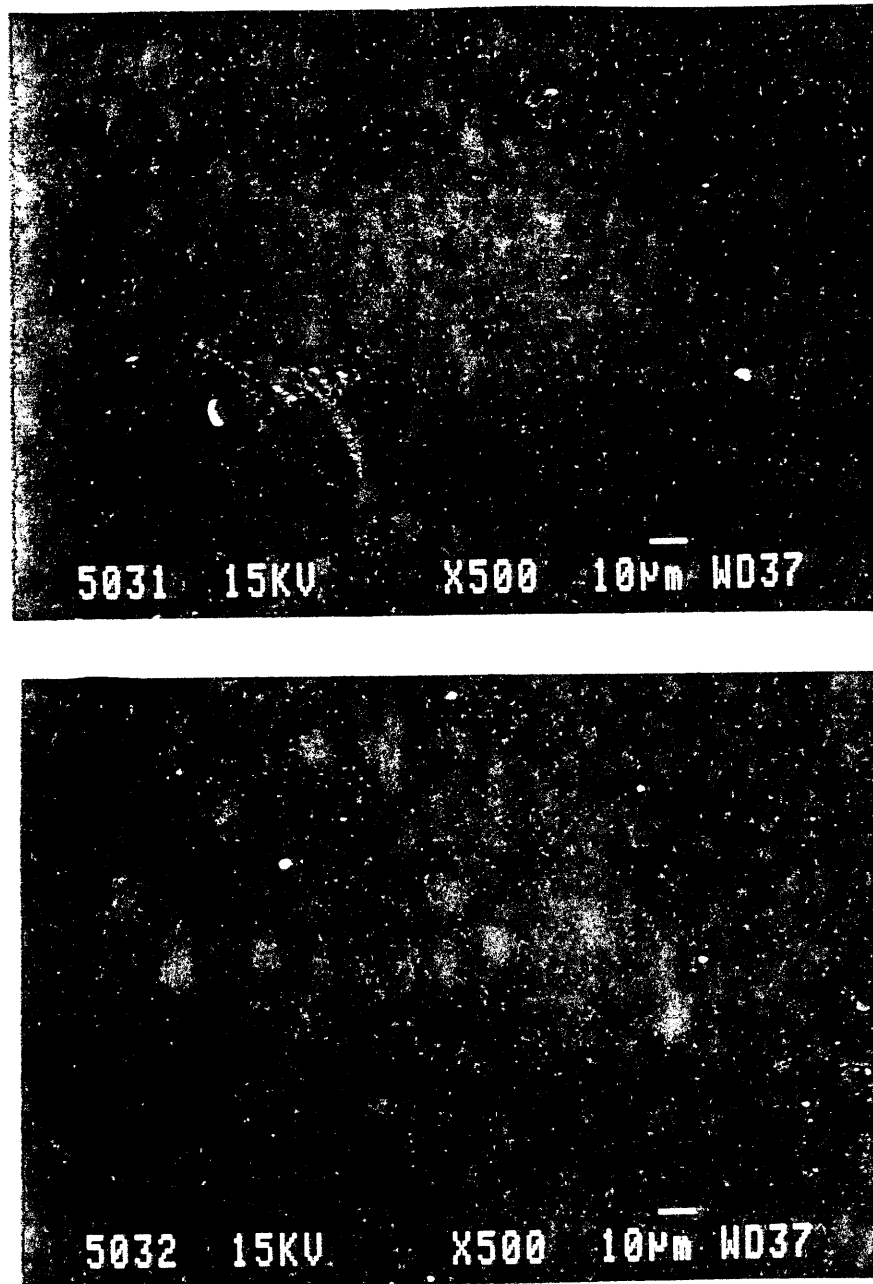


Figure 3.4.9: Top micrograph shows the morphology of a dielectric film deposited onto sapphire at 9.0 mTorr with argon to oxygen ratio of 2.0:1.0. The bottom micrograph shows the morphology of the dielectric film deposited onto sapphire at 6 mTorr with argon to oxygen ratio of 3.0:1.0.

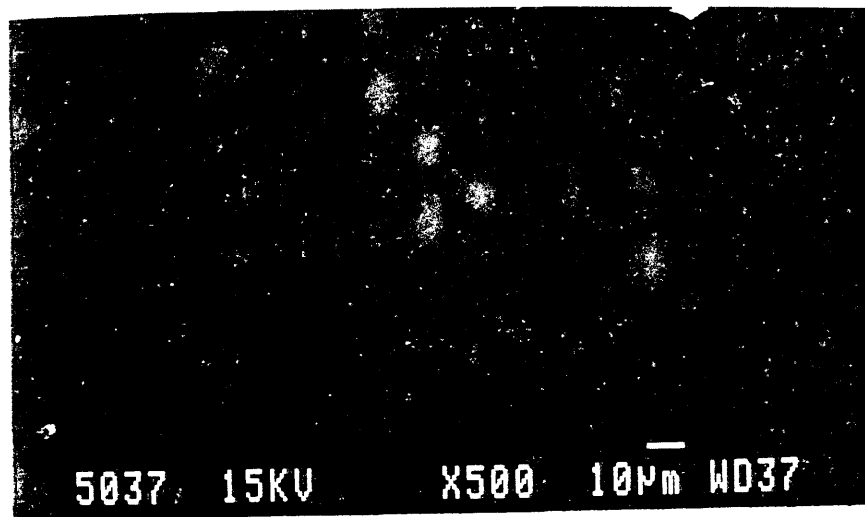
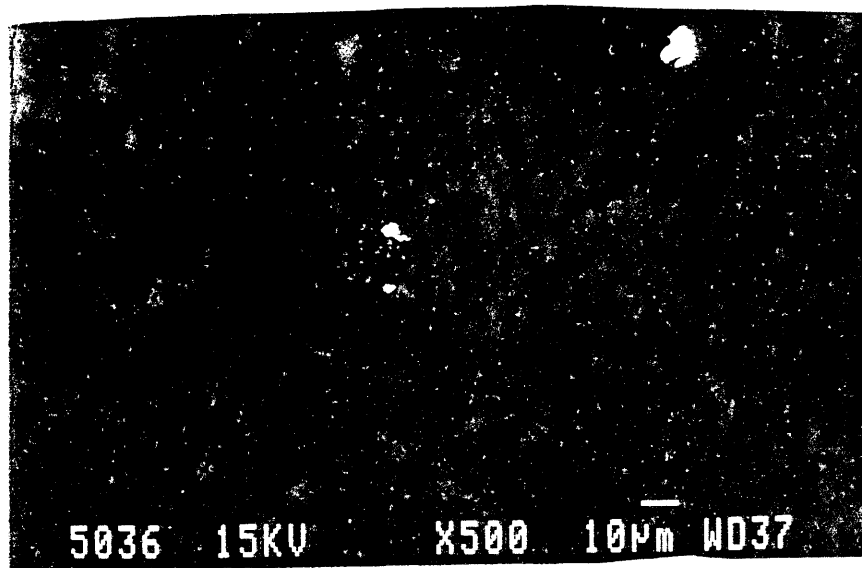


Figure 3.4.10: Top micrograph shows the morphology of a dielectric film deposited onto sapphire at 9.1 mTorr with argon to oxygen ratio of 3.0:1.0. The bottom micrograph shows the morphology of the dielectric film deposited onto sapphire at 12 mTorr with argon to oxygen ratio of 3.0:1.0.

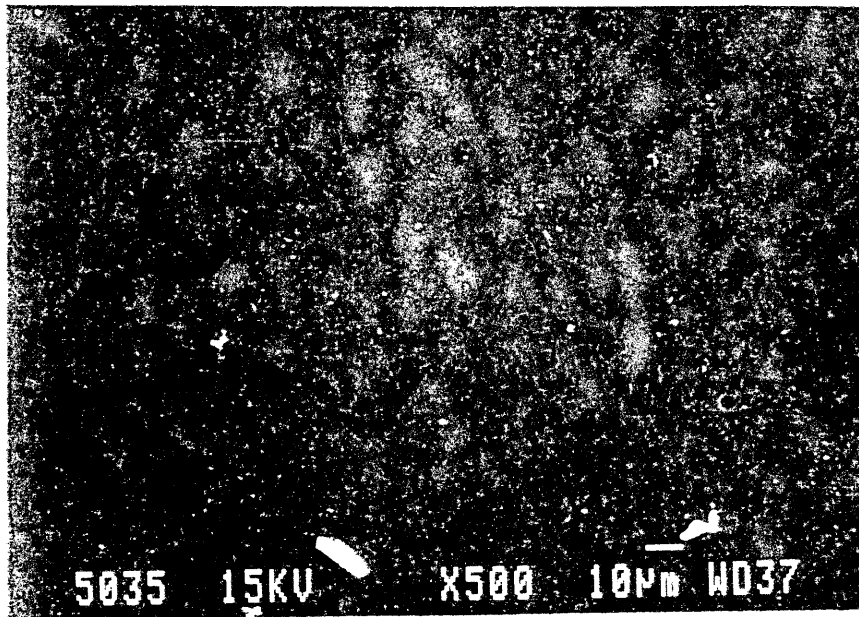
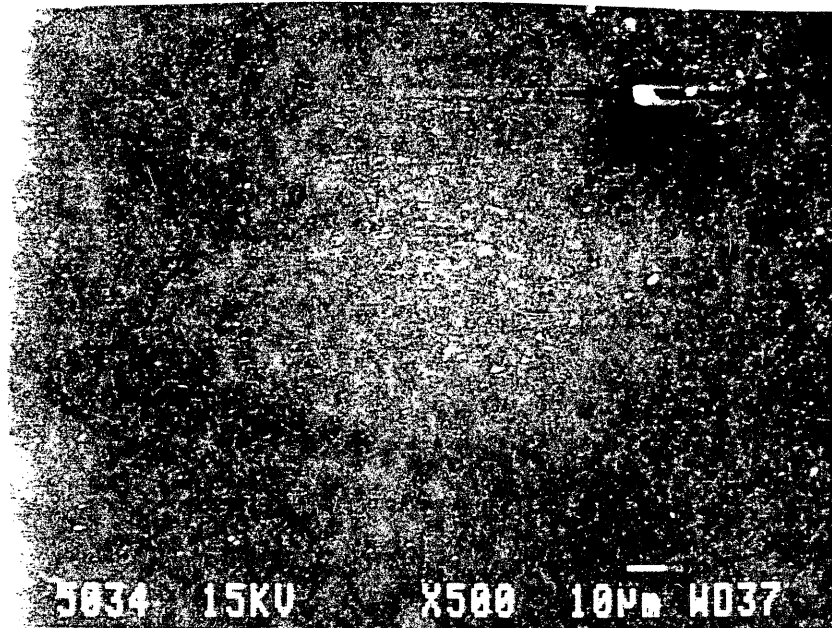


Figure 3.4.11: Top micrograph shows the morphology of a dielectric film deposited onto silicon at 9.0 mTorr with argon to oxygen ratio of 2.0:1.0. The bottom micrograph shows the morphology of the dielectric film deposited onto silicon at 6 mTorr with argon to oxygen ratio of 3.0:1.0.

for a 2θ scan. The Bragg diffraction peaks in the scan are difficult to identify since the substrate and films were not aligned parallel with the incident beam. For similar reasons as stated in earlier sections we can conclude that the as-deposited films are not polycrystalline. The diffraction peaks located at approximately 5° are attributed to the clay used to mount the samples onto the goniometer since the d-spacing is so large. The other Bragg diffractions in the diffraction patterns are probably from the substrate even though their d-spacings do not match the reported d-spacings for sapphire. The incorrect positions of the Bragg peaks are due to the misalignment of the substrate. The alignment procedure was later modified to correct this problem by aligning both the substrate and film parallel with the incident x-ray beam.

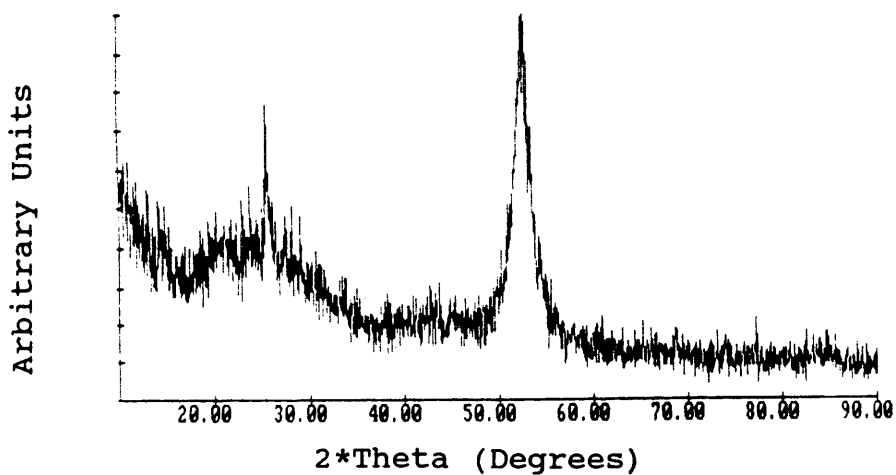
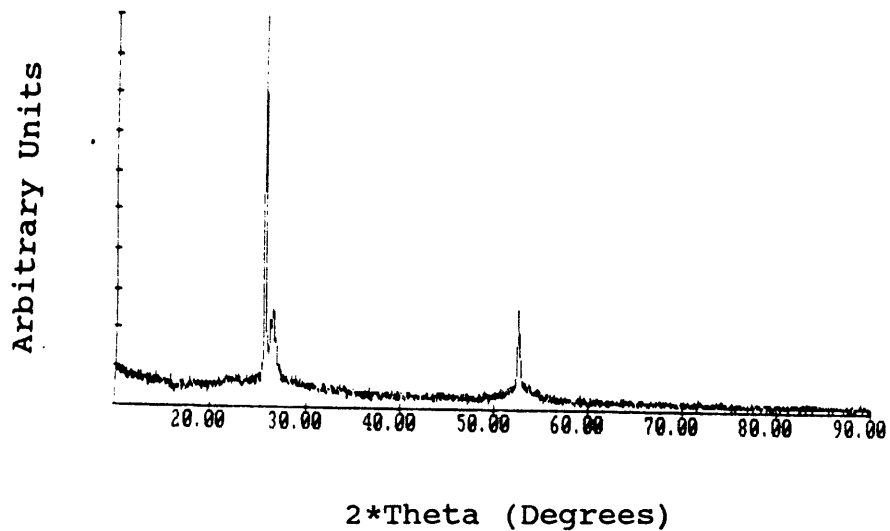


Figure 3.4.12: Top XRD pattern for the dielectric film deposited onto sapphire at 3.7 mTorr with argon to oxygen ratio of 2.2:1.0. The bottom XRD pattern for the dielectric film deposited onto sapphire at 10 mTorr with argon to oxygen ratio of 3.3:1.0.

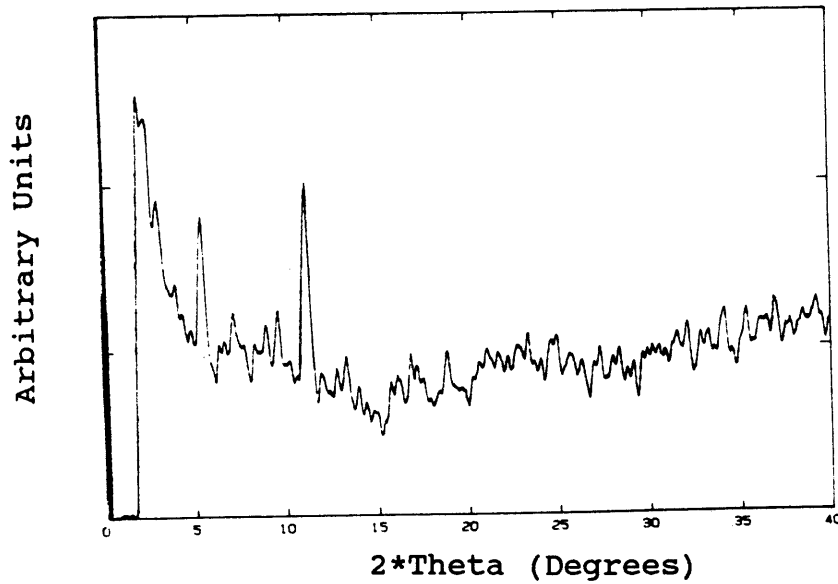
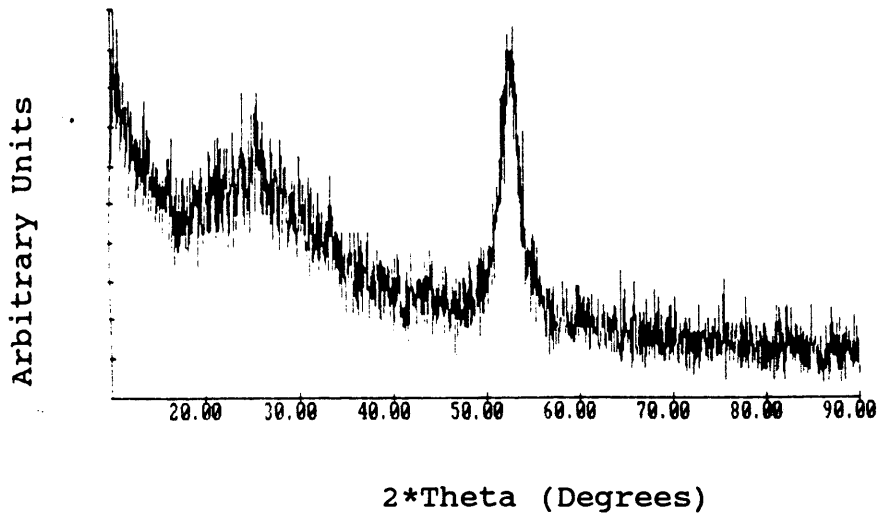


Figure 3.4.13: The top XRD pattern for the dielectric film deposited onto sapphire at 9.0 mTorr with argon to oxygen ratio of 2.0:1.0. The bottom XRD pattern for the dielectric film deposited onto sapphire at 6 mTorr with argon to oxygen ratio of 3.3:1.0.

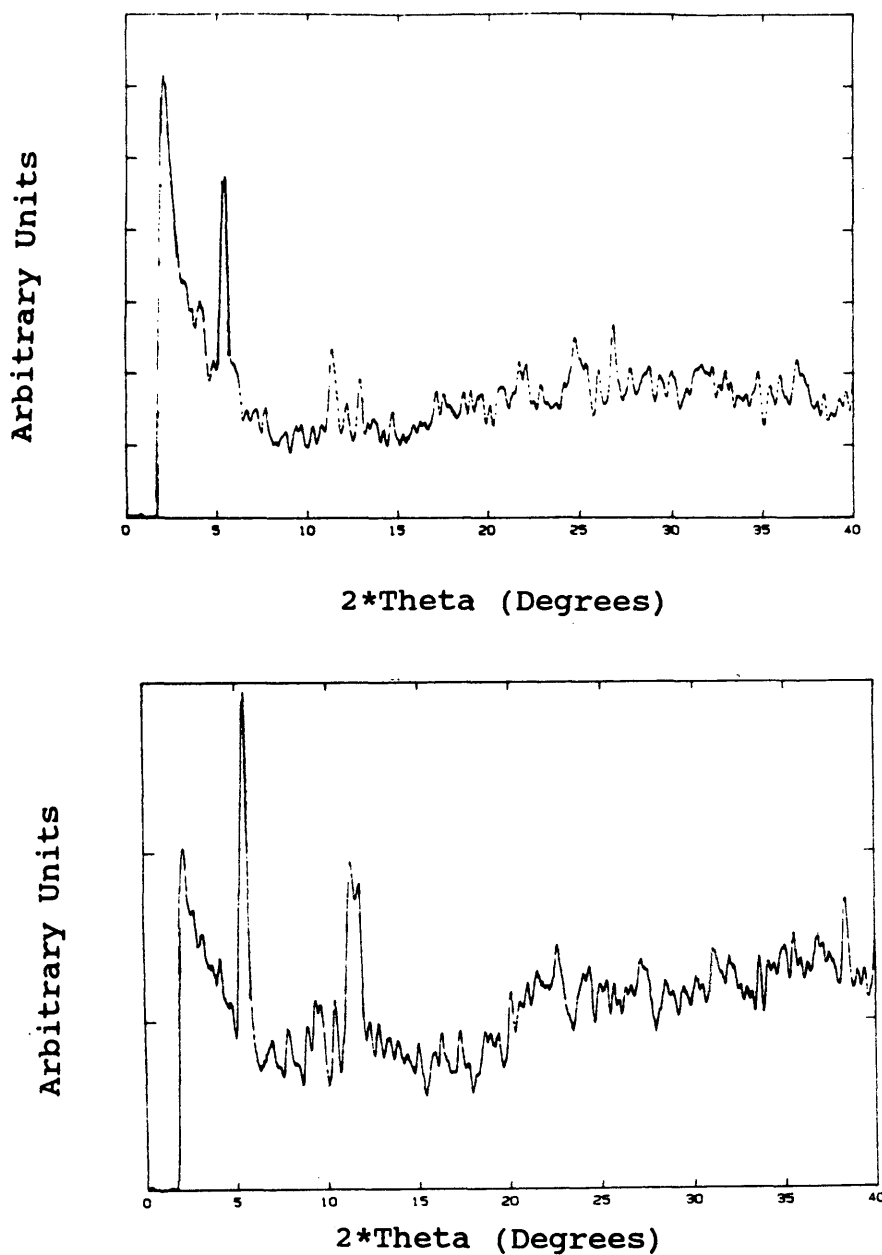


Figure 3.4.14: The top XRD pattern for the dielectric film deposited onto sapphire at 9.1 mTorr with argon to oxygen ratio of 2.0:1.0. The bottom XRD pattern for the dielectric film deposited onto sapphire at 12 mTorr with argon to oxygen ratio of 3.0:1.0.

Table 3.4.14

XRD Analysis Results for Dielectric Films
Deposited onto Sapphire With Different
Sputtering Gas Pressures

| Sample ID | 2θ (Degrees) | d-spacing (Å) | Normalized Peak Height | Diffraction Peak Identification |
|-----------|---------------------|---------------|------------------------|--|
| LAO-1 | 25.67 | 3.468 | 100.0 | 102 Sapphire Not Al_2O_3 , La_2O_3 , LaAlO_3 , and Ag. |
| | 26.50 | 3.361 | 25.2 | |
| LAO-2 | 52.61 | 1.738 | 25.6 | 204 Sapphire |
| | 25.83 | 3.450 | 77.0 | 102 Sapphire |
| | 52.80 | 1.730 | 100.0 | 204 Sapphire |
| LAO-3 | 53.00 | 1.727 | 100.0 | 102 Sapphire |
| LAO-5 | 5.52 | 7.38 | 93.0 | Clay |
| | 11.21 | 3.64 | 100.0 | |
| LAO-6 | 5.52 | 7.38 | 100.0 | Clay |
| | 11.29 | 3.61 | 66.1 | |
| | 38.45 | 1.08 | 57.6 | |
| LAO-7 | 5.50 | 7.41 | 100.0 | Clay |
| | 11.38 | 3.58 | 43.3 | |
| | 12.93 | 3.16 | 30.0 | |
| | 26.78 | 1.53 | 41.8 | |

3.4.4 POST-ANNEALING EFFECTS ON LANTHANUM ALUMINATE FILMS

A post-annealing study was performed on as-deposited films on sapphire and silicon substrates. The qualities of the as-deposited and post-annealed films were compared. Table 3.4.15 lists the deposition parameters used in this study. An SEM micrograph of an as-deposited film on sapphire shows a rough granular microstructure and on silicon a smooth microstructure (Figure 3.4.15). The EDS compositional analysis for these as-deposited films results

TABLE 3.4.15

Deposition Parameters For Post-Annealing Study
of Lanthanum Aluminate Films on Sapphire
and Silicon Substrates

| Deposition Parameters | |
|--|---------------------------|
| Target | LaAlO ₃ |
| Orientation | Off-Axis |
| Heated Stationary Substrate Holder | |
| RF-Power | 150 W |
| Substrate Height | 2 cm |
| Substrate Distance | 4 cm |
| Substrate Temperature | 650°C |
| Base Pressure | 9 x 10 ⁻⁵ Torr |
| Average Total Sputtering Gas Pressure | 9.0 mTorr |
| Average Argon Pressure | 6.8 mTorr |
| Average Oxygen Pressure | 2.2 mTorr |
| Deposition Time | 4 Hours |

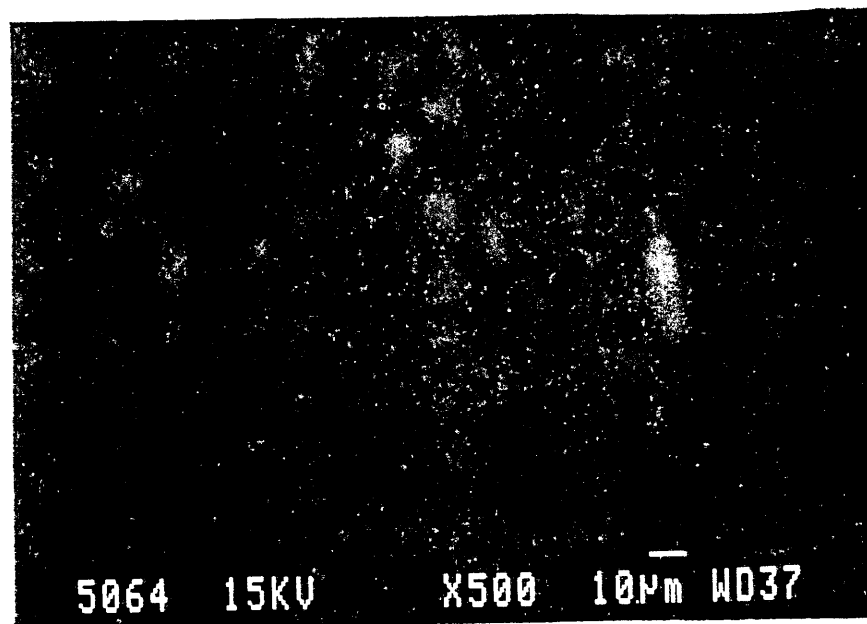
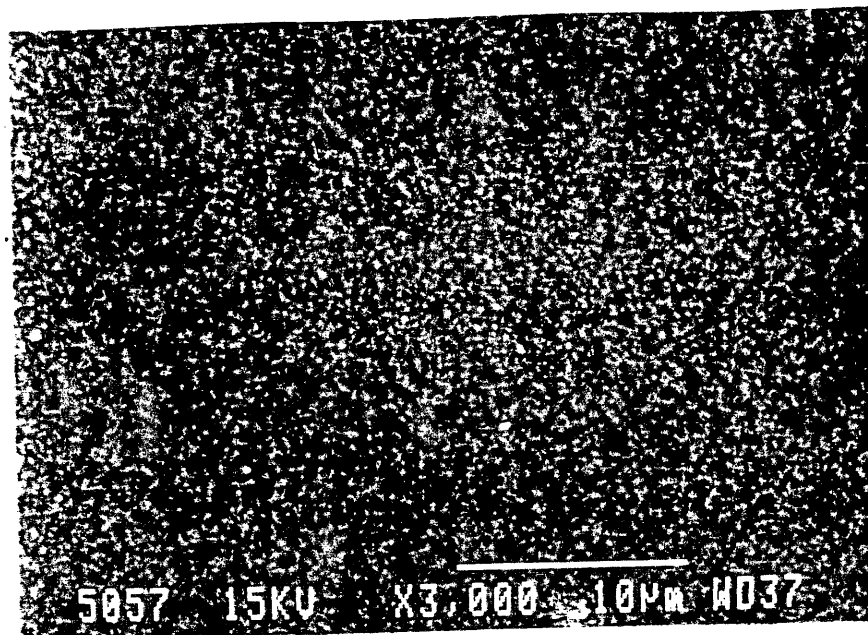


Figure 3.4.15: Top micrograph shows the morphology of the amorphous, granular LaAlO₃ film deposited onto sapphire. Bottom micrograph shows the morphology of the amorphous, smooth LaAlO₃ film deposited onto silicon.

are listed in Table 3.4.16. The stoichiometries of these films are close to the expected 1:1 ratio for lanthanum to aluminum. It is also interesting to note that both films have approximately the same stoichiometries. This observation will be discussed in more detail in Section 3.4.6. X-ray diffraction patterns for the as-deposited films indicate that the films are amorphous (Figure 3.4.16).

The samples were post-annealed in the furnace with the heat treatment listed in Table 3.4.17. The samples were placed into an alumina crucible and heated in air. After annealing both films were cloudy and did not reflect light as well as before. SEM micrographs for films on sapphire and silicon substrates show large cracks and peeling away from the substrate (Figure 3.4.17). The cracks are most likely caused by the large mismatch in coefficients of thermal expansion (CTE) of the film and substrate (See Table 1.2.4). The percent difference of CTE between lanthanum aluminate and sapphire, or silicon are 12 and 78 respectively. The CTE for sapphire used in these calculations is the average CTE and not the actual CTE along the [1102] direction. EDS compositional analysis shows that the film compositions remain the same as for the as-deposited film (Table 3.4.18).

The x-ray diffraction patterns for the samples contain lanthanum aluminate Bragg diffraction peaks as shown in

TABLE 3.4.16

Compositional Analysis of As-deposited Films
onto Sapphire and Silicon Substrates

| Substrate | Element | Atomic Percent |
|-----------|---------|----------------|
| Sapphire | La | 45.25 ± 1.0 |
| | Al | 54.75 ± 1.0 |
| Silicon | La | 44.77 ± 1.0 |
| | Al | 52.70 ± 1.0 |
| | Si | 2.53 ± 1.0 |

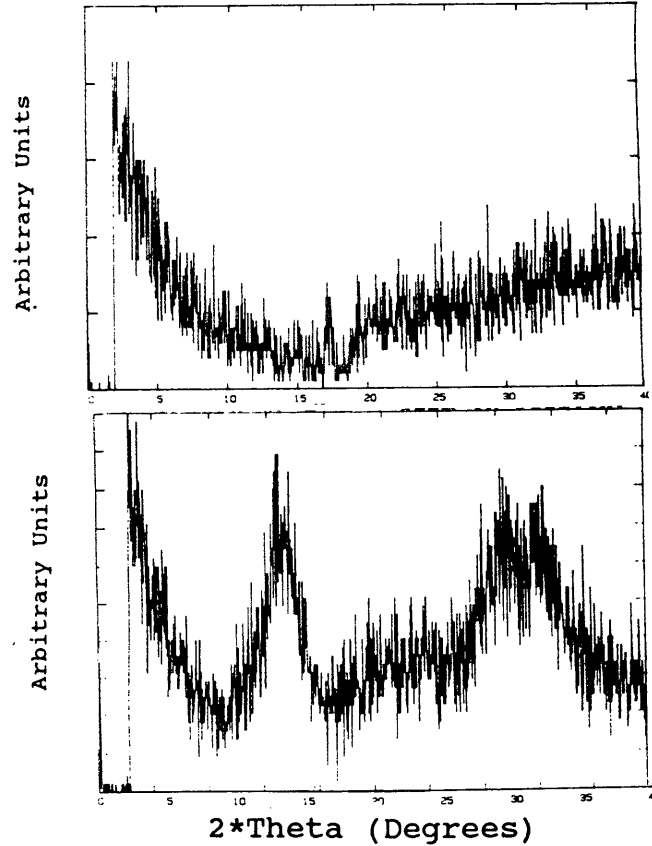


Figure 3.4.16: The top XRD pattern for as-deposited amorphous LaAlO_3 film on sapphire. The bottom XRD pattern for as-deposited amorphous LaAlO_3 film on silicon.

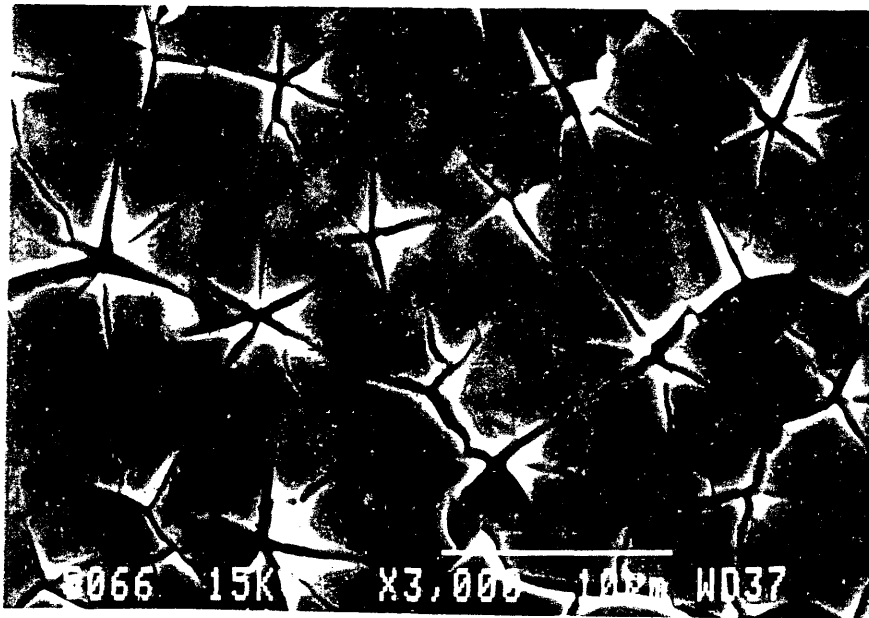
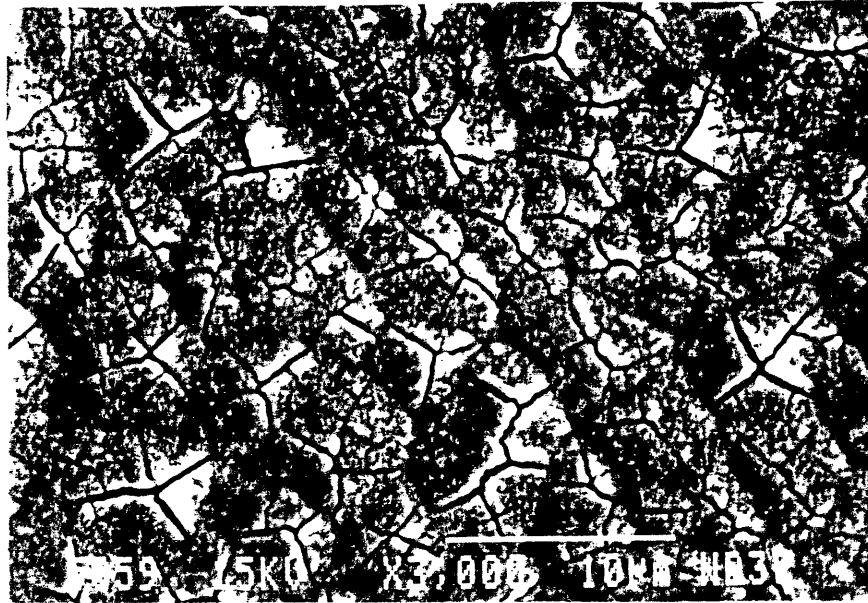


Figure 3.4.17: Top micrograph shows the morphology of the cracked post-annealed LaAlO_3 film on sapphire. Bottom micrograph shows the morphology of the cracked post-annealed LaAlO_3 film on silicon.

TABLE 3.4.17

Post-Annealing Conditions for Lanthanum
Aluminate Deposited onto Sapphire
and Silicon Substrates

| | |
|-----------------------|-----------|
| Heating Rate | 10°C/Min. |
| Annealing Temperature | 850°C |
| Annealing Time | 1 Hour |
| Cooling Rate | 10°C/Min. |
| Heating Environment | Air |

TABLE 3.4.18

Compositional Analysis of Post-Annealed
Lanthanum Aluminate Films Deposited
onto Sapphire and Silicon

| Substrate | Element | Atomic Percent |
|-----------|---------|----------------|
| Sapphire | La | 45.16 ± 1.0 |
| | Al | 54.62 ± 1.0 |
| | Cl | 0.22 ± 1.0 |
| Silicon | La | 40.59 ± 1.0 |
| | Al | 46.99 ± 1.0 |
| | Si | 12.43 ± 1.0 |

Figure 3.4.18. The lanthanum aluminate film on silicon has the (100), (110), (111), (200), (210), and (211) diffraction peaks. The film on sapphire is missing (100) and (110) lanthanum aluminate diffraction peaks, but contains (111), (200), (210), (220) peaks. There may have been an problem with the alignment of the sample and incident x-ray beam which could account for the missing Bragg diffraction peaks. Also there are some diffraction peaks that are not associated with lanthanum aluminate. The diffraction peak at 17.18° is (111) silver from the silver paste used to mount the substrates. The peak located at 5.46° has been observed in other diffraction patterns and is most likely from the clay used to mount the sample onto the pin, because of the large d-spacing value. The diffraction peaks at 9.12° and 11.28° are not sapphire, lanthanum chloride or aluminum chloride and remain unidentified.

Since both diffraction patterns contain all or most of the diffraction peaks listed in the powder diffraction tables for lanthanum aluminate, the films are randomly oriented. The absence of a well defined peak in the rocking curve analyses of these films confirmed that the films were randomly oriented (Figure 3.4.19). The d-spacings for the diffraction peaks are listed in Table 3.4.19. The d-spacings were calculated using Equation 2.2 as previously described in Section 2.4. The relative peak heights for the

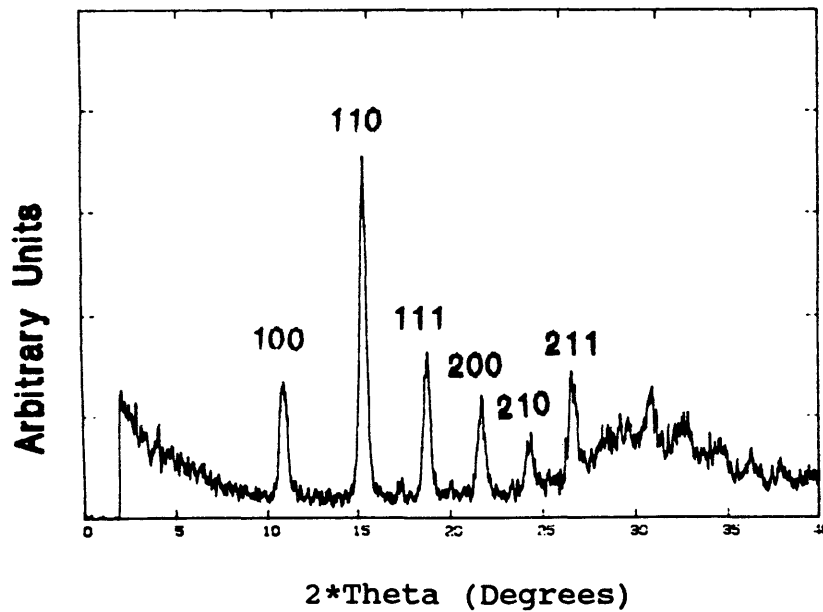
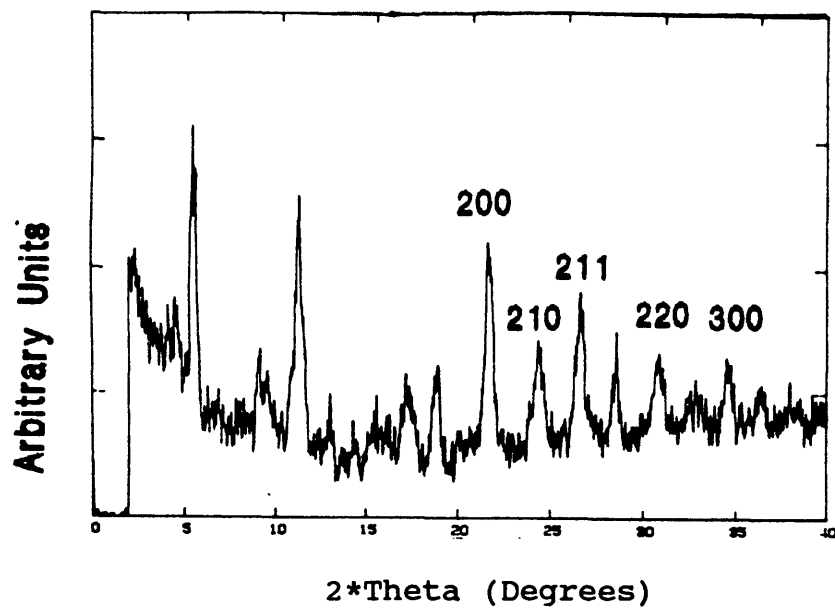


Figure 3.4.18: The top XRD pattern showing the post-annealed LaAlO_3 film on sapphire is randomly oriented. The bottom XRD pattern showing the post-annealed LaAlO_3 film on silicon is randomly oriented.

LaAlO₃ on sapphire were difficult to compare with that of the LaAlO₃ powder reported in Table 3.3.1 since the first three diffraction peaks are missing in the pattern. The normalized peak heights for LaAlO₃ on silicon did not match those measured for LaAlO₃ powder (Table 3.3.1). The average pseudo-cubic lattice parameters calculated from the diffraction patterns are 3.774 ± 0.016 Å and 3.766 ± 0.011 Å for sapphire and silicon substrates, respectively. Compared to the lattice constant for lanthanum aluminate powder (3.788 ± 0.009 Å) the lattice constant for the film on sapphire was within the experimental uncertainty. The lattice constant for the film on silicon was essentially the same the powder lattice constant.

Another post-annealing study was performed to determine the minimum post-annealing temperature required to crystallize the lanthanum aluminate films. Lanthanum aluminate was deposited onto sapphire and silicon with the depositions condition listed in Table 3.4.20. The thickness of these films measured with the quartz-crystal oscillator was approximately 3500 Å. The diffraction patterns for the as deposited films are amorphous (Figure 3.4.20). The Bragg diffraction peaks observed in the diffraction pattern for the as-deposited film on sapphire are identified as sapphire (102) and (204) peaks. The films were post-annealed for one hour in air beginning at 500 °C and increasing by steps of

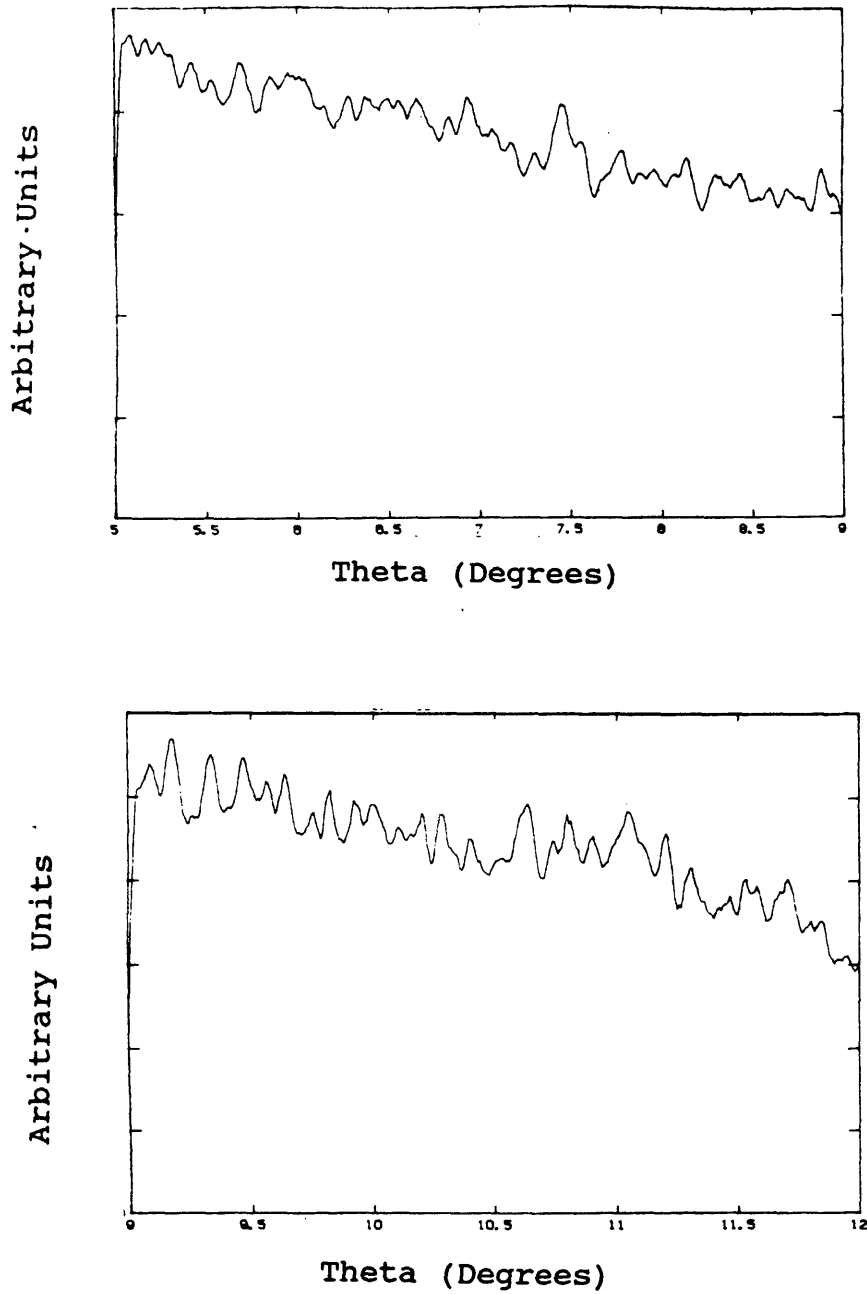


Figure 3.4.19: The top rocking curve for post-annealed LaAlO_3 film on sapphire confirmed that the film was randomly oriented. The bottom rocking curve for post-annealed LaAlO_3 film on silicon confirmed that the film was randomly oriented.

TABLE 3.4.19

Calculated d-Spacings for Post-Annealed
Lanthanum Aluminate Films

| Substrate | $2*\theta$ | d-Spacing (Å) | Normalized Peak Height | LaAlO ₃ hkl |
|-----------|------------|------------------|---------------------------|---------------------------|
| Sapphire | 5.46 | 7.46 | 100.0 | |
| | 9.12 | 4.47 | 33.9 | |
| | 11.28 | 3.616 | 96.6 | |
| | 17.18 | 2.379 | 32.9 | |
| | 18.92 | 2.162 | 39.7 | |
| | 21.60 | 1.896 | 78.3 | 200 |
| | 24.32 | 1.687 | 40.7 | 210 |
| | 26.62 | 1.544 | 57.2 | 211 |
| | 30.84 | 1.336 | 27.9 | 220 |
| | 34.50 | 1.198 | 27.9 | 300 |
| Silicon | 10.88 | 3.748 | 37.4 | 100 |
| | 15.34 | 2.663 | 100.0 | 110 |
| | 18.82 | 2.174 | 44.0 | 111 |
| | 21.72 | 1.886 | 30.8 | 200 |
| | 24.42 | 1.680 | 15.4 | 210 |
| | 26.60 | 1.545 | 30.0 | 211 |
| | 30.90 | 1.334 | 18.7 | 220 |

Table 3.4.20

Deposition Parameters for Minimum Crystallization
Temperature for Post-Annealed Lanthanum
Aluminate Films

RF-Sputtering Parameters

| | |
|---------------------------------------|-----------------------------|
| Target | LaAlO ₃ |
| Orientation | Off-Axis |
| Stationary Heated Substrate Holder | |
| Substrate Height | 1.5 cm |
| Substrate Distance | 4.5 cm |
| Substrate Temperature | 750°C |
| RF-Power | 75 W |
| Base Pressure | 1.6 x 10 ⁻⁴ Torr |
| Argon Pressure | 12 mTorr |
| Oxygen Pressure | 4.1 mTorr |
| Total Sputtering Gas Pressure | 16 ± 2 mTorr |
| Deposition Time | 2 Hours |

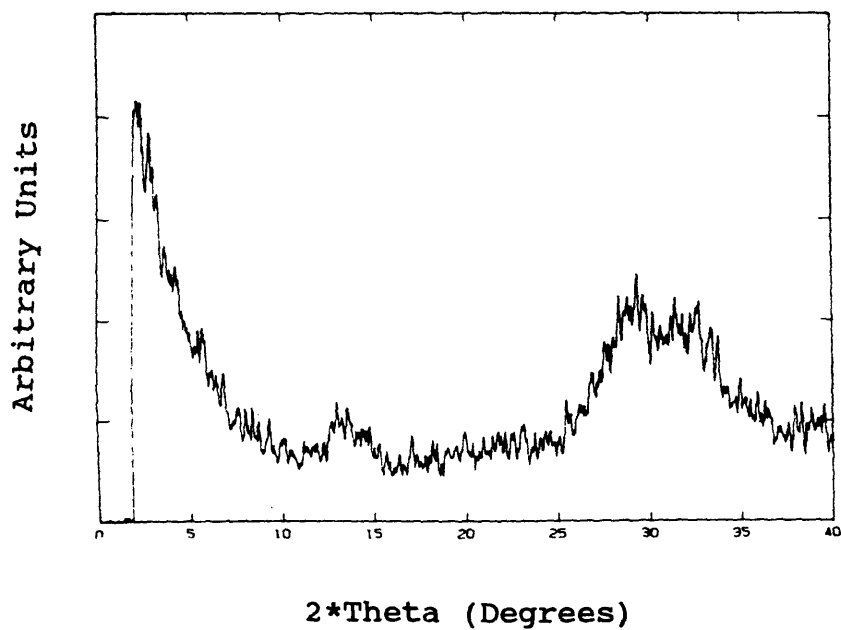
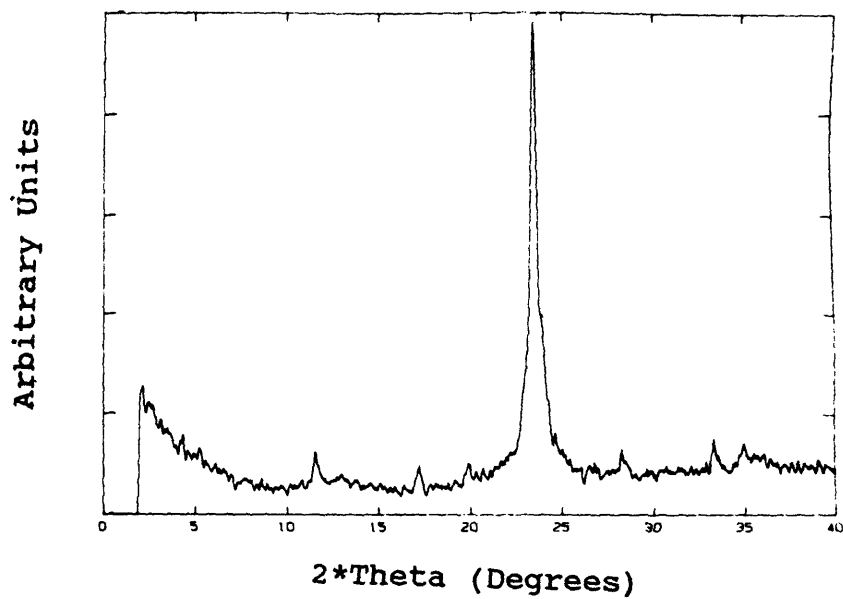


Figure 3.4.20: The top XRD pattern for amorphous LaAlO_3 film deposited onto sapphire. The bottom XRD pattern for amorphous LaAlO_3 film deposited onto silicon.

The films were post-annealed for one hour in air beginning at 500 °C and increasing by steps of 50°C to a maximum temperature of 900°C. A typical heating cycle is listed in Table 3.4.21. After each heat treatment the films were characterized with XRD. The films annealed at 800°C and below were amorphous. However the XRD patterns for films annealed at 850°C have (100), (110), (111), and (200) lanthanum aluminate diffraction peaks (Figure 3.4.21). The rest of the lanthanum aluminate powder diffraction peaks cannot be distinguished from background in these diffraction patterns. The d-spacings and relative intensities are listed in Table 3.4.22. The relative peak heights on the post-annealed LaAlO_3 film on sapphire match fairly well with the measured relative peak heights for the LaAlO_3 powder (Table 3.3.1). The largest deviation observed was the relative intensity for the (100) peak which was 62.8 instead of 49.3. The relative peak heights for the post-annealed LaAlO_3 film on silicon also matched closely with the measured intensities for LaAlO_3 powder. Again, the largest deviation for relative peak height was seen in the (100) peak. The relative peak height was 74.0. EDS compositional measurements were performed on the samples after they were annealed at 850°C, since earlier post-annealing study showed that the film compositions do not vary significantly using these post-annealing conditions.

TABLE 3.4.21

Heating Conditions for Minimum Crystallization
Temperature Study

| | |
|--|-----------|
| Heating Rate | 10°C/Min. |
| Cooling Rate | 10°C/Min. |
| Annealing Time at Maximum Temperature | 1 Hour |
| Air Annealing Environment | |

TABLE 3.4.22

Summary of XRD Analysis For Post-Annealed LaAlO₃
Films on Sapphire and Silicon Substrates

| Substrate | 2* θ (Degrees) | d-Spacing (Å) | Normalized Peak Height | Bragg Peak Identification |
|-----------|--------------------------|------------------|---------------------------|------------------------------|
| Sapphire | 5.1 | 8.0 | | Clay |
| | 10.69 | 3.815 | 62.8 | (100) LaAlO ₃ |
| | 15.17 | 2.692 | 100.0 | (110) LaAlO ₃ |
| | 18.53 | 2.207 | 47.3 | (111) LaAlO ₃ |
| | 21.83 | 1.877 | 37.6 | (200) LaAlO ₃ |
| Silicon | 10.74 | 3.797 | 74.0 | (100) LaAlO ₃ |
| | 15.28 | 2.673 | 100.0 | (110) LaAlO ₃ |
| | 18.62 | 2.197 | 48.1 | (111) LaAlO ₃ |
| | 21.58 | 1.898 | 48.4 | (200) LaAlO ₃ |

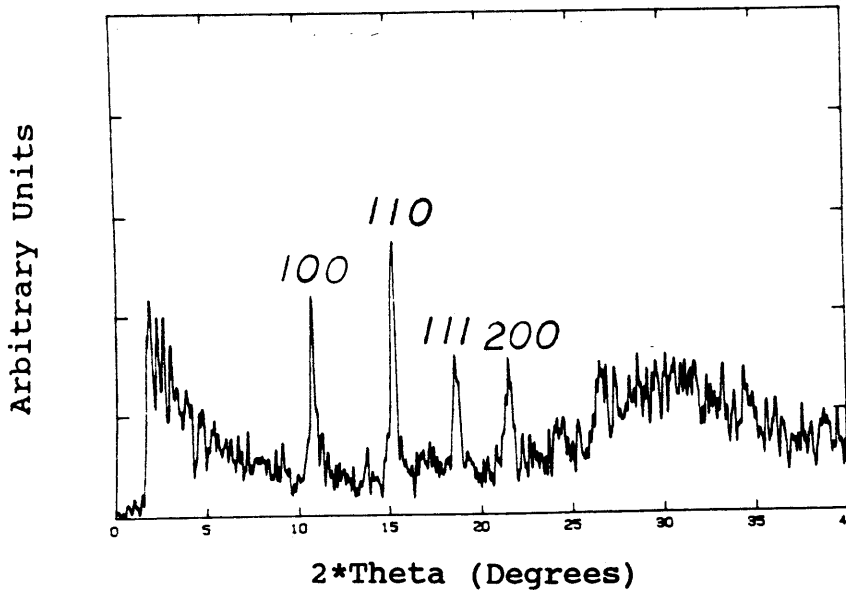
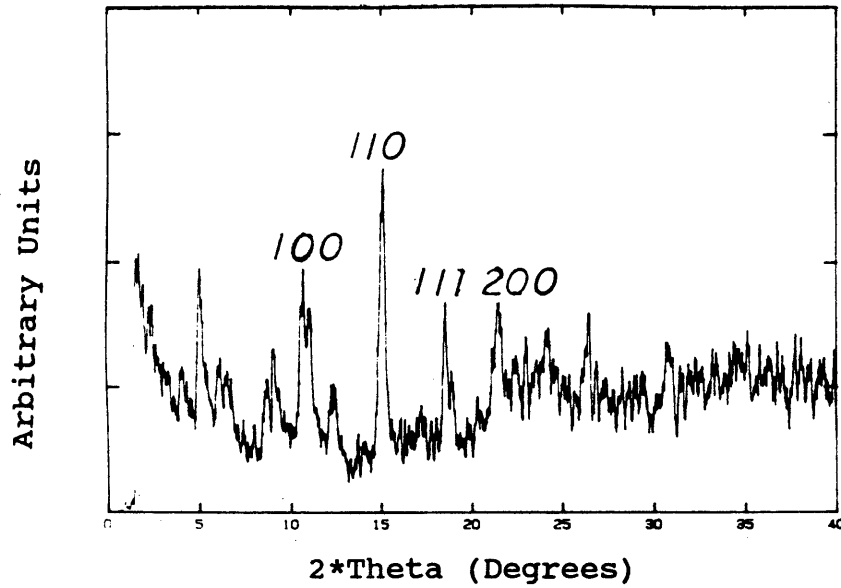


Figure 3.4.21: The top XRD pattern for post-annealed (850°C) LaAlO_3 film on sapphire. The bottom XRD pattern for post-annealed (850°C) LaAlO_3 film on silicon.

The EDS compositional results are listed in Table 3.4.23. SEM analysis shows the films are rough and cracked. However, the cracking does not appear to be as severe as seen in the previous study. This is most likely due to the thinner thickness of the films (Figure 3.4.22).

TABLE 3.4.23

Compositional Results for Minimum Crystallization Temperature Study

| Substrate | Element | Atomic Percent | |
|-----------|---------|----------------|-------------|
| | | Overall Film | Particle |
| Sapphire | La | 19.18 ± 1.0 | 25.96 ± 1.0 |
| | Al | 80.82 ± 1.0 | 74.04 ± 1.0 |
| Silicon | La | 18.85 ± 1.0 | 31.41 ± 1.0 |
| | Al | 19.59 ± 1.0 | 41.93 ± 1.0 |
| | Si | 61.56 ± 1.0 | 23.71 ± 1.0 |
| | Ag | 0.0 | 2.94 ± 1.0 |

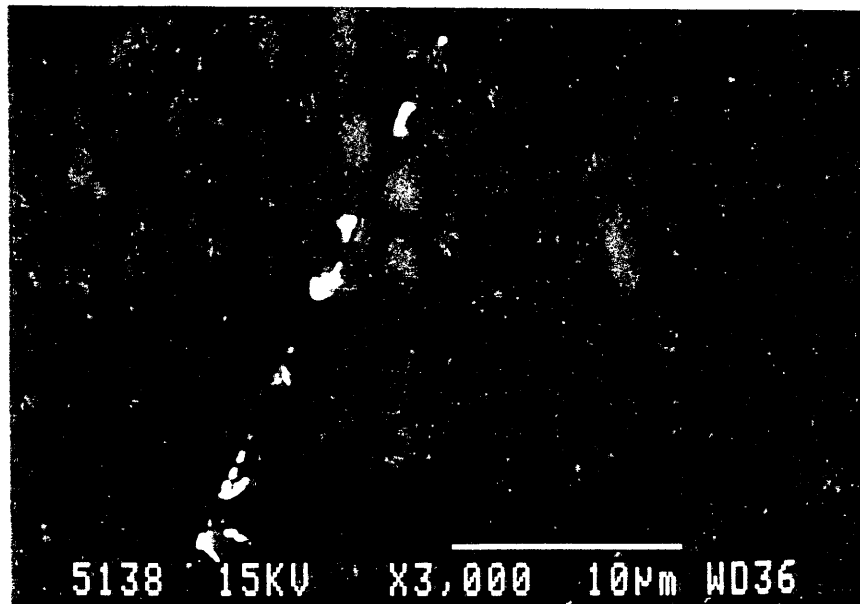
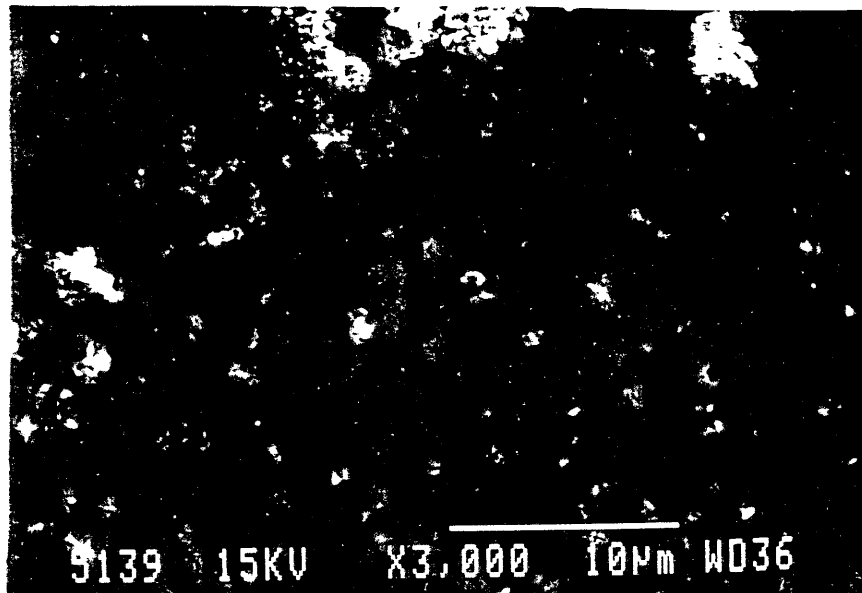


Figure 3.4.22: Top micrograph shows the morphology of LaAlO₃ film on sapphire post-annealed at 850°C. The bottom micrograph shows the morphology of the LaAlO₃ film on silicon post-annealed at 850°C.

3.4.5 METALLIC BUFFER LAYERS

One of the most critical parameters in growing epitaxial films is that the substrate lattice parameter should match very closely with that of the epitaxial film. Several studies have reported the deposition of superconducting films onto metallic buffer layers on sapphire and silicon substrates (24,54,55). The deposition of metallic buffer layers is simpler than ceramic oxide layers since oxygen depletion in the buffer layer is not a problem. Copper and silver lattice constants match closely with the pseudo-cubic lattice constant of lanthanum aluminate. The lattice parameters are listed in Table 3.4.24. Copper and silver can easily be deposited onto sapphire and silicon by using evaporation. For these reasons a study investigating the quality of lanthanum aluminate films deposited onto copper and silver buffer layers on sapphire and silicon substrates was initiated.

Initially, copper was deposited onto silicon and sapphire substrates by rf-sputtering. (See Table 3.4.25 for sputtering parameters used to deposited the copper films.) Visual inspection of the copper films showed the surfaces to be rough. The copper film had an unknown thickness, but is assumed to be thick since the films were not transparent and copper has a much greater deposition rate than ceramic

TABLE 3.4.24

Comparison of Metallic Lattice Constants
With Lanthanum Aluminate, Sapphire
and Silicon

| Material | Lattice Constant (Å) | Reference |
|---------------------------|----------------------|-----------|
| LaAlO ₃ | 3.778 | (11) |
| Sapphire [1 $\bar{1}$ 02] | 3.479 | (9) |
| Silicon (110) | 3.840 | (16) |
| Ag | 4.086 | (16) |
| Cu | 3.6153 | (16) |

TABLE 3.4.25

Deposition Parameters for RF-Sputtering
Copper Buffer Layer onto Sapphire
and Silicon Substrates

| RF-Sputtering Parameters | |
|---------------------------------------|-----------------------------|
| Target | LaAlO ₃ |
| Orientation | Off-Axis |
| Stationary Heated Substrate Holder | |
| Substrate Height | 2 cm |
| RF Power | 50 W |
| Base Pressure | 1.5 x 10 ⁻⁴ Torr |
| Argon Pressure | 10 mTorr |
| Oxygen Pressure | 0 mTorr |
| Total Sputtering Gas Pressure | 10 mTorr |
| Deposition Time | 15 Minutes |

oxides.

Lanthanum aluminate was then deposited onto the films (Table 3.4.26). After lanthanum aluminate deposition the copper began to peel away from the substrates indicating a film adhesion problem. The copper films also were black in color indicating that they were oxidized during the deposition of the lanthanum aluminate. The adhesion problem of LaAlO_3 / Cu film on sapphire was so severe that the sample could not be characterized using XRD, SEM, and EDS. LaAlO_3 / Cu on silicon did have a white colored area on the film. This area was analyzed and the diffraction pattern did have lanthanum aluminate diffraction peaks (Figure 3.4.23). These peaks suggests that the lanthanum aluminate film is randomly oriented and polycrystalline. The d-spacings and relative peak heights are listed Table 3.4.27. Again the relative peak heights differ slightly from those measured for the LaAlO_3 powder. The relative peak height for (100) peak was less than the (111) peak. The rest of the relative peak heights are slightly lower than the powder peak heights. The d-spacings not associated with lanthanum aluminate were compared with the d-spacings for CuO , Cu_2O , Si , SiO_2 , Ag , Al_2O_3 , and La_2O_3 . After the d-spacing comparisons, the Bragg diffraction peaks located at 15.18° and 28.95° remain unidentified. Both the copper and lanthanum aluminate films on silicon had granular

TABLE 3.4.26

Deposition Parameters for Depositing Lanthanum
Aluminate onto Copper Buffer Layers

| RF-Sputtering Parameters | |
|---------------------------------------|-----------------------------|
| Target | LaAlO ₃ |
| Orientation | Off-Axis |
| Stationary Heated Substrate Holder | |
| Substrate Height | 2 cm |
| Substrate Distance | 4 cm |
| RF Power | 150 W |
| Base Pressure | 1.1 x 10 ⁻⁴ Torr |
| Argon Pressure | 8 mTorr |
| Oxygen Pressure | 3 mTorr |
| Total Sputtering Gas Pressure | 11 mTorr |
| Deposition Time | 5 Hours |

TABLE 3.4.27

XRD Analysis Summary for LaAlO₃ deposited onto
a Thick Copper buffer Layer on Silicon

| 2*θ (Degrees) | d-Spacing (Å) | Normalized Peak Height | Bragg Peak Identification |
|------------------|------------------|---------------------------|------------------------------|
| 10.62 | 3.840 | 40.7 | (100) LaAlO ₃ |
| 13.02 | 3.134 | 22.0 | (111) Si |
| 15.18 | 2.690 | 100.0 | (110) LaAlO ₃ |
| 16.03 | 2.649 | 15.3 | - |
| 17.70 | 2.310 | 15.3 | (111) & (200) CuO |
| 18.74 | 2.183 | 44.1 | (111) LaAlO ₃ |
| 20.34 | 2.013 | 15.3 | (111) Cu |
| 21.62 | 1.895 | 33.9 | (200) LaAlO ₃ |
| 24.27 | 1.690 | 16.9 | (210) LaAlO ₃ |
| 26.55 | 1.548 | 42.4 | (211) LaAlO ₃ |
| 28.95 | 1.422 | 42.4 | - |
| 30.97 | 1.331 | 28.8 | (220) LaAlO ₃ |

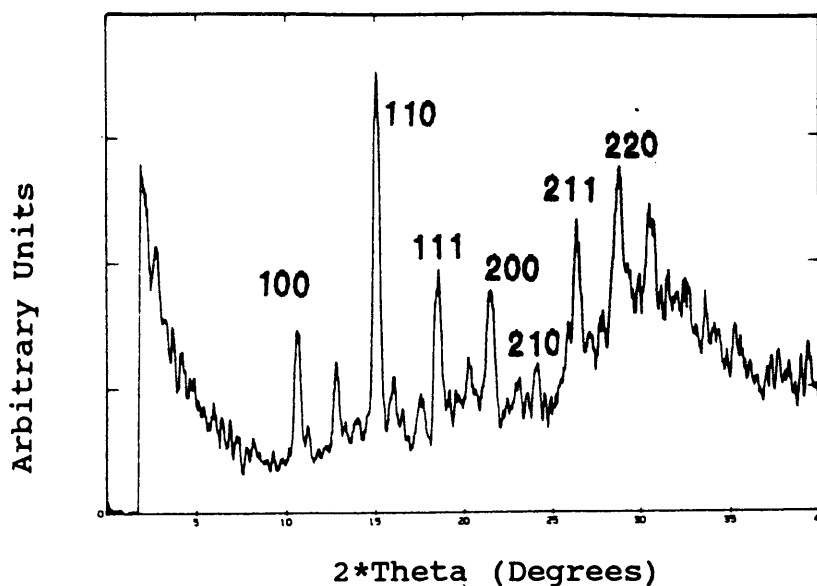


Figure 3.4.23: XRD pattern for LaAlO_3 film deposited onto a copper buffer layer on silicon.

microstructures (Figure 3.4.24). There was an adhesion problem between the lanthanum aluminate and copper films (Figure 3.4.24). EDS composition results are presented in Table 3.4.28.

A thinner copper film was deposited onto sapphire and silicon substrates by evaporation. These films were transparent indicating that their thickness was less than the previous copper film. Lanthanum aluminate was then deposited onto these buffer layers (Table 3.4.29). For the first 1000 Å of lanthanum aluminate deposition only argon

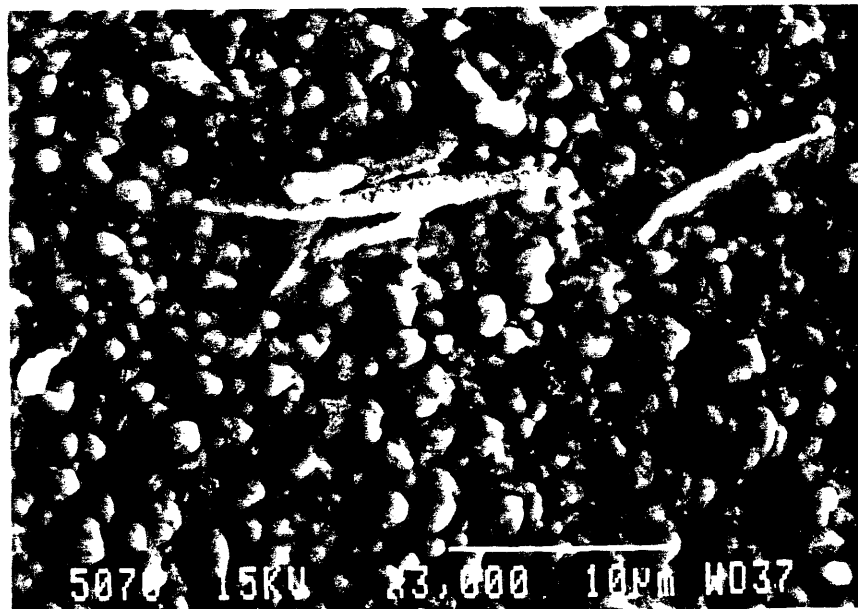
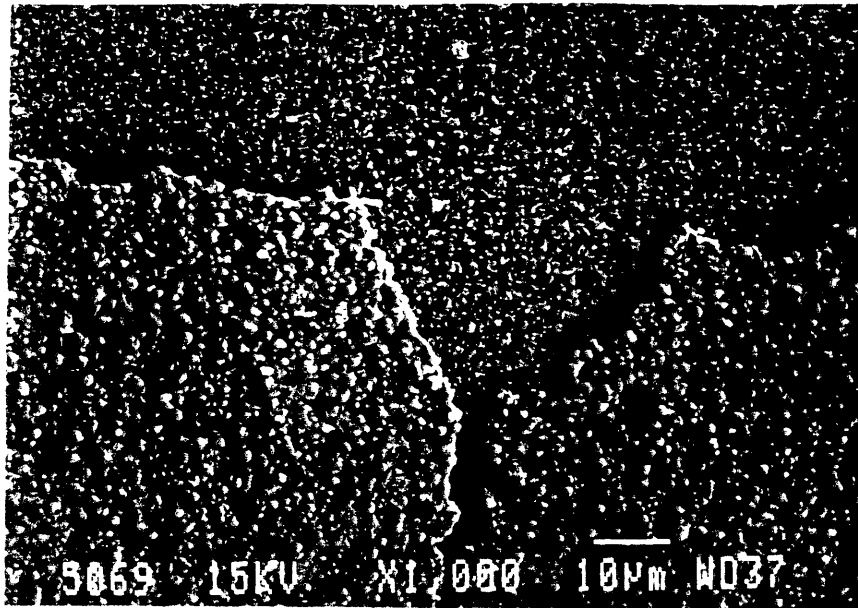


Figure 3.4.24: Top SEM micrograph shows the morphologies of the copper buffer layer and the LaAlO₃ overlayer. The bottom SEM micrograph shows the morphology of the LaAlO₃ film in greater detail.

TABLE 3.4.28

Compositional Results of LaAlO_3 / Cu Films
on Silicon Substrate

| Element | Atomic Percent | | |
|---------|-----------------------|---------------------------|-------------|
| | LaAlO_3 Film | LaAlO_3 Particle | Cu Film |
| La | 40.35 ± 1.0 | 40.60 ± 1.0 | 0.0 |
| Al | 50.97 ± 1.0 | 52.18 ± 1.0 | 0.0 |
| Cu | 8.68 ± 1.0 | 7.22 ± 1.0 | 25.79 ± 1.0 |
| Si | 0.0 | 0.0 | 74.21 ± 1.0 |

TABLE 3.4.29

Deposition Parameters of LaAlO_3 onto Sapphire
and Silicon with a Copper Buffer Layer

| RF-Sputtering Parameters | |
|------------------------------------|------------------------------|
| Target Orientation | LaAlO_3 Off-Axis |
| Stationary Heated Substrate Holder | |
| RF Power | 75 W |
| Substrate Height | 2 cm |
| Substrate Distance | 4 cm |
| Substrate Temperature | 700°C |
| Base Pressure | 1.9×10^{-4} Torr |
| Argon Pressure | 8 mTorr |
| Oxygen Pressure | 3 mTorr |
| Total Sputtering Gas Pressure | 11 mTorr |
| Deposition Time | 1.5 Hours |
| Final Thickness | 2832 Å |

gas was used for the sputtering gas to minimize the oxidation of the copper film. The XRD patterns show that the lanthanum aluminate films are amorphous (Figure 3.4.25 shows LaAlO_3 film on sapphire.) The film composition on silicon was more stoichiometrically correct than on sapphire (Tables 3.4.30 and 3.4.31). This observation may be due to sampling of the substrate as well as the LaAlO_3 film in the EDS analysis. The microstructure of the film on silicon had both star-like and rod-like particles (Figure 3.4.26). The star-like particles contain more aluminum and the rods have a higher concentration of lanthanum. The smaller dot particles contain a nearly 1:1 ratio of lanthanum to aluminum. In contrast the morphology of the film deposited onto Cu/sapphire consists of rounded and randomly dispersed particles varying from approximately 0.33 to 2 microns in size (Figure 3.4.27).

Thin transparent silver buffer layers were evaporated onto sapphire and silicon substrates and lanthanum aluminate was then deposited onto the silver buffer layers. The XRD patterns for these samples show only the silver (111) Bragg peak (Figure 3.4.28). The films on sapphire and silicon were continuous with large particles randomly distributed (Figure 3.4.29). The size of the particles ranged from approximately 0.2 to 2 microns. Approximately the same amount of lanthanum was deposited onto the silver buffer

TABLE 3.4.30

Composition of Film Deposited onto Cu/Sapphire

| Element | Atomic Percent | |
|---------|----------------|-------------|
| | Overall Film | Particle |
| La | 25.24 ± 1.0 | 24.25 ± 1.0 |
| Al | 64.84 ± 1.0 | 51.95 ± 1.0 |
| Cu | 9.91 ± 1.0 | 23.80 ± 1.0 |

TABLE 3.4.31

Composition of Film Deposited onto Cu/Silicon

| Element | Overall Film | Atomic Percent (± 1%) | | |
|---------|--------------|-----------------------|---------------|--------------|
| | | Dot Particle | Star Particle | Rod Particle |
| La | 17.68 | 21.98 | 10.83 | 21.76 |
| Al | 20.12 | 26.66 | 18.76 | 18.75 |
| Cu | 2.32 | 36.06 | 16.84 | 22.74 |
| Si | 59.89 | 15.30 | 52.39 | 36.74 |
| Cl | - | - | 1.18 | - |

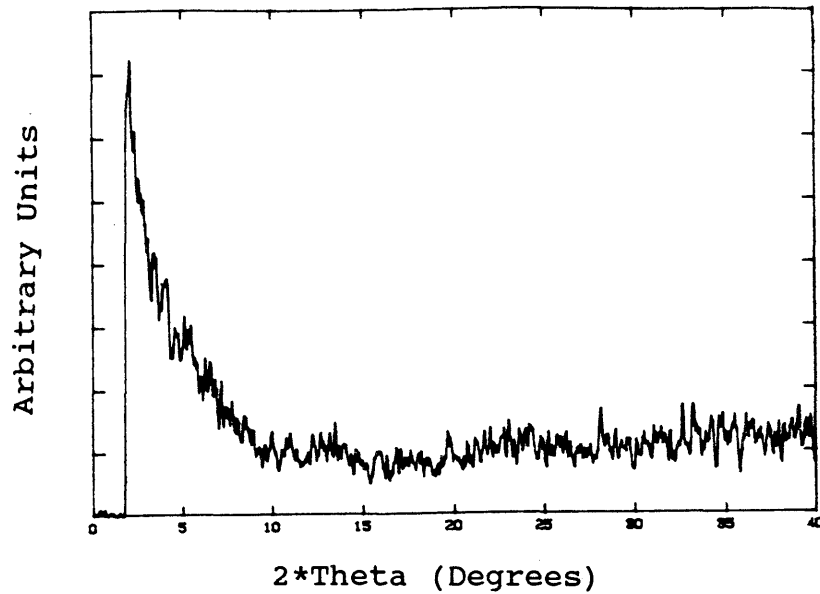


Figure 3.4.25: XRD pattern for LaAlO_3 deposited onto a thin copper buffer layer on sapphire.

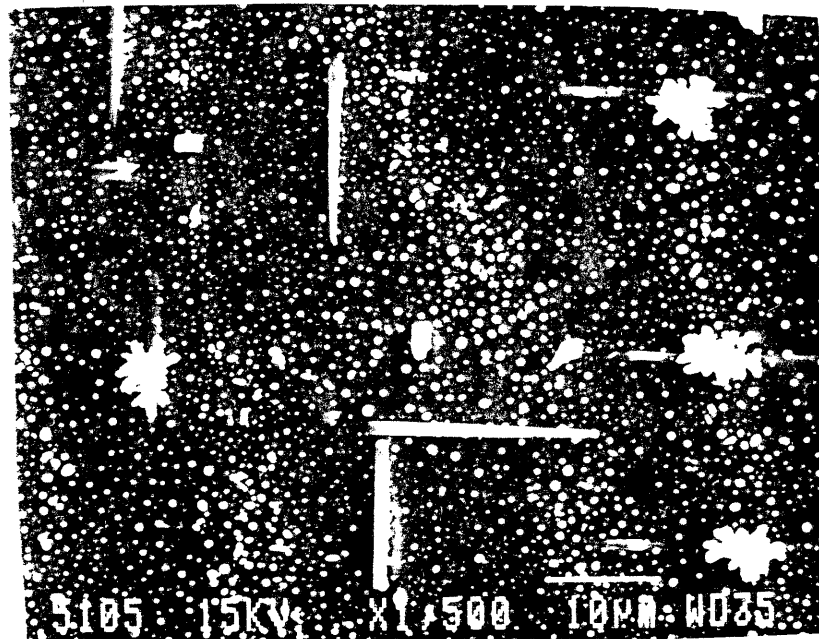


Figure 3.4.26: SEM micrograph showing the morphology of the LaAlO_3 film deposited onto a thin copper buffer layer on silicon.

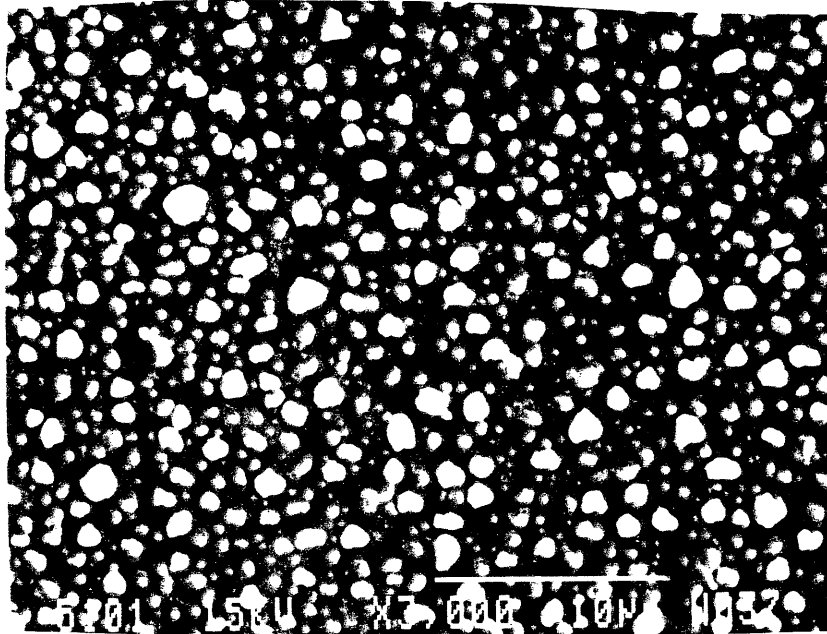


Figure 3.4.27: SEM micrograph showing the morphology of the LaAlO₃ film deposited onto a thin copper buffer layer on sapphire.

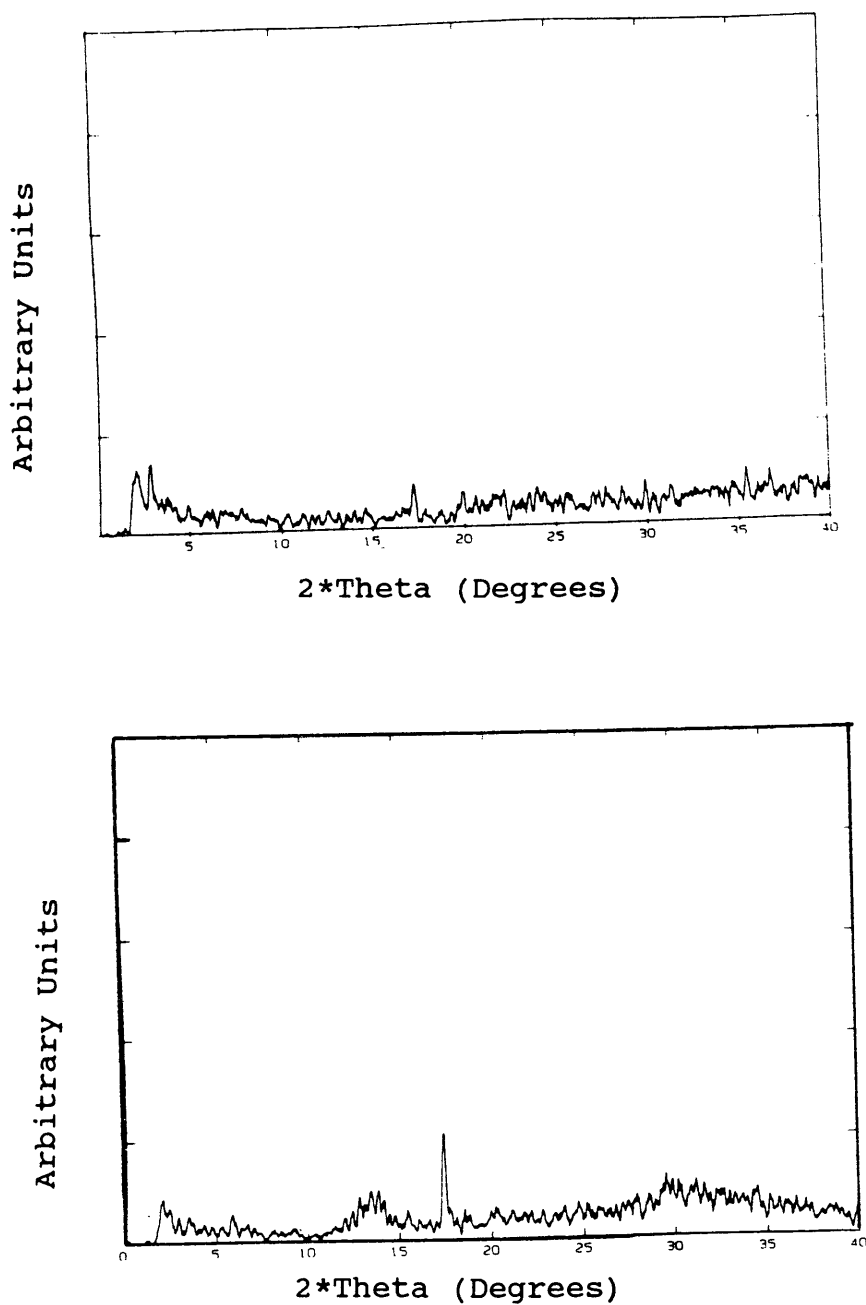


Figure 3.4.28: The top XRD pattern for LaAlO_3 film deposited onto a thin silver buffer layer on sapphire. The bottom XRD pattern for LaAlO_3 film deposited onto a thin silver buffer layer on silicon.

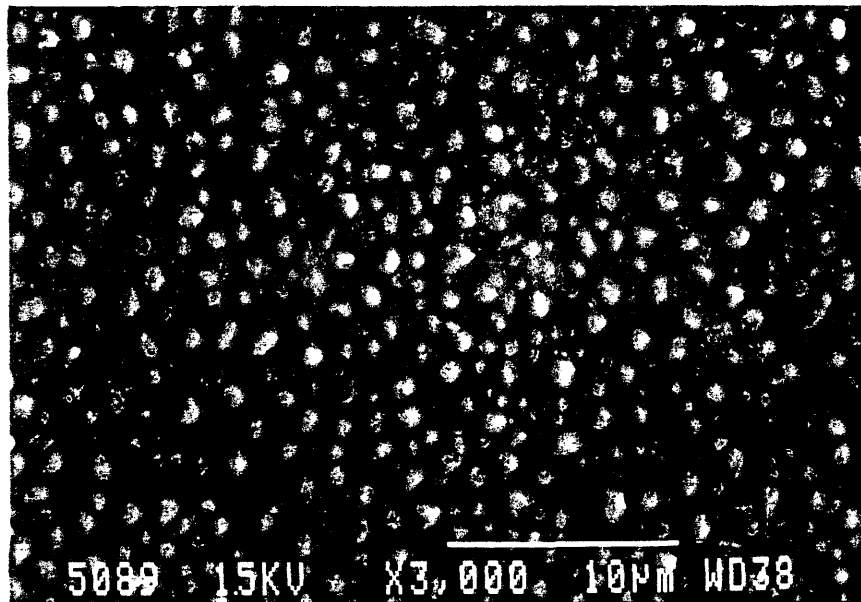
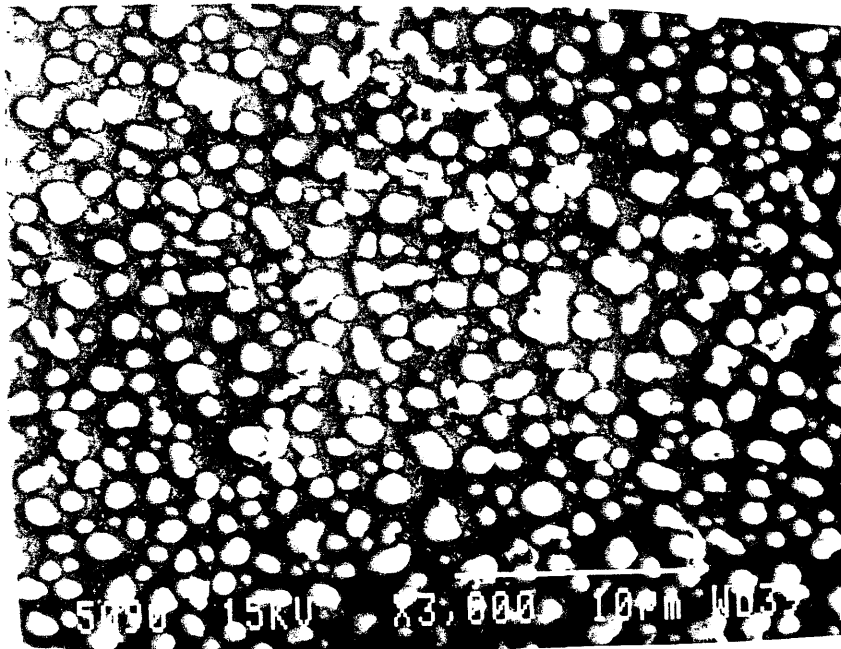


Figure 3.4.29: The top SEM micrograph shows the LaAlO₃ film deposited onto a thin silver buffer layer on sapphire. The bottom SEM micrograph shows the LaAlO₃ film deposited onto a thin silver buffer layer on silicon.

layer. Approximately the same amount of lanthanum was deposited onto the silver buffer layers on both sapphire and silicon substrates (see Tables 3.4.32 and 3.4.33).

The samples mounted 2 cm high were post-annealed according to the heat treatment conditions in Table 3.4.34. Post-annealing had no visible effects on the morphology of the films (Figure 3.4.30). The composition of the post-annealed films remained unchanged from the as deposited films (Table 3.4.35). The lanthanum aluminate film crystallized in the post-annealing treatment as seen in the diffraction pattern (Figure 3.4.31). The calculated d-spacings and relative peak heights are listed in Table 3.4.36. The pseudo-cubic lattice constant was calculated to be 3.8107 Å with a standard deviation of 0.004 Å. This matches well with the lattice constant, 3.788 ± 0.009 Å, for lanthanum aluminate (Table 3.3.1). The relative peak heights for the post-annealed LaAlO_3 film match very closely with the peak heights measured for the LaAlO_3 powder (Table 3.3.1) unlike previous post-annealed samples in the Section 3.4.4.

TABLE 3.4.32

Deposition Parameters of Lanthanum Aluminate
onto Silver Buffer Layer on Sapphire
and Silicon Substrates

| RF-Sputtering Parameters | |
|------------------------------------|-----------------------------|
| Target | LaAlO ₃ |
| Orientation | Off-Axis |
| Stationary Heated Substrate Holder | |
| Substrate Height | 1 cm and 2 cm |
| Substrate Distance | 3.8 cm |
| Substrate Temperature | 650°C |
| RF Power | 150 W |
| Base Pressure | 1.0 x 10 ⁻⁴ Torr |
| Argon Pressure | 8 mTorr |
| Oxygen Pressure | 3 mTorr |
| Deposition Time | 3 Hours |

TABLE 3.4.33

Compositional Analysis of Lanthanum Aluminate
Deposited onto Ag/Sapphire and
Ag/Silicon

| Substrate | Element | Atomic Percent ($\pm 1\%$) | | |
|-------------|---------|------------------------------|----------|-----------------|
| | | Overall Film | Particle | Continuous Film |
| Ag/Sapphire | La | 37.07 | 39.73 | - |
| | Al | 61.62 | 57.94 | - |
| | Ag | 1.31 | 2.33 | - |
| Ag/Silicon | La | 38.06 | 37.72 | 37.77 |
| | Al | 47.61 | 55.17 | 46.66 |
| | Si | 11.18 | 2.78 | 13.91 |
| | Ag | 3.15 | 4.34 | 1.66 |

TABLE 3.4.34

Post-Annealing Conditions of Lanthanum
Aluminate Films Deposited onto
Silver Buffer Layers

| | |
|--|-----------------------|
| Heating Rate | 10°C/Min. |
| Cooling Rate (800 °C to 350 °C) (350 °C to Room Temp.) | 1°C/Min. 10°C/Min. |
| Annealing Temperature | 800°C |
| Annealing Time | 10 Hours |

TABLE 3.4.35

Compositional Results of Post-Annealed Lanthanum
Aluminate Deposited onto Silver Buffer Layers

| Substrate | Element | Atomic Percent ($\pm 1\%$) | |
|-------------|---------|------------------------------|-----------|
| | | Overall Film | Particles |
| Ag/Sapphire | La | 37.19 | 36.17 |
| | Al | 61.25 | 61.26 |
| | Ag | 1.56 | 2.58 |
| Ag/Silicon | La | 35.85 | 35.73 |
| | Al | 47.03 | 51.27 |
| | Ag | 2.63 | 2.10 |
| | Si | 14.48 | 10.90 |

TABLE 3.4.36

d-Spacings for Post-Annealed Lanthanum Aluminate
Film on Ag/Sapphire

| hkl | 2θ | d-Spacing (Å) | Normalized Peak Height |
|-----|-----------|---------------|---------------------------|
| 100 | 10.68 | 3.818 | 52.0 |
| 110 | 15.16 | 2.694 | 100.0 |
| 111 | 18.60 | 2.199 | 47.7 |
| 200 | 21.48 | 1.907 | 39.2 |
| 210 | 24.12 | 1.701 | 23.9 |
| 211 | 26.40 | 1.556 | 43.2 |
| 220 | 30.60 | 1.347 | 26.1 |

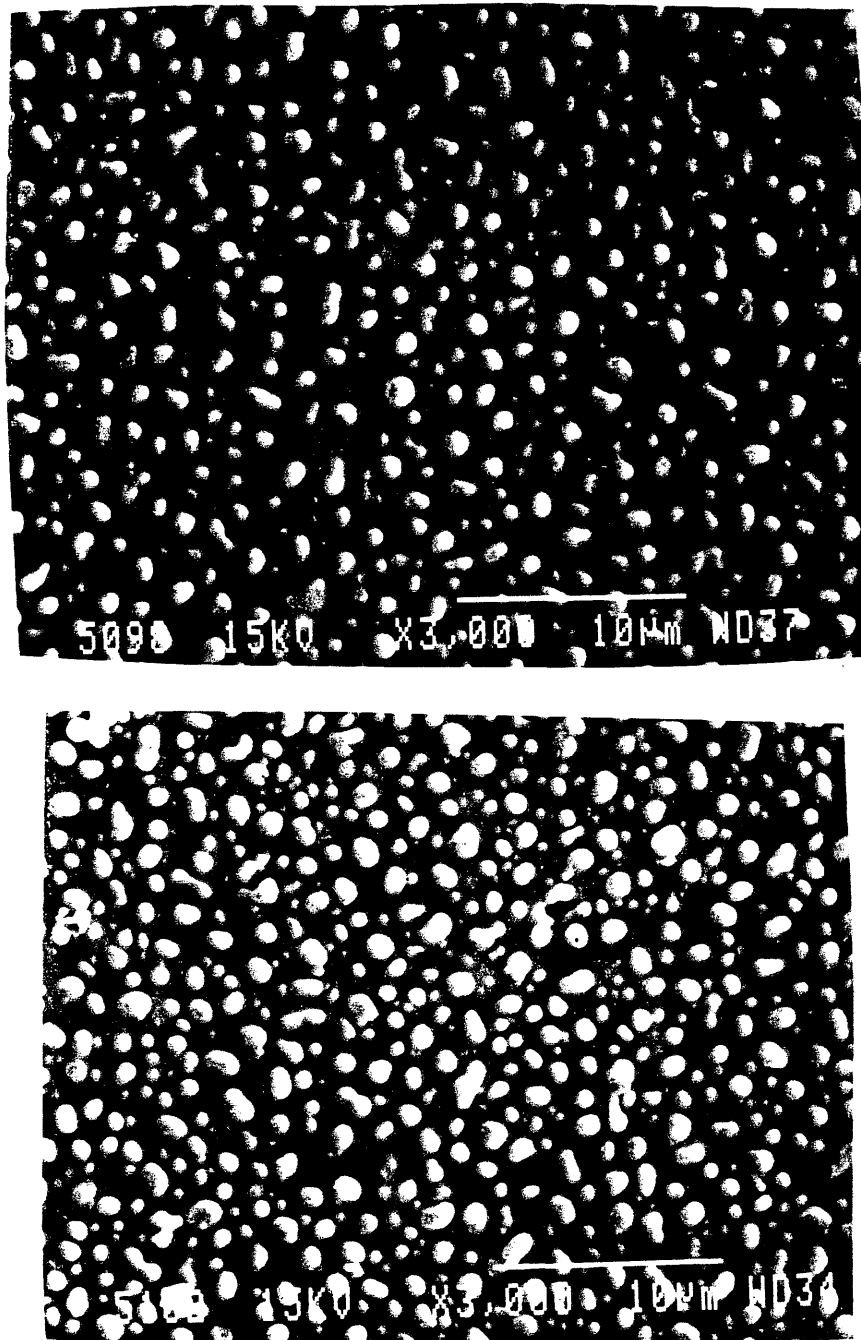


Figure 3.4.30: The top SEM micrograph showing the unchanged morphology of the post-annealed LaAlO_3 film on Ag/sapphire. The bottom SEM micrograph showing the morphology of the post-annealed LaAlO_3 film on Ag/silicon.

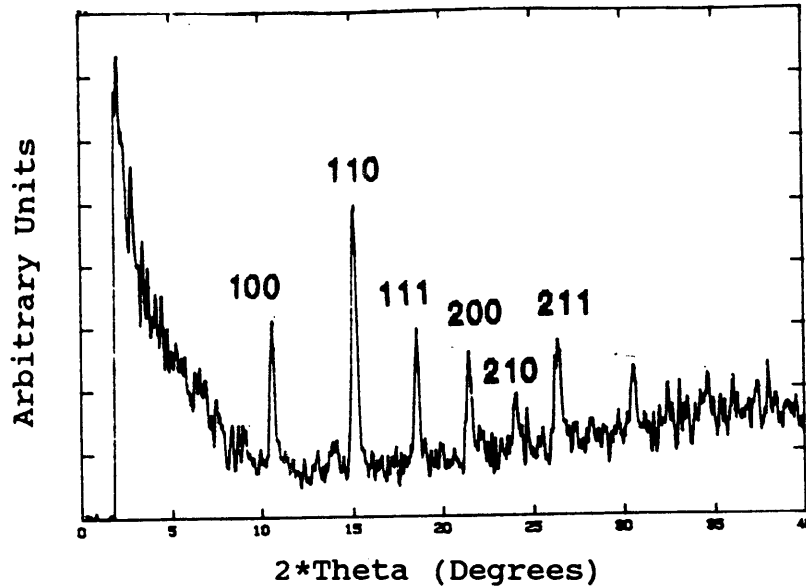


Figure 3.4.31: XRD pattern for post-annealed LaAlO_3 film deposited onto Ag/sapphire.

3.4.6 POST IN-SITU ANNEALING OF LANTHANUM ALUMINATE FILMS

A series of post in-situ annealing studies was performed to see if this type of processing method would produce good quality crystalline lanthanum aluminate films. Lanthanum aluminate films were deposited onto sapphire, magnesium oxide (MgO), and yttrium-stabilized zirconia (YSZ) substrates. The deposition parameters are listed in Table

3.4.37. Initial deposition parameters matched the optimal deposition parameters previously determined in the pressure study (Section 3.4.3). Several research groups have recently reported high quality, c-axis oriented YBCO films on substrates whose lattice constants do not match with the YBCO basal plane. In these reports the films were typically deposited at higher pressures (5,56-58). Therefore the sputtering gas pressures were increased in this study to see if higher sputtering and post-in-situ annealing pressures would affect the film quality.

The EDS compositional results for the overall films are listed in Table 3.4.38. The overall film composition seems to be dependent on the substrate material. The lanthanum aluminate films deposited onto MgO and YSZ are rich in aluminum even though the lanthanum aluminate target has approximately a 1:1 ratio of lanthanum to aluminum. Films deposited onto YSZ are closer to the desired stoichiometry of 1:1 for lanthanum to aluminum than films deposited onto MgO. Since a large portion of the substrate is included in the EDS compositional analysis it is difficult to determine if the film deposited onto sapphire is stoichiometrically correct. However, in previous studies thicker films deposited onto sapphire and silicon matched closely with the composition of the same lanthanum aluminate target (Section 3.4.4). The deposition rate for lanthanum and aluminum were

TABLE 3.4.37

Deposition and Post-In-Situ Annealing Parameters
For Lanthanum Aluminate Films Deposited
onto Sapphire, MgO and YSZ Substrates

| Deposition Parameters | LAO Sample Identification | | | | | | |
|---------------------------------------|---------------------------|-----|-----|-----|------|------|-----|
| | 25 | 26 | 27 | 28 | 31 | 32 | 33 |
| RF Power (Watts) | 75 | 75 | 100 | 100 | 100 | 100 | 100 |
| Sputtering Gas Pressure (mTorr) | 16 | 16 | 30 | 30 | 40 | 40 | 40 |
| Argon Pressure (mTorr) | 12 | 12 | 20 | 20 | 30 | 30 | 30 |
| Oxygen Pressure (mTorr) | 4 | 4 | 10 | 10 | 10 | 10 | 10 |
| Deposition Temperature (C) | 720 | 675 | 700 | 750 | 750 | 745 | 700 |
| Deposition Time (Hours) | 0.5 | 0.5 | 1 | 1.5 | 2 | 0.3 | 2 |
| Annealing Temperature (C) | 725 | 675 | 700 | 800 | 800+ | 775 | - |
| Annealing Time (Hours) | 2 | 2 | 2 | 1.5 | 1 | 1.25 | - |
| Annealing Pressure (mTorr) | 16 | 16 | 30 | 30 | 2000 | 2000 | - |

Table 3.4.38

EDS Compositional Results for Post-In-Situ
Annealing Study of Lanthanum Aluminate
Films Deposited onto Sapphire,
MgO and YSZ Substrates

| Substrate | Sample Id. | Atomic Percent ($\pm 1\%$) | | |
|-----------|------------|------------------------------|-------|---------|
| | | La | Al | La / Al |
| Sapphire | 25 | 7.00 | 93.00 | - |
| | 26 | 6.13 | 93.87 | - |
| | 27 | 10.92 | 89.08 | - |
| | 28 | 13.66 | 86.34 | - |
| | 31 | 7.73 | 92.27 | - |
| | 32 | 1.09 | 98.91 | - |
| | 33 | 2.03 | 97.97 | - |
| MgO | 25 | 6.58 | 9.11 | 0.722 |
| | 26 | 6.12 | 9.16 | 0.668 |
| | 27 | 2.26 | 19.48 | 0.6294 |
| | 28 | 15.64 | 23.45 | 0.6670 |
| | 31 | 6.46 | 10.47 | 0.617 |
| | 32 | 1.54 | - | - |
| | 33 | - | - | - |
| YSZ | 25 | 11.16 | 14.43 | 0.773 |
| | 26 | - | - | - |
| | 27 | 18.29 | 23.35 | 0.7833 |
| | 28 | 22.11 | 25.54 | 0.8657 |
| | 31 | 14.33 | 16.08 | 0.8912 |
| | 32 | 2.44 | 3.02 | 0.8079 |
| | 33 | 5.87 | 5.37 | 1.093 |

greater for films deposited onto YSZ than MgO. Similarly, the deposition rate for lanthanum was greater for films deposited onto YSZ than for sapphire.

The EDS compositional analysis for Sample 32 deposited onto MgO contains no aluminum. However, a compositional analysis of the star-like particle in the film had a La:Al ratio which was approximately equal to 1:1 (Figure 3.4.32). This result suggests the overall film compositional measurement was not correct and that the deposited film contains both lanthanum and aluminum.

The morphologies of the films deposited onto sapphire post-in-situ annealed at 725°C or below were smooth and featureless (Figure 3.4.33). However, films post-in-situ annealed at temperatures ranging from 775 to 800+°C had small star-like and branch-like particles. This change in the film morphology may be associated with initial stages of crystallization of the films. Additional transmission electron microscopy (TEM) and selected area diffraction (SAD) studies need to be performed to confirm this hypothesis. The morphologies of the films deposited onto MgO and YSZ also seemed to be dependent on the post-in-situ annealing temperatures. Films post-in-situ annealed at temperatures greater than 775°C had more textured areas and again some star-like particles (Figures 3.4.34-3.4.35), again suggesting that some type of structural change began

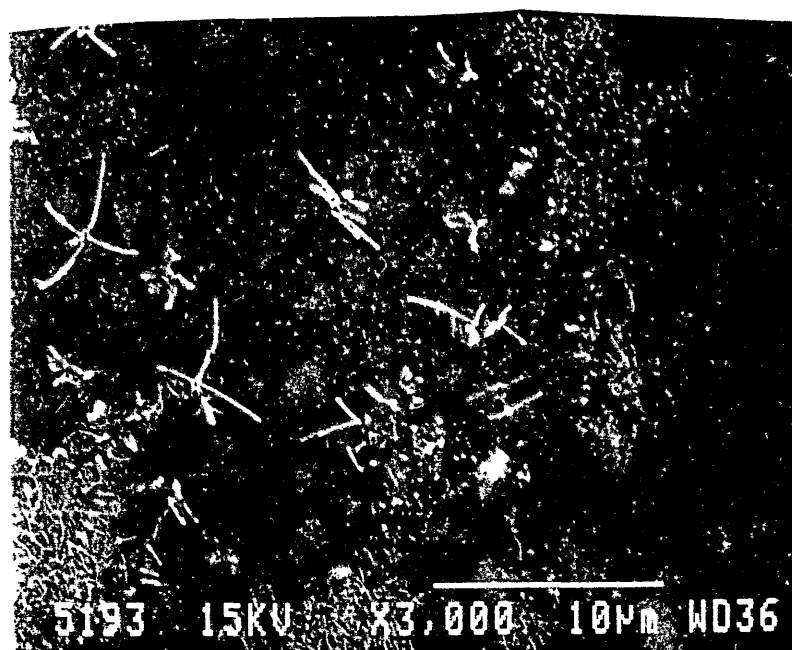


Figure 3.4.32: SEM micrograph showing the film deposited onto MgO substrate (Sample LAO-32).

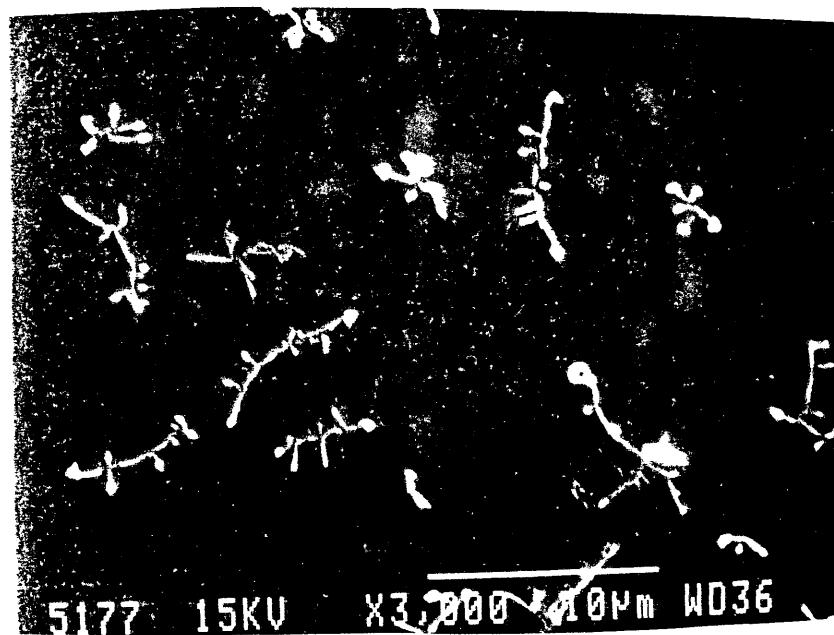
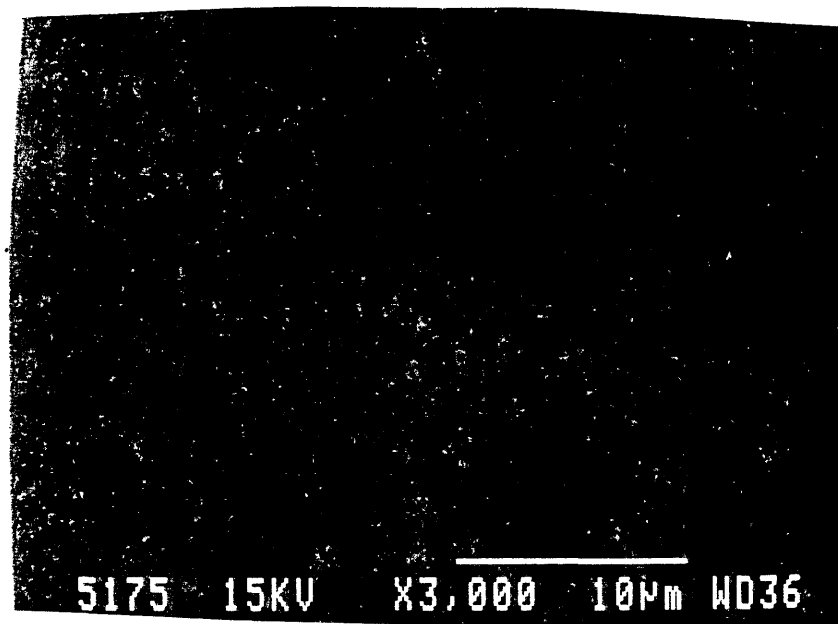


Figure 3.4.33: SEM micrographs showing the morphologies of the post-in-situ annealed films on sapphire. The top micrograph is sample LAO-27 and the bottom LAO-28.

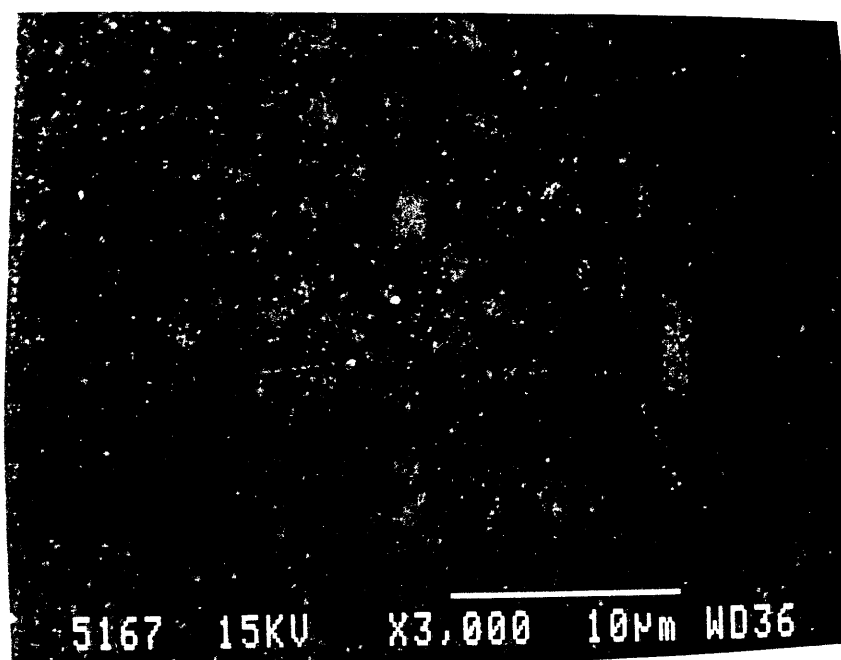
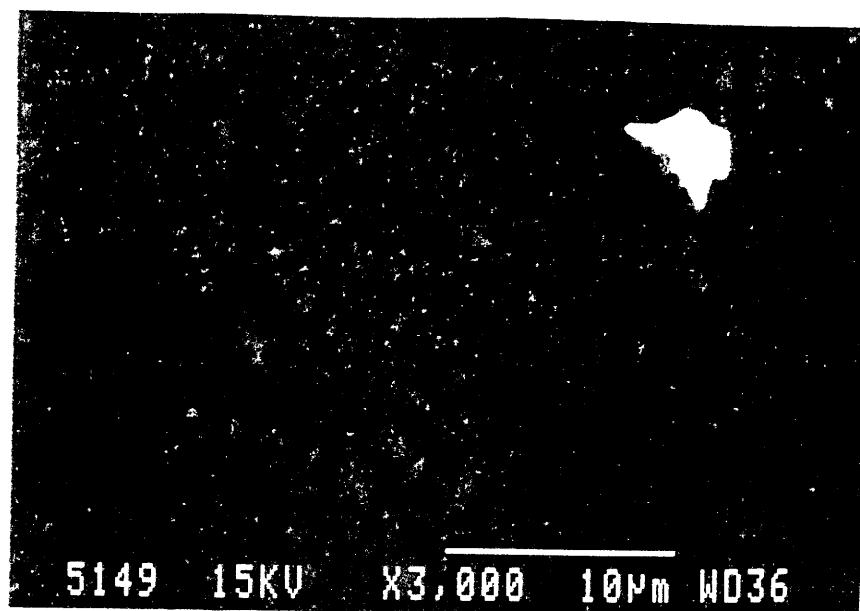


Figure 3.4.34: SEM micrographs showing the morphologies of the post-in-situ annealed films on MgO. The top micrograph is sample LAO-25 and the bottom LAO-26.

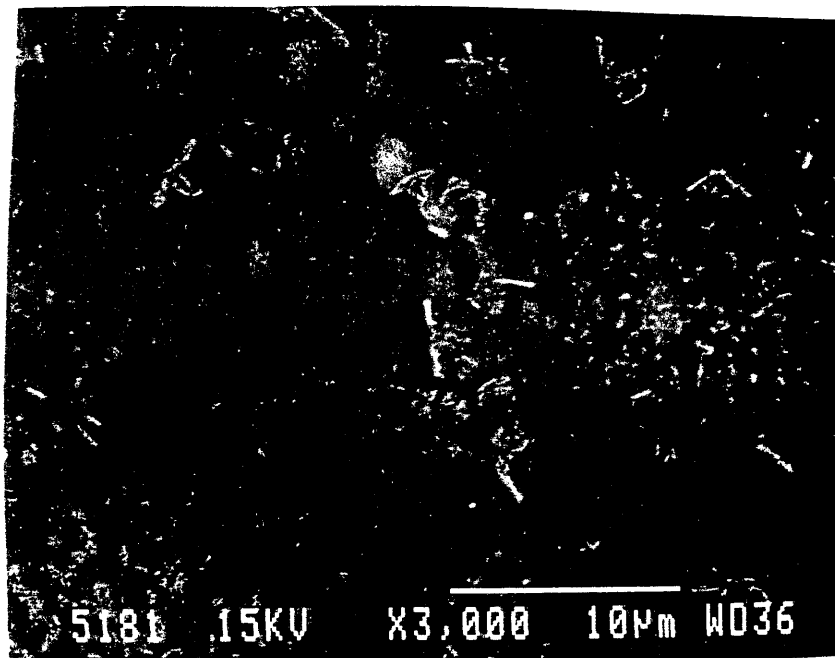
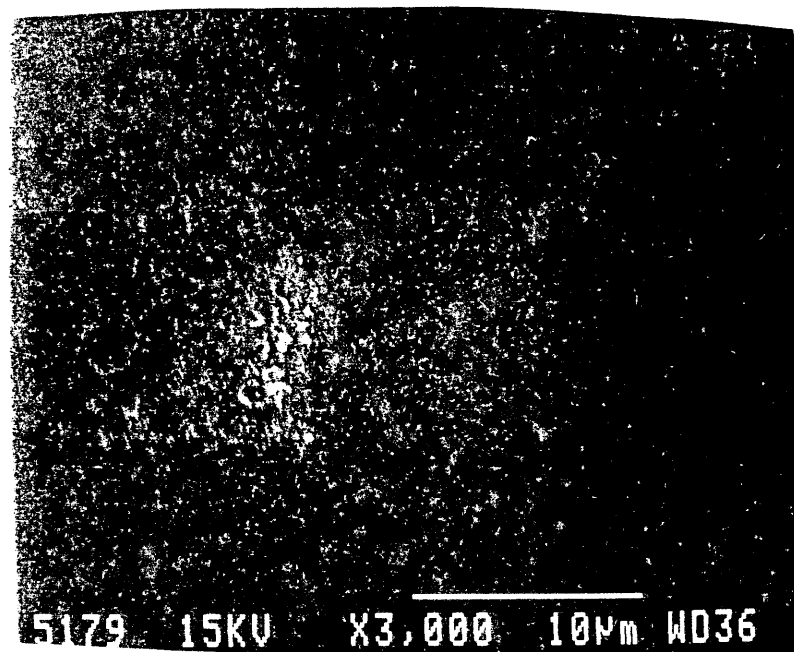


Figure 3.4.35: SEM micrographs showing the morphologies of the post-in-situ annealed films on YSZ. The top micrograph is sample LAO-27 and the bottom LAO-28.

to occur in the films at these higher post-in-situ annealing temperatures. These results are consistent with the post deposition annealing results where the crystallization temperature for lanthanum aluminate was determined to be between 800 and 850°C.

The XRD analyses of the films showed that all the films are amorphous. The only diffraction peaks observed in these samples belonged to the substrates or the silver paste. These results indicate that changes in the structure observed in the morphology of the post-in-situ annealed films may not be significantly large enough to be detected by XRD measurements.

3.4.7 LATTICE MATCHING

A study was performed to duplicate Dr. A. Lee's deposition of crystalline lanthanum aluminate buffer layers onto crystalline EBCO films. Using similar rf-sputtering parameters, lanthanum aluminate was deposited onto a EBCO film on SrTiO_3 as well as MgO and sapphire substrates (See Table 3.4.39). Before depositing lanthanum aluminate, the EBCO film was analyzed using XRD, resistance versus temperature, and SEM measurements. The XRD pattern confirmed the EBCO to be c-axis oriented (Figure 3.4.36).

The mosaic spread of the film was 0.26° at full-width half-maximum (Figure 3.4.36). The lattice constant for the EBCO film was calculated to be 11.751 \AA . The c-axis of the EBCO film was accurately determined by calculating the "q" values for each (00l) Bragg peak observed in the diffraction pattern. Then the q value was plotted against the respective order of the (00l) value. The distance between diffraction planes in reciprocal is q and it is described by the following equation:

$$q = \frac{4\pi \sin(\theta)}{\lambda} \quad (3.4.1)$$

where θ is half the diffraction angle and λ is the radiation wavelength. The above Equation (3.4.1) was solved for $\sin \theta / \lambda$ and substituted into Bragg's law (Equation 2.2) to get the following expression:

$$\frac{n}{d_n} = \frac{q}{2\pi} \quad (3.4.2)$$

Then the above equation was linearized to get:

$$q = \frac{2\pi n}{d_n} \quad (3.4.3)$$

The slope of the line was accurately determined from the above equation by performing a linear regression. (See Figure 3.4.37 for the graph of this line.) The c-axis lattice constant was computed from the slope of the line to be $11.751 \pm 0.001 \text{ \AA}$. The uncertainty of q was calculated

TABLE 3.4.39

Deposition Parameters of Lanthanum Aluminate
onto Crystalline EBCO Film, Sapphire,
and MgO Substrates

RF-Sputtering Parameters

| | |
|-----------------------|-----------------------------|
| Target | LaAlO ₃ |
| Off-Axis Orientation | |
| Substrate Temperature | 730 °C |
| Substrate Height | 2.5 cm |
| Substrate Distance | 5.0 cm |
| RF-Power | 100 W |
| Base Pressure | 1.0 x 10 ⁻⁴ Torr |
| Argon Pressure | 40 mTorr |
| Oxygen Pressure | 30 mTorr |
| Total Sputtering | |
| Gas Pressure | 70 mTorr |
| Deposition Time | 2 Hours |

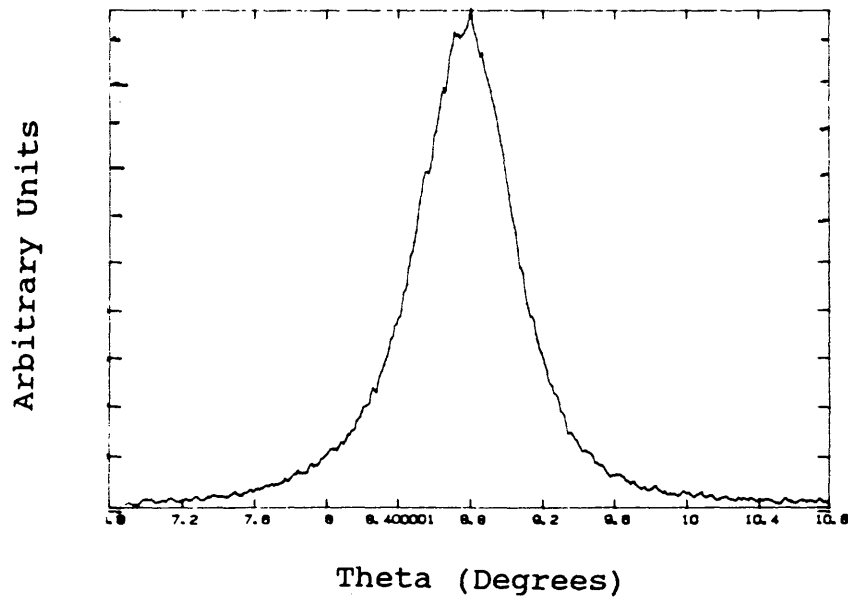
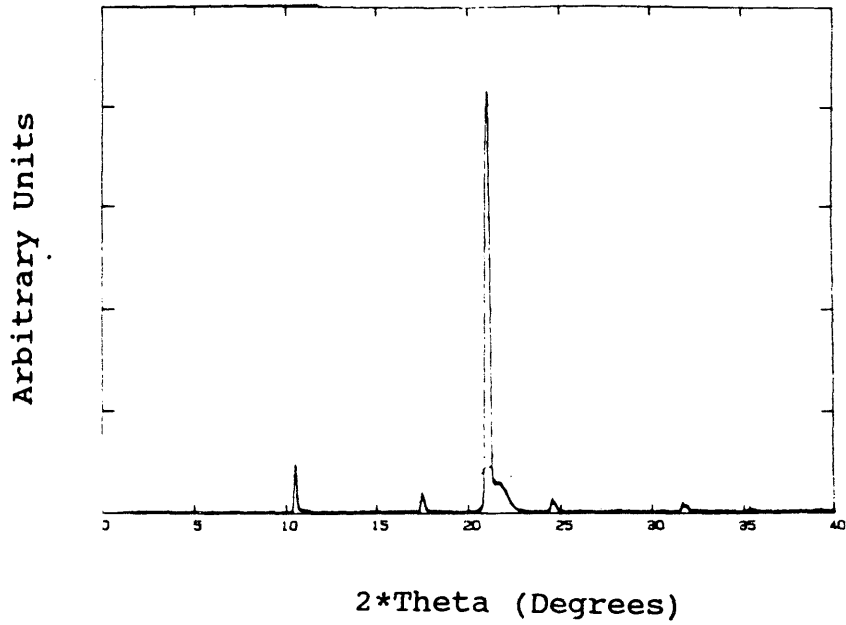


Figure 3.4.36: Top XRD pattern shows the c-axis oriented EBCO film. Bottom rocking curve analysis shows that the EBCO film was well oriented.

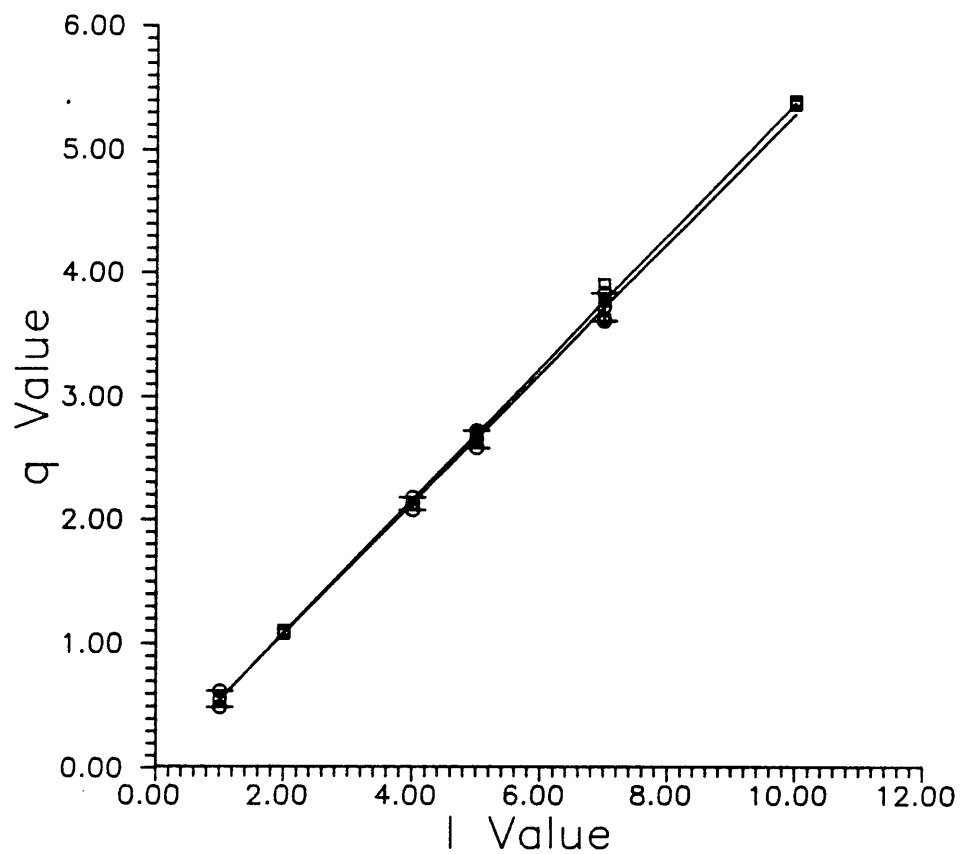


Figure 3.4.37: Plot of q versus (001) . Circles represent q calculated before LaAlO_3 deposition and squares represent q calculated after LaAlO_3 .

from the following equation:

$$\Delta q = \frac{4\pi\Delta\theta\cos(\theta)}{\lambda} \quad (3.4.4)$$

where $\Delta\theta$ is the full-width-half-maximum measured directly from the XRD pattern.

The resistance versus temperature measurements showed a superconducting transition at 90 K. The room temperature resistance of the film was 5.4 ohms (Figure 3.4.38). The SEM micrograph of the EBCO showed a smooth continuous film with what appeared to be randomly dispersed black pinholes (Figure 3.4.39). The EDS compositional results are listed in Table 3.4.40. From the EDS compositional analysis the ratios for Er:Ba:Cu and Sr:Ti were calculated to be 1:0.94:1.7 and 1:1.79, respectively. The energy of the x-rays collected in the EDS measurement overlapped significantly affecting the ability of the software to accurately resolve the quantitative amounts of each element present in the sample (see Figure 3.4.40) and making it difficult to draw any conclusions about the EBCO film composition before lanthanum aluminate deposition. Since the film had good resistance versus temperature properties, the composition of the film must have been fairly close to the expected 1:2:3 ratio of Er:Ba:Cu.

TABLE 3.4.40

Compositional Analysis of EBCO Film on SrTiO_3
Before Lanthanum Aluminate Film Deposition

| Element | Atomic Percent | |
|---------|-----------------|-----------------|
| | Overall Film | Black Pinhole |
| Er | 14.36 \pm 1.0 | 16.25 \pm 1.0 |
| Ba | 13.49 \pm 1.0 | 7.63 \pm 1.0 |
| Cu | 25.01 \pm 1.0 | 6.04 \pm 1.0 |
| Sr | 16.92 \pm 1.0 | 23.70 \pm 1.0 |
| Ti | 30.23 \pm 1.0 | 46.38 \pm 1.0 |

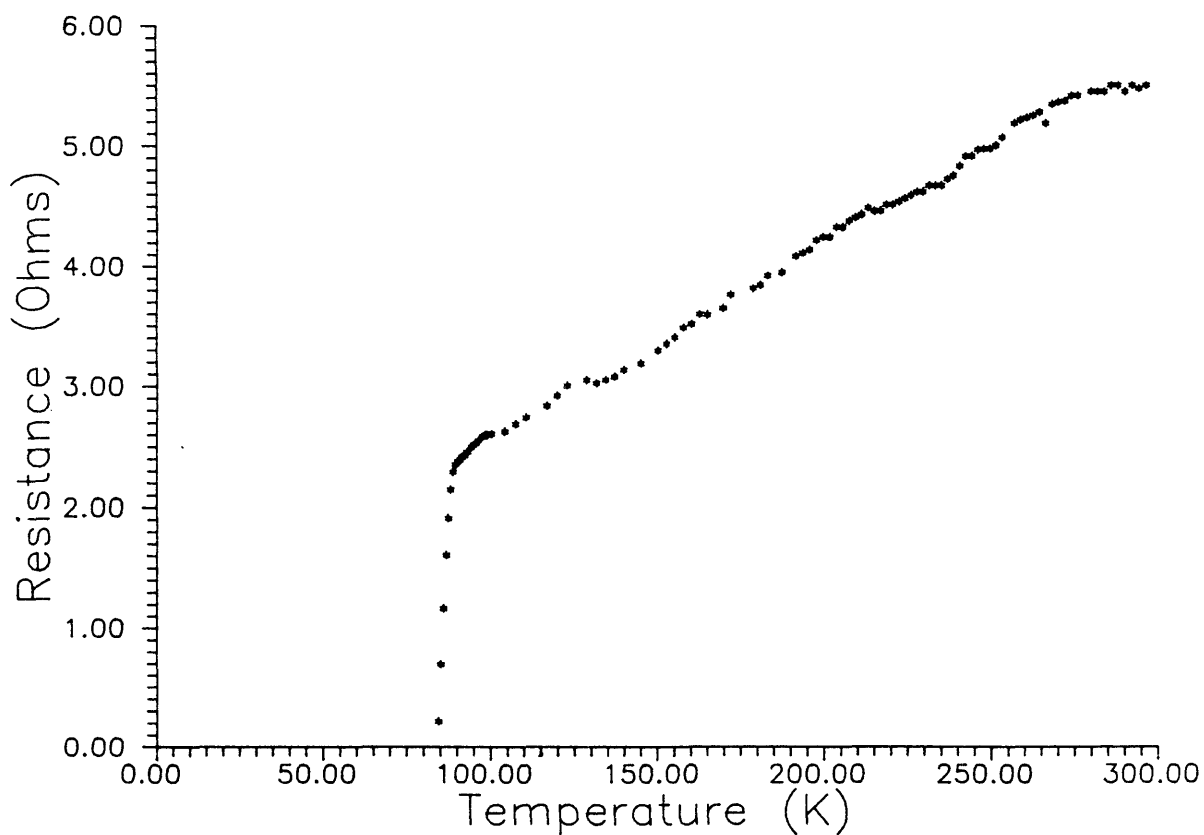


Figure 3.4.38: Resistance versus temperature curve for EBCO superconducting film.

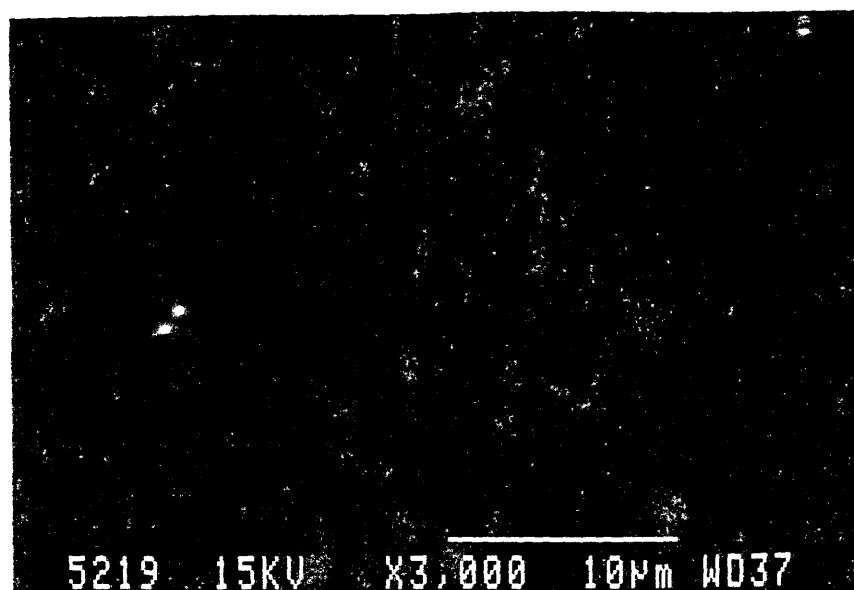


Figure 3.4.39: SEM micrograph showing the morphology of the EBCO film before the deposition of LaAlO_3 film.

TN-5500 Colorado School of Mines / JEOL FRI 20-JUL-90 10:42
 Cursor: 0.000keV = 0

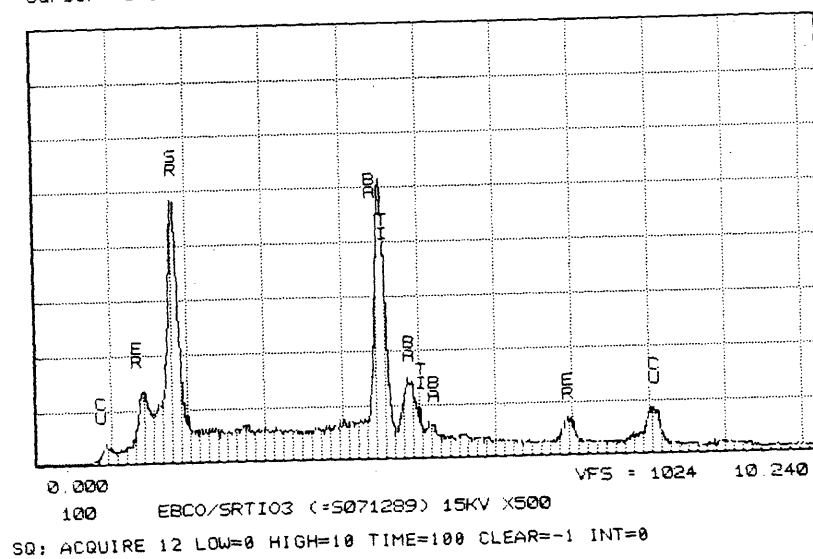


Figure 3.4.40: Graph showing the EDS data collected for compositional analysis of EBCO film.

The lanthanum aluminate film was analyzed using XRD and SEM/EDS. The XRD pattern for $\text{LaAlO}_3/\text{EBCO}/\text{SrTiO}_3$ had lanthanum aluminate (100), (200), and (300) Bragg diffraction peaks indicating that the film was crystalline and oriented along the (h00) direction (see Figure 3.4.41 and Table 3.4.41). The average pseudo-cubic lattice parameter was calculated to be 3.81 Å (Table 3.4.41). This value is slightly larger than the lattice parameter measured for lanthanum aluminate powder 3.788 ± 0.009 Å. Rocking curve analysis of the lanthanum aluminate (100) peak gave full-width half-maximum value of 0.29° , reaffirming that the lanthanum aluminate crystalline film is well oriented (Figure 3.4.41). The c-axis was calculated by performing a linear regression of Equation 3.4.5 as previously described (Figure 3.4.37). The c-axis of the EBCO film was calculated to be 11.926 ± 0.02 Å. As seen Figure 3.4.37 the two lines are within the experimental uncertainty of q . This result indicates that there was no degradation to the EBCO film during the LaAlO_3 deposition. There is one unidentified Bragg peak at 2θ equal to 27.70° ; it is not from the silver paste. The XRD patterns for the films on sapphire and MgO only showed substrate diffraction peaks indicating that the deposited films were amorphous.

All the deposited films were smooth as can be seen in the SEM micrographs (Figure 3.4.42). However, the lanthanum

TABLE 3.4.41

Calculated d-Spacing for XRD Pattern of
 LaAlO_3 Deposited onto Crystalline
 EBCO Superconducting Film

| $2*\theta$ | d-Spacing (Å) | SrTiO_3 hkl | $\text{ErBa}_2\text{Cu}_3\text{O}_x$ hkl | LaAlO_3 hkl |
|------------|------------------|-------------------------|---|-------------------------|
| 3.6 | 11.31 | | 010 | |
| 10.46 | 3.899 | 100 | | |
| 10.76 | 3.790 | | | 100 |
| 13.82 | 2.954 | | 040 | |
| 17.26 | 2.368 | | 050 | |
| 20.96 | 1.954 | 200 | | |
| 21.40 | 1.914 | | | 200 |
| 24.28 | 1.690 | | 070 | |
| 27.70 | 1.485 | | | |
| 31.62 | 1.304 | 300 | | |
| 31.82 | 1.296 | | 090 | |

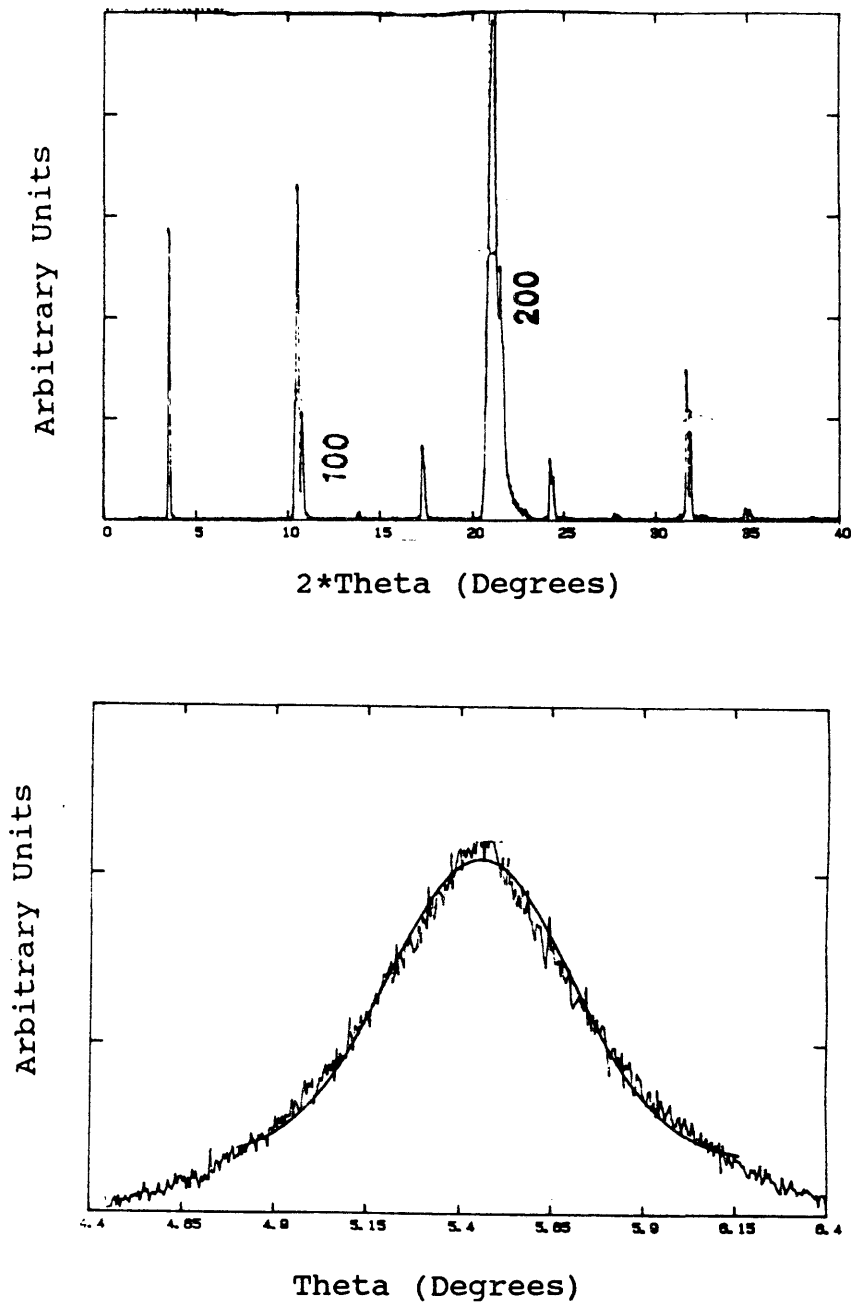


Figure 3.4.41: XRD pattern showing the oriented LaAlO_3 film on EBCO superconducting film. Rocking curve analysis showing that the LaAlO_3 film is well oriented.

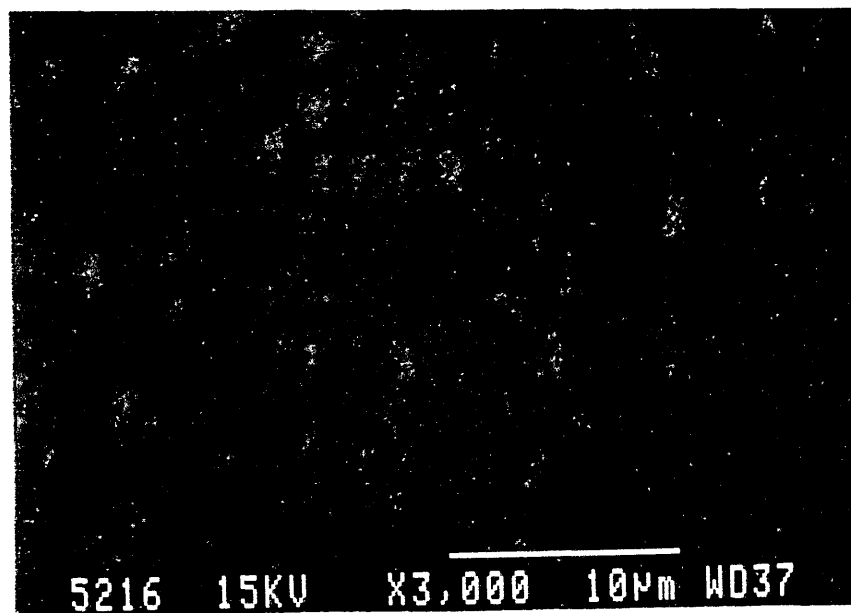
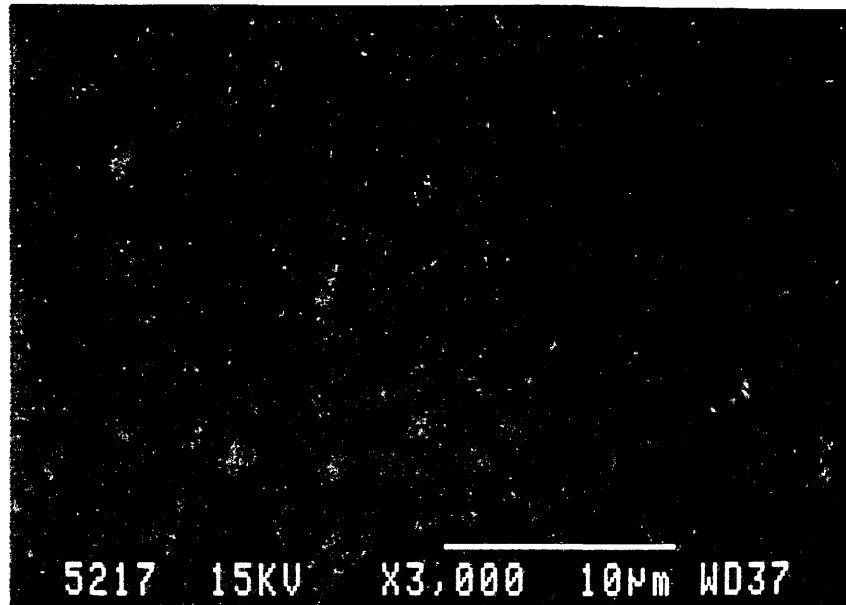


Figure 3.4.42: SEM micrographs showing the morphologies of LaAlO₃ films deposited onto sapphire (top) and MgO (bottom).

aluminate film on EBCO had light grey, medium grey, and black particles randomly throughout the film (Figure 3.4.43). The EDS compositional data for these films are presented in Tables 3.4.42-3.4.43. Again, for the reasons previously mentioned it is difficult to draw any conclusions about the compositions of the LaAlO_3 and EBCO films.

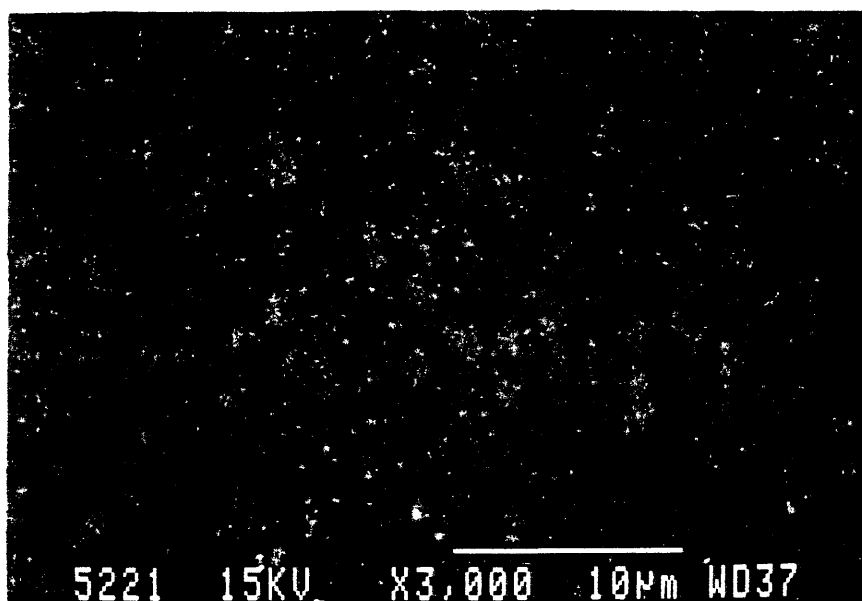


Figure 3.4.43: SEM micrograph showing the morphology of LaAlO_3 film deposited onto EBCO crystalline film.

TABLE 3.4.42

Compositional Analysis for Lanthanum Aluminate
Deposited onto EBCO Film on SrTiO₃

| Element | Atomic Percent ($\pm 1\%$) | | |
|---------|------------------------------|----------------|---------------|
| | Overall Film | Light Particle | Dark Particle |
| La | 15.74 | 17.68 | 14.96 |
| Al | 26.34 | 30.65 | 19.19 |
| Er | 8.46 | 8.04 | 11.71 |
| Ba | 11.43 | 13.50 | 10.90 |
| Cu | 19.56 | 14.42 | 12.81 |
| Sr | 5.81 | 5.26 | 9.47 |
| Ti | 12.66 | 10.44 | 20.97 |

TABLE 3.4.43

Compositional Analysis for Lanthanum Aluminate
Deposited onto Sapphire and MgO Substrates

| Substrate | Element | Overall Film (Atomic Percent) |
|-----------|---------|----------------------------------|
| Sapphire | La | 13.18 \pm 1.0 |
| | Al | 86.82 \pm 1.0 |
| MgO | La | 10.64 \pm 1.0 |
| | Al | 18.69 \pm 1.0 |
| | Mg | 70.67 \pm 1.0 |

3.5 LANTHANUM ALUMINATE THIN FILM DEPOSITION SUMMARY

The radial compositional study (Section 3.4.2) of lanthanum aluminate films deposited onto 1-2-3 superconducting films showed that there was no correlation between film composition and radial positioning of samples on the rotating substrate holder. These results are consistent with other studies which have shown correlations between superconducting film compositions and substrate distance radially away from the target, since in the radial compositional study all the substrates were essentially located at the same distance from the center of the target.

Small changes in total sputtering gas pressure, from 6 to 12 mTorr, did not greatly affect the quality of the lanthanum aluminate films deposited onto sapphire and silicon substrates. The deposition rates were slightly greater for an argon to oxygen ratio of 3:1 than for 2:1. Surprisingly, the deposited film compositions contained no chlorine or potassium impurities while the target did. The film composition deposited onto silicon was richer in lanthanum than was that of the target. The ratio of lanthanum to aluminum for the films typically ranged from 0.78 to 0.89 with one unexplained exception of 0.59, while the target had a ratio of 0.70. All of the films deposited at these pressures were amorphous in structure and typically

had a smooth and featureless morphology.

The crystallization temperature of the amorphous lanthanum aluminate films was determined to be between 800 and 850°C. XRD results showed that the annealed films were randomly oriented and crystalline in structure when annealed at temperatures between 800 and 850°C. Unfortunately, the high post annealing temperatures caused the films to severely crack. The cracking was attributed to the difference in the thermal expansion coefficients for lanthanum aluminate and the substrates (sapphire and silicon). These results led to studies of lanthanum aluminate film depositions at lower processing temperatures such as depositing films onto heated substrates (650 to 775°C) and metallic buffer layers.

Most of the lanthanum aluminate films deposited onto metallic buffer layers were amorphous even though the lattice constants of the metallic layers matched closely with the lattice constant for lanthanum aluminate. The buffer layers greatly affected the morphology of the deposited films.

Post-in-situ annealing studies reconfirmed the minimum crystallization temperature for lanthanum aluminate films to be about 800°C. The structure in the film morphology was temperature dependent. At annealing temperatures greater than 775°C the films on sapphire began to show star-like

structures dispersed randomly throughout the film. Similar structure changes were observed in films on MgO and YSZ at annealing temperatures greater than 775°C. More importantly, the composition of the films was dependent on the substrate material and rf-sputtering parameters or annealing conditions.

A study was performed to deposit a crystalline film of lanthanum aluminate onto a EBCO film and compare simultaneous depositions onto sapphire, MgO, and YSZ. Higher sputtering gas pressure was used to reduce the deposition rate of the films. This study reaffirmed the importance of lattice matching of the film and substrate materials when growing epitaxial films. The increase of the c-axis parameter of the EBCO indicated that oxygen depletion may have occurred in the superconducting film during the lanthanum aluminate film deposition.

4.0 RECOMMENDATIONS FOR FUTURE STUDIES OF LANTHANUM ALUMINATE FILM DEPOSITIONS

The deposition studies described in this thesis have reaffirmed the importance of lattice matching the film and substrate when trying to grow epitaxial films. Even though

initial attempts to deposit lanthanum aluminate onto thin copper and silver buffer layers on sapphire and silicon were not successful, a study with modified deposition parameters could be initiated. Since copper and silver lattice constants match closely with lanthanum aluminate, it should be possible to deposit epitaxial layers of lanthanum aluminate using similar deposition parameters as were described in Section 3.4.7.

Crystalline deposition of oriented lanthanum aluminate onto substrates whose lattice parameters do not match well with lanthanum aluminate will require careful processing. Higher sputtering pressures were more effective in reducing the deposition rate than was lowering the rf-power supplied. Therefore, higher sputtering gas pressures are recommended for crystalline deposition of lanthanum aluminate onto lattice mismatched substrates such as sapphire, MgO, and YSZ. Other alternatives, such as chemical enhancement of the substrates before and after film deposition are also recommended for further studies.

The post-in-situ annealing studies suggest that annealing temperatures greater than 775°C produce structural changes in the films. Further investigation of post-in-situ annealing with longer annealing times would determine if this process can produce acceptable quality polycrystalline lanthanum aluminate films on a variety of substrates.

However, before implementation of this type of study is made, it is recommended that a more reliable substrate heater be installed. The present substrate heater has difficulty in maintaining high annealing temperatures for prolonged periods of time.

5.0 OVERALL SUMMARY

A reliable processing method for making high purity and high quality lanthanum aluminate powder which can be used to make sputtering targets has been developed. The optimal processing method for preparing lanthanum aluminate powder was determined to be mixing a one-to-one molar ratio of lanthanum and aluminum ions in solution followed by hydrolysis and filtration. The calcination temperature required to decompose the hydrolysis byproducts was 950°C. The starting materials which yielded the highest purity products were lanthanum hydroxide and aluminum chloride. The concentration of nitrate present in the solutions greatly affected the purity of the products. If the nitrate concentration was too high then the powder products had a high impurity concentration. A possible hypothesis to explain this effect is that an unidentified nitrate compound, not listed in Table 2.2.4, is present in the

solution and has a decomposition temperature greater than 950°C.

The effects of substrate location, sputtering gas pressure, post-annealing, metallic buffer layers, in-situ-post annealing, and substrate lattice matching on the quality of lanthanum aluminate films deposited by rf-magnetron sputtering were investigated. Substrates were positioned at different radial distance on a rotating substrate holder. The distance between the target center and substrate holder was approximately 4 cm. The previous studies that correlated substrate-target distances with YBCO film compositions and phases did not vary the radial distances of the substrates. This study showed that there is no correlation was observed between the compositions of the films and the radial distance. The coverage of film positioned at the center of the substrate holder was more uniform.

The sputtering gas pressure study compared film qualities that were deposited at pressures of 6, 9, and 12 mTorr. The compositions of the films were different from the that of the target. The ratio of lanthanum to aluminum was closer to 1:1 for the as-deposited films. The films had lower impurity concentrations than the target. The deposition rate was slightly higher for an argon-oxygen ratio of 3:1. The films deposited with these sputtering

conditions were smooth, continuous and amorphous.

Polycrystalline films could be prepared by post-annealing amorphous lanthanum aluminate films at 850°C for one hour in air. These films were severely cracked and thus unsuitable for superconducting thin-film device applications. The cracking of the films was attributed to differences in coefficients of thermal expansion between the films and the substrates. The crystallization of post-annealed films occurred at temperatures greater than 800°C. The post-in-situ studies showed changes in the film morphology, indicating that the films might have started to crystallize. The rough and textured morphology of the films especially on MgO and YSZ substrates indicates that the differences in thermal expansion coefficients of the film and substrate may again reduce the quality of the film.

The metallic buffer layer study showed that thick copper films do not adhere well to sapphire and silicon substrates and are not suitable for thin film applications. The as-deposited films on copper and silver buffer layers were amorphous. The morphology of the as-deposited and post-annealed films on the buffer layers appeared to be not suitable for thin film application, since small particles and crystals were surface of the films. The XRD pattern for the post-annealed film on silver most accurately duplicated that of the lanthanum aluminate powder.

The importance of matching the film and substrate lattice parameters was reaffirmed since the only epitaxial lanthanum aluminate film was grown on a well-oriented crystalline EBCO film. The epitaxial lanthanum aluminate film was deposited onto a crystalline EBCO film on SrTiO_3 while the films simultaneously deposited onto sapphire and MgO were amorphous. These results are in agreement with those reported by Dr. A. Lee (59) where epitaxial growth of lanthanum aluminate was observed only on SrTiO_3 and lanthanum aluminate substrates. The morphology the crystalline lanthanum aluminate film was smooth at 3000X magnification. These results suggests that the single crystalline LaAlO_3 film would be suitable for device applications. However, to be certain of this conclusion the morphology of the film should be inspected at higher magnifications. The composition of the deposited films was found to be dependent on the substrate material. The compositions of the films deposited onto sapphire and silicon matched the composition of the rf-sputtering target. The compositions of the films deposited onto MgO and YSZ were rich in aluminum in comparison to the target.

REFERENCES

- 1) Simon, R. 1989. High-Temperature Superconductors for Microelectronics. Solid State Technology September: 141-146.
- 2) Trefny, J. Superconductivity Class Lecture notes. Fall 1989.
- 3) Readey, D. Properties of Ceramics Class Lecture notes. Spring 1990.
- 4) Cheung, C.T. and Ruckenstein, E. 1989. Superconductor-substrate interactions of the Y-Ba-Cu oxide. J. Mater. Res. 4 (1): 1-15.
- 5) Char, K., Fork, D.K., Geballe, T.H., Laderman, S.S., Taber, R.C., Jacowitz, R.D., Bridges, F., Connell, G.A.N., and Boyce, J.B. 1990. Properties of epitaxial $\text{YBa}_2\text{Cu}_3\text{O}_7$ thin films on Al_2O_3 {1012}. Appl. Phys. Lett. 56 (8): 785-787.
- 6) Leskela M., Truman J.K., Mueller C.H., and Holloway P.H. 1989. Preparation of superconducting Y-Ba-Cu-O thin films. J. Vac. Sci. Technol. A 7 (6): 3147-3171.
- 7) Williams, J., Beno, M., Douglas, K., Geiser, U., Ivy Kao, H., Kini, A., Porter, L., Schultz, A., Thorn, R., Wang, H., Whangbo, M., and Evian, M. 1988. High Transition Temperature Inorganic Oxide Superconductors: Synthesis, Crystal Structure, Electrical Properties, and Electronic Structure. Accounts of Chemical Research 21 (1): 1-7.
- 8) JCPDS-ICDD, Card no. 38-1433, 1988.
- 9) Swanson and Fuyat 1953. Natl. Bur. Std. Cir. 539 Vol II: 20-23.
- 10) Talvacchio, J. and Wagner, G.R. 1990. High- T_c film development for electronic applications. Superconductivity Applications for Infrared and Microwave Devices, SPIE Proc. Vol. 1292 (To be published).
- 11) Wyckoff, R.W.G. 1964. Crystal Structures, 2nd ed. Volume II. New York: Interscience Publishers. pp. 393-412.

- 12) JCPDS-ICDD, Card no. 35-734, 1988.
- 13) JCPDS-ICDD, Card no. 4-829, 1988.
- 14) JCPDS-ICDD, Card no. 30-1468.
- 15) JCPDS-ICDD, Card no. 24-1125.
- 16) Donnay, J.D.H. and Ondik, H.M. eds. 1973. Crystal Data Determinative Tables, 3rd ed. Volume II. Washington DC: U.S. Department of Commerce, National Bureau Standards, and Joint Committee on Powder Diffraction Standards.
- 17) Berkowski, M., Pajaczkowska, A., Gierlowski, P., Lewandowski, S., Sobolewski, R., Gorshunov, B., Kozlov, G., Ludmirsky, D., Syrotynsky, O., Saltykov, P., Soltner, H., Poppe, U., Buchal, Ch., and Lubig, A. CaNdAlO₄ Perovskite Substrate for Microwave and Far-infrared Applications of Epitaxial High-T_c Superconducting Thin Films. (To be published).
- 18) Simon, R. and Smith, A. 1988. Superconductors Conquering Technology's New Frontier. New York: Plenum Press.
- 19) Wangsness, R.K. 1979. Electromagnetic Fields. New York: John Wiley and Sons.
- 20) Cheng, D. 1989. Field and Wave Electromagnetics. 2nd ed. Reading, Massachusetts: Addison-Wesley Publishing Company.
- 21) Simon, R., Lee, A., Platt, C., Daly, K., Luine, J., Eom, C., Rosenthal, P., Wu, X., and Venkatesan, T. 1989. Growth of High Temperature Superconductor Thin Films On Lanthanum Aluminate Substrates, in: Proceedings of SERI Conference on Science and Technology of Thin Film Superconductors, R.D. McConnell and S.A. Wolf, (eds). New York: Plenum Press. pp. 337-346.
- 22) Giess, E. A., Sandstrom, R., Gallagher, W., Gupta, A., Shinde, S., Cook, R., Cooper, E., O'Sullivan, E., Roldan, J., Segmuller, A., and Angilello, J. Lanthanide Gallate Perovskite-Type Substrates for High-Temperature Superconducting Cuprate Films. (To be published).

- 23) Belohoubek, E., Kalokitis, D., Fathy, A., Pendrick, V., Brown, R., Matey, J., Nazar, L., Wilkens, B., Venkatesan, T., Inam, A., Wu, X.D., and Dutta, B. 1989. Microwave Measurements on Patterned High Temperature Superconducting Thin Film Circuits, in: Processing of Films for High T_c Superconducting Electronics, Volume 1187, pp. 348-358. SPIE - The International Society for Optical Engineering.
- 24) Simon, R., Platt, C., Daly, K., Lee, A., and Wagner, M. 1989. Improvement Of Average Film Quality in $\text{RBa}_2\text{Cu}_3\text{O}_{7-x}$ Sputtered Films. IEEE Transactions on Magnetics 25 (2): 2433-2436.
- 25) Bono, A. 1989. Diffusive interactions between $\text{YBa}_2\text{Cu}_3\text{O}_{7-x}$ and LaAlO_3 . Senior Thesis, Colorado School of Mines, Golden, Colo.
- 26) Wu, X., Inam, A., Hegde, M., Wilkens, B., Chang, C., Hwang, D., Nazar, L., Venkatesan, T., Miura, S., Matsubara, S., Miyasaka, Y., and Shohata, N. 1989. High critical currents in epitaxial $\text{YBa}_2\text{Cu}_3\text{O}_{7-x}$ thin films on silicon with buffer layers. Appl. Phys. Lett. 56 (8): 754-756.
- 27) Lee, J., Migliuolo, M., Stamper, A., Greve, D., Laughlin, D., and Schlesinger, T. 1989. Microstructure of superconducting $\text{YBa}_2\text{Cu}_3\text{O}_{7-\delta}$ thin films on Si and alumina substrates with buffer layers. J. Appl. Phys. 66 (10): 4886-4890.
- 28) Atomergic Chemetals Corporation. Lanthanum Aluminate Single Crystal.
- 29) Kingery, W. 1963. Introduction to Ceramics. New York: John Wiley and Sons.
- 30) Mark, H., McKetta, J., Othmer, D., and Standen, A., eds. 1966. Kirk-Othmer Encyclopedia of Chemical Technology, 2nd ed., Volume 18. New York: Interscience Publishers.
- 31) Weasted, R. ed. 1987. Handbook of Chemistry and Physics, 69th ed. Baton, Florida: CRC Press Inc.
- 32) Geller, S., and Bala, V. 1956. Crystallographic Studies of Perovskite-like Compounds. II. Rare Earth Aluminates. Acta Cryst. 9: 1019-1025.

- 33) Simon, R., Platt, C., Lee, A., Lee, G., Daly, K., Wire, M., Luine, J., and Urbanik, M. 1988. Low-loss substrate for epitaxial growth of high-temperature superconductor thin films. Appl. Phys. Lett. **53** (26): 2677-2679.
- 34) Roth, R. 1957. Classification of Perovskite and other ABO_3 - Type Compounds. Journ. Res. Natl. Bur. Stds. **58** (2): 75-88.
- 35) Keith, M., and Roy, R. 1954. Structural Relations Among Double Oxides of Trivalent Elements. Amer. Miner. **39** (1,2): 1-23.
- 36) Golub, A., Maidukova, T., and Limar, T. 1969. Preparation of Lanthanum Aluminate by Joint Precipitation. Ceramic Abstracts. Izv. Akad Nauk SSSR Neorgan. Materialy **2** (9): 179-181.
- 37) Vidyasagar, K., Gopalakrishnan, J., and Rao, C. 1985. Synthesis of Complex Metal Oxides Using Hydroxide, Cyanide and Nitrate Solid Solution Precursors. Journ. of Solid State Chemistry **58**: 29-37.
- 38) Krylov, V., Belova, I., Magunov, R., Kozlov, V., Kalinichenko, A., and Krot'ko, N. 1973. Preparation of Rare Earth Monaluminates from Aqueous Solutions. Chemical Abstracts. Izv. Akad. Nauk SSSR, Neorg. Mater. **9** (8): 1388-1390.
- 39) Watanabe, N., Hisao, K., Kawagoe, H., and Matsuda, S. Patent 20 July 1988. Manufacturing of a heat-resistant aluminum-rare earth metal multiple oxide catalyst support. Chemical Abstracts. Jpn. Kokai Tokkyo Koho JP 63/175642 A2[88/175642].
- 40) Limar, T., Cherednichenko, I., Reshetnikova, L., Lisker, K., and Mudrolyubova, L. Patent 30 March 1980. Powders for manufacture of ceramics. Chemical Abstracts. U.S.S.R. SU 724475.
- 41) Kadogawa, Y. 1986. Effect of Transition Metal Compounds on the formation of Lanthanum Aluminum Oxide ($LaAlO_3$) by the sol-gel Method. Chemical Abstracts. Denki Kagaku Oyobi Kogyo Butsuri Kagaku **54** (4): 362-365.
- 42) Aslanyan, K., Nadzharyan, A., and Nikogosyan, R. 1981. Synthesis of some rare earth metal aluminates, Chemical Abstracts. Arm. Khim. Zh. **34** (1): 13-17.

- 43) Reed, J. 1988. Introduction to the Principles of Ceramic Processing. New York: John Wiley and Sons.
- 44) March, J., and Windwer, S. 1979. General Chemistry. New York: Macmillan Publishing Co., Inc.
- 45) Latimer, W., and Hildebrand, J. 1951. Reference Book of Inorganic Chemistry. New York: The Macmillan Company.
- 46) Kirk, R., and Orthmer, D. eds. 1972. Encyclopedia of Chemical Technology. 2nd ed., Volume 17. New York: Interscience
- 47) Schwartz, L., and Cohen, J. 1987. Diffraction from Materials. 2nd ed. New York: Springer-Verlag.
- 48) Mizuno, M., et al. 1974. JCPDS-ICDD, Card no. 31-22. Yogyo Kyokaishi, (J. Ceram. Assoc. Jpn.) **82**: 631.
- 49) Bondar, I., and Vinogradova, N. 1964. Phase equilibria in the system lanthanum oxide-alumina. Izv. Akad. Nauk. SSSR, Ser. Khim. **5**: 785-790.
- 50) Westwood, W. 1988. Sputtering Deposition Processes. MRS Bulletin : December 1988 46-51.
- 51) Cullity, B. 1978. Elements of X-Ray Diffraction. 2nd ed. Reading, Massachusetts: Addison-Wesley Publishing Company, Inc.
- 52) Goldstein, J., Newbury, D., Echlin, P., Joy, D., Fiori, C., and Lifshin, E. 1981. Scanning Electron Microscopy and X-Ray Microanalysis A Text for Biologists, Materials Scientists, and Geologists. New York: Plenum Press.
- 53) Matsutani, K., Terada, N., Jo, M., and Ihara, H. 1990. Compositional Change of Sputtered $\text{YBa}_2\text{Cu}_3\text{O}_y$ Films with Substrate Location. Japanese Journal of Applied Physics **29** (1): 79-80
- 54) Witanachchi, S., Patel, S., Shaw, D., and Kwok, H. 1989. Effect of buffer layers on low-temperature growth of mirror superconducting thin films on sapphire. Appl. Phys. Lett. **55** (3): 295-297.

- 55) Mossner, C., Ufer, K., Kopfer, P., Rupertus, V., and Oechsner, H. 1989. Characterization Of Ion-Beam- and Magnetron-Sputtered $\text{YBa}_2\text{Cu}_3\text{O}_{7-x}$ High T_c Superconducting Films By Secondary Neutral Mass Spectrometry Depth Profiling. Thin Films 174: 255-262.
- 56) Gao, J., Hauser, B., and Rogalla, H. 1990. High critical current density ultrathin $\text{YBa}_2\text{Cu}_3\text{O}_x$ films made by a modified rf-magnetron sputtering technique. J. Appl. Phys. 67 (5): 2512-2515.
- 57) Eom, C., Sun, J., Yamamoto, K., Marshall, A., Luther, K., Geballe, T., and Laderman, S. 1989. In situ grown $\text{YBa}_2\text{Cu}_3\text{O}_{7-d}$ thin films from single-target magnetron sputtering. Appl. Phys. Lett. 55 (6): 595-597.
- 58) Char, K., Newman, N., Garrison, S., Barton, R., Taber, R., Laderman, S., and Jacowitz, R. 1990. Microwave Surface Resistance of Epitaxial YBCO Thin Films on Sapphire. To be Published.
- 59) Lee, A., Platt, C., Burch, J., Simon, R., Goral, J., and Al-Jassim, M. Epitaxially-grown sputtered LaAlO_3 films. To be published.